This is the author's peer reviewed, accepted manuscript. However, the online version of record will be different from this version once it has been copyedited and typeset

PLEASE CITE THIS ARTICLE AS DOI: 10.1063/5.0209887

### Simulating Multipulse NMR Spectra of Polycrystalline Solids in the Frequency Domain

Deepansh J. Srivastava<sup>1, a)</sup> and Philip J. Grandinetti<sup>2, b)</sup>

<sup>1)</sup> Hyperfine, Inc., Guilford, CT, USA

An approach is presented for simulating multipulse Nuclear Magnetic Resonance (NMR) spectra of polycrystalline solids directly in the frequency domain. The approach integrates the symmetry pathway concept for multipulse NMR with efficient algorithms for calculating spinning sideband amplitudes and performing interpolated finite-element numerical integration over all crystallite orientations in a polycrystalline sample. The numerical efficiency is achieved through a set of assumptions used to approximate the evolution of a sparse density matrix through a pulse sequence as a set of individual transition pathway signals. The utility of this approach for simulating spectra of complex materials, such as glasses and other structurally disordered materials, is demonstrated.

### I. INTRODUCTION

Nuclear Magnetic Resonance (NMR) spectroscopy. II-5 has long played an essential role in determining the structure and dynamics of matter on various length scales. At the atomic scale, such information is encoded in the tensorial interactions between the electromagnetic moments of the nucleus and its surrounding magnetic and electric fields. In fluid phases, the effect of these anisotropic interactions on the NMR transition frequency is averaged out by rapid molecular tumbling, leaving only isotropic contributions to the NMR spectrum. In solid phases, however, these anisotropic interactions are preserved. This leads to a richer array of spectral features in solids that can reveal significantly more details about the structure and dynamics of the solid. Unfortunately, the presence of these anisotropic frequency contributions also increases the level of complexity of the measurements and the interpretation of results. For this reason, solid-state NMR measurements often require the expertise of a solid-state NMR spectroscopist to set up, process, and interpret. Compared to the liquid state, solid-state NMR has never been a technique that can be approached casually, even on commercial instruments.

The ability to simulate solid-state NMR spectra is central to their analysis and interpretation. It also plays a vital role in developing new solid-state NMR methods. Currently, there are two approaches to simulating solid-state NMR spectra. The first numerically solves a quantum master equation, e.g., the Louiville von Neumann equation, to simulate a time-domain signal whose Fourier transform gives the frequency-domain spectrum. This first-principles approach can be highly versatile in its ability to simulate multi-pulse NMR methodologies in rotating samples, but it is computationally expensive. Consequently, it is often not practical for simulating

the spectra of disordered materials, where the number of unique spin systems can be large. The second and more approximate approach focuses on spin systems with non-degenerate eigenvalues where analytical expressions for the NMR transition frequencies and amplitudes for each spin system can be summed to obtain the frequency-domain spectrum directly. While existing software packages implementing this approximate approach are significantly faster than the first-principles approach, they are often hard-coded for a small subset of NMR methods. [20] [27]

In principle, implementing a general-purpose multipulse NMR simulation directly in the frequency domain should be no more challenging than in the time domain, although admittedly, there are few examples in the literature of numerical algorithms being developed for such cases. Here, we present a theoretical approach supporting algorithms for a general-purpose multi-pulse NMR simulation of solid-state NMR spectra directly in the frequency domain. In this effort, we combine concepts from the symmetry pathway approach to multi-pulse NMR experiments with efficient algorithms for calculating spinning sideband amplitudes and for performing numerical integration of the spectra over all crystallite orientations in a polycrystalline sample. In the symmetry pathway approach, a multi-pulse NMR method is described in terms of a set of transition symmetry pathways, which, when combined with a given spin system, are mapped into a set of transition pathways. Each transition pathway corresponds to a single resonance in a multi-dimensional NMR spectrum in a static sample or a single centerband resonance flanked by a series of spinning sideband resonances in a rotating sample. By focusing on individual transition pathways, the finiteelement integration and interpolation algorithm of Alderman, Solum, and Grant<sup>[20]</sup> (ASG) for rapid simulation of one-dimensional NMR spectra of polycrystalline sample in the frequency domain can be extended to the simulation of multidimensional NMR spectra. Taken together, this frequency domain approach can perform simulations of multi-pulse NMR spectra in polycrystalline

<sup>&</sup>lt;sup>2)</sup> Department of Chemistry, Ohio State University, 100 West 18th Avenue, Columbus, OH 43210, USA

<sup>&</sup>lt;sup>a)</sup>Electronic mail: dsrivastava@hyperfine.io

b) Electronic mail: grandinetti.1@osu.edu

PLEASE CITE THIS ARTICLE AS DOI: 10.1063/5.0209887

This is the author's peer reviewed.

solids in significantly less time than conventional time domain simulations. The theoretical approach and algorithms described here are implemented in the Python package MRSimulator for simulating multi-dimensional NMR spectra of polycrystalline solids and will be described elsewhere.

### II. THEORETICAL APPROACH

### A. Fundamental assumptions

The state of a quantum-mechanical system of a set  $\mathcal{I}$  of  $n_{\mathcal{I}}$  coupled spins can be described by a vector in a  $\Upsilon$ -dimensional Hilbert space according to

$$|\psi(t)\rangle = \sum_{i=1}^{\Upsilon} c_i(t)|i\rangle, \text{ where } \Upsilon_{\left\{I_1, I_2, \dots, I_{n_{\mathcal{I}}}\right\}} = \prod_{u=1}^{n_{\mathcal{I}}} (2I_u + 1), \tag{1}$$

where  $|i\rangle$  is the  $i^{\text{th}}$  eigenstate of the (Zeeman) Hamiltonian, and  $c_i(t)$  is the complex amplitude of the  $i^{\text{th}}$  eigenstate. Here,  $I_u$  is the total spin angular momentum quantum number of the  $u^{\text{th}}$  nucleus.

For an ensemble of identical quantum-mechanical systems, we can define the density operator

$$\hat{\rho}(t) = \overline{|\psi(t)\rangle\langle\psi(t)|} = \sum_{j=1}^{\Upsilon} \sum_{i=1}^{\Upsilon} \overline{c_j(t)c_i^*(t)} |j\rangle\langle i|, \quad (2)$$

where the  $\overline{c_i(t)}c_i^*(t)$  represent the population of the  $i^{\text{th}}$  stationary eigenstate, and the  $\overline{c_j(t)}c_i^*(t)$  represent the complex amplitude of the  $i \to j$  transition. The  $i \to j$  transition is one of  $\Upsilon!/(\Upsilon-2)!$  possible transitions between  $\Upsilon$  levels. Here, we count  $i \to j$  and  $j \to i$  as different transitions.

We assume that the equilibrium density operator is diagonal in the Zeeman eigenstates with populations given by the Boltzmann distribution. In the high-temperature approximation, the density operator at thermal equilibrium is approximated according to

$$\hat{\rho}_{eq} = \frac{e^{-\hat{\mathcal{H}}/k_B T}}{Z} \approx -\sum_{u=1}^{n_{\mathcal{I}}} \frac{\hbar \omega_{0,u}}{k_B T \left(2I_u + 1\right)} \hat{I}_{u,z}, \quad (3)$$

where  $\hat{\mathcal{H}}$  is the Hamiltonian,  $Z = \text{Tr}(e^{-\hat{\mathcal{H}}/k_BT})$  is the partition function,  $k_B$  is the boltzmann constant, T is the thermodynamic temperature,  $\hbar \hat{I}_{u,z}$  is the z-component of the angular momentum operator for the  $u^{\text{th}}$  nucleus, and  $\omega_{0,u}$  is the Larmor frequency of the  $u^{\text{th}}$  nucleus.

At the most general level, the theoretical description of an NMR experiment starts with the time evolution of the density operator,  $\hat{\rho}(t)$ , through a quantum master equation. The form of this equation can vary depending on the application. We focus on applications where relaxation processes can be neglected, allowing the quantum master equation to be reduced to the Louiville von

Neumann equation<sup>3</sup>

$$\frac{d\hat{\rho}(t)}{dt} = -\frac{i}{\hbar} \left[ \hat{\mathcal{H}}(t), \hat{\rho}(t) \right], \tag{4}$$

where  $\hat{\mathcal{H}}(t)$  is a Hamiltonian having only coherent time dependences due to radio-frequency (RF) excitation and sample rotation, such as magic-angle (MAS) and variable-angle (VAS) sample spinning. It has the general form

$$\hat{\mathcal{H}}(t) = \hat{\mathcal{H}}_Z + \hat{\mathcal{H}}_{RF}(t) + \sum_{\lambda \in \Gamma} \hat{\mathcal{H}}_{\lambda}^{(1)}(t), \tag{5}$$

where  $\mathcal{H}_Z$  is the Zeeman Hamiltonian,  $\hat{\mathcal{H}}_{RF}(t)$  is the RF excitation Hamiltonian, and  $\hat{\mathcal{H}}_{\lambda}^{(1)}(t)$  are the parts of the Hamiltonian arising from some set  $\Gamma$  of nuclear spin couplings internal to the sample. In NMR, the  $\hat{\mathcal{H}}_{\lambda}^{(1)}$  are often expressed in terms of irreducible tensor elements of ranks  $L=0,\ 1,\ \mathrm{and}\ 2$  in the lab coordinate system as

$$\hat{\mathcal{H}}_{\lambda}^{(1)} = \Lambda^{\{\lambda\}} \sum_{L=0}^{2} \sum_{m=-L}^{L} (-1)^m R_{L,-m}^{\{\lambda\}} \hat{T}_{L,m}^{\{\lambda\}} (\vec{\hat{U}}, \vec{V}).$$
 (6)

Here, the  $\Lambda^{\{\lambda\}}$  depend on the identity of the nuclei involved in the interaction and are given in Table S7 of the Supplementary Material. The  $R_{L,-m}^{\{\lambda\}}$  are the spherical tensor elements, and  $\hat{T}_{L,m}^{\{\lambda\}}(\vec{U},\vec{V})$  are the irreducible spherical tensor element operators, formed from the tensor product of two vectors  $\vec{U}$  and  $\vec{V}$ . The vector  $\vec{U}$  is a nuclear spin vector operator, whereas the vector  $\vec{V}$  can be the same nuclear spin vector operator (quadrupolar interaction), another nuclear spin vector operator (dipolar and J coupling), or the external magnetic field vector (Zeeman, paramagnetic shift, and nuclear shielding interactions). Further details on the Cartesian and spherical tensor conventions are given in the Supplementary Material. We further assume that  $||\hat{\mathcal{H}}_Z|| \gg ||\sum_{\lambda} \hat{\mathcal{H}}_{\lambda}^{(1)}(t)||$ , and the time-dependence due to sample rotation is in the adiabatic limit,  $||\vec{\mathcal{H}}||^2$  allowing the Hamiltonian to be written in a series expansion

$$\hat{\mathcal{H}}(t) \approx \hat{\mathcal{H}}_Z + \hat{\mathcal{H}}_{RF}(t) + \sum_{\lambda \in \Gamma} \hat{D}_{\lambda}^{(1)}(t) + \sum_{\lambda \in \Gamma} \sum_{\lambda' \in \Gamma} \hat{D}_{\lambda,\lambda'}^{(2)}(t) + \cdots,$$
(7)

where  $\hat{D}_{\lambda}^{(1)}(t)$  and  $\hat{D}_{\lambda,\lambda'}^{(2)}(t)$  are the first- and second-order perturbation theory corrections. 37

An  $n_{\text{dim}}$ -dimensional multi-pulse NMR experiment can be modeled using the density operator according to

$$\hat{\rho}(t_1, \dots, t_{n_{\text{dim}}}) = \hat{\mathcal{U}}(t_1, \dots, t_{n_{\text{dim}}}) \,\hat{\rho}(0) \,\hat{\mathcal{U}}^{\dagger}(t_1, \dots, t_{n_{\text{dim}}}), \tag{8}$$

where

$$\hat{\mathcal{U}}(t_1, \dots, t_{n_{\text{dim}}}) = \prod_{v=1}^{n_{\text{dim}}} \hat{\mathcal{U}}_v(t_v), \tag{9}$$

PLEASE CITE THIS ARTICLE AS DOI: 10.1063/5.0209887

This is the author's peer reviewed.

and  $\hat{\mathcal{U}}_{v}(t_{v})$  is the *spectral dimension* propagator modeling the evolution through the  $v^{th}$  spectral dimension.

Each spectral dimension propagator can be further broken down into a product of  $n_{\rm v}$  events, given by

$$\hat{\mathcal{U}}_{\mathbf{v}}(t_{\mathbf{v}}) = \prod_{k=1}^{n_{\mathbf{v}}} \hat{U}_{\mathbf{v},k},\tag{10}$$

where  $\hat{U}_{v,k}$  is either a free evolution propagator,  $\hat{U}_{v,k}(\tau_{v,k})$  or  $\hat{U}_{v,k}(x_{v,k}t_v)$ , or a mixing propagator,  $\hat{P}_{v,k}(\tau_{v,k})$ . The  $\hat{P}_{v,k}(\tau_{v,k})$  and  $\hat{U}_{v,k}(\tau_{v,k})$  are propagators of constant duration  $\tau_{v,k}$ , which we will refer to as a mixing event and delay event propagator, respectively. The  $\hat{U}_{v,k}(x_{v,k}t_v)$  denotes a variable duration free evolution propagator, which we will refer to as a spectral event propagator and  $x_{v,k}$  is the fraction of the free evolution period  $t_v$  that the  $k^{\text{th}}$  propagator is active in  $\hat{\mathcal{U}}_v(t_v)$ . We define  $x_{v,k}=0$  whenever the  $k^{\text{th}}$  propagator is not a spectral event propagator, and require

$$\sum_{k=1}^{n_{\mathbf{v}}} x_{\mathbf{v},k} = 1. \tag{11}$$

The assumptions made so far are similar to those found in many conventional NMR simulations and are commonly used to analyze high-field solid-state NMR spectra. In developing our frequency domain simulation approach, we obtain significant efficiency gains in the simulation algorithms by making the following additional assumptions:

- I. There are no degeneracies in the eigenvalues of  $\hat{\mathcal{H}}(t)$  for all t, i.e., all the dipolar and J couplings remain in the weak limit.
- II. Time dependences in  $\hat{\mathcal{H}}_{\lambda}^{(1)}(t)$  are not on or near resonant with any NMR transition frequencies. 38-40
- III. Internal couplings can be neglected during RF excitation, i.e.,  $||\hat{\mathcal{H}}_{RF}(t)|| \gg ||\sum_{\lambda} \hat{\mathcal{H}}_{\lambda}^{(1)}(t)||$ . Therefore, for the mixing propagator,  $\hat{P}_{\mathbf{v},k}$ , the effect of an RF pulse on the density operator is approximated by a pure rotation of  $\theta$  about an axis defined by  $\psi$  in the x-y plane.
- IV. Transition frequencies can be calculated analytically.

Assumptions I and II are essential for reducing the density operator to a set of individual transition pathway signals with no mixing among transitions during free evolution periods, i.e., the free evolution propagator matrices,  $\hat{U}_{v,k}(\tau_{v,k})$  or  $\hat{U}_{v,k}(x_{v,k}t_v)$ , remain diagonal. Assumptions III and IV are not essential but are made to reduce computational overhead in calculating the transition pathway signals. While these four assumptions might be considered restrictive for a general-purpose NMR simulation package, they are not uncommon for many high-field solid-state NMR experiments, where the dipolar and J couplings are weak and the RF excitation is strong.

### B. Transition Pathways

When simulating the solid-state NMR spectrum arising from a multi-pulse sequence, it is helpful to keep in mind that NMR experiments are typically performed as a set of difference measurements designed to isolate the signal from a specific set of transition pathway signals. Much of the experimental design and implementation of an NMR method is identifying the desired transition pathways and finding ways to acquire their signals while eliminating all undesired transition pathway signals. Transition pathway signal isolation is experimentally accomplished through various approaches, such as RF phase cycling, pulse length optimizations, selective pulses, multiple quantum filters, or field gradients.

In numerical simulations of multi-pulse NMR experiments, the undesired transition pathway signals in the density matrix are eliminated by zeroing the corresponding undesired matrix elements. The density matrix can become sparse in this process, making it computationally inefficient to propagate the full density matrix through the pulse sequence. In such cases, it is more efficient to propagate the single transition operators through each transition pathway separately.

Consider the illustration of a 2D pulse sequence shown in Fig.  $\square$  where the desired signal for the method is associated with a particular transition pathway,  $\hat{\chi}_A \to \hat{\chi}_B \to \hat{\chi}_C \to \hat{\chi}_D$ . Here  $\hat{\chi}_A$  and  $\hat{\chi}_B$  are the transitions associated with the two spectral events in the  $t_1$  spectral dimension with  $x_A + x_B = 1$ . The  $\hat{\chi}_C$  is the transition associated with the delay event with constant delay  $\tau$ , and  $\hat{\chi}_D$  is the transition associated with the spectral event, with  $x_D = 1$ , along the  $t_2$  spectral dimension, respectively. The pulses shown as solid black rectangles are the four mixing events. Through the first spectral dimension, we can write the evolution as

$$(u_{0A})e^{-i\Omega_A x_A t_1} \hat{\chi}_A \to (u_{0A} u_{AB})e^{-i(\Omega_A x_A + \Omega_B x_B)t_1} \hat{\chi}_B.$$
 (12)

Here,  $u_{0A}$  is the amplitude of the initial single transition operator  $\hat{\chi}_A$ , and  $u_{AB}$  is the mixing amplitude for the transfer from  $\hat{\chi}_A$  to  $\hat{\chi}_B$ . The Fourier transform of the transition pathway signal as a function of  $t_1$  derives its average frequency,  $\overline{\Omega}_1$ , from a weighted average of the  $\hat{\chi}_A$  and  $\hat{\chi}_B$  transition frequencies. After reaching the final transition,  $\hat{\chi}_D$ ,

$$\cdots \to \underbrace{\left[ (u_{0A} u_{AB} u_{BC} u_{CD}) e^{-i\Omega_C \tau} \right]}_{s(0,0)} e^{-i\overline{\Omega}_1 t_1} e^{-i\Omega_D t_2} \hat{\chi}_D,$$

the transition pathway signal has acquired a  $t_1$  and  $t_2$  dependent phase modulation,  $e^{-i\overline{\Omega}_1t_1}e^{-i\Omega_Dt_2}$ , and a complex amplitude, s(0,0), where  $u_{BC}$  and  $u_{CD}$  are the mixing amplitudes for the transfer from  $\hat{\chi}_B$  to  $\hat{\chi}_C$  and  $\hat{\chi}_C$  to  $\hat{\chi}_D$ , respectively. A 2D Fourier transform of the transition pathway signal gives

$$s(\omega_1, \omega_2) = s(0, 0)\delta(\omega_1 - \overline{\Omega}_1)\delta(\omega_2 - \Omega_D), \tag{14}$$

PLEASE CITE THIS ARTICLE AS DOI: 10.1063/5.0209887

This is the author's peer reviewed.

### Transition pathway signal $\overline{\Omega_1}t_1$

FIG. 1. An illustration of a two-dimensional NMR pulse sequence leading up to the acquisition of the signal from a single transition pathway.

where  $\delta(x)$  is the Dirac delta function. This process can be repeated for other desired transition pathway signals. which are summed to the total signal,

$$S(\omega_1, \omega_2) = \sum_{z \in \mathcal{T}} s_z(\omega_1, \omega_2), \tag{15}$$

where  $\mathcal{T}$  is the set of all desired transition pathways. This approach is advantageous when the number of desired transition pathways is significantly less than the total number of possible transition pathways. Further details on how the transition pathway signals are calculated are provided in the following sections.

### C. Transition Frequencies

Calculating the desired transition pathway spectrum is more efficient when analytical expressions for transition frequencies are available. This section briefly reviews these expressions for a spin-system with  $n_{\tau}$  sites. For a detailed overview of their derivation, see the Supplemen-

Here, we consider frequency contributions arising from the first- and second-order perturbation terms, which are summed to give the total transition frequency,  $\Omega(\Theta, i, j)$ , for the  $i \to j$  transition as 28

$$\Omega(\Theta, i, j) = \sum_{k} \omega_k \,\Xi_L^{(k)}(\Theta) \,\xi^{(k)}(i, j), \qquad (16)$$

where  $\omega_k$  is the size,  $\Xi_L^{(k)}(\Theta)$  is the sample's spatial orientation function corresponding to the  $L^{\text{th}}$  rank spatial irreducible spherical tensor, and  $\xi^{(k)}(i,j)$  is the spin transition symmetry function of the  $k^{th}$  frequency contribution A review of spin transition symmetry functions is given in Appendix A.

The spatial orientation functions,  $\Xi_L^{(k)}(\Theta)$ , in Eq. (16), are defined in the laboratory frame, where the z-axis is the direction of the external magnetic field. Here,  $\Theta(t)$  are the Euler angles that determine the sample's lattice spatial orientation, which can carry a time dependence due to sample rotation. We can expand the orientation dependence of a given transition frequency using a series of rotations from the common frame of each frequency contribution to the laboratory frame and re-express Eq. (16) as

$$\Omega(t,i,j) = \sum_{k} \underbrace{\left[ \sum_{m_0 = -L_k}^{L_k} \mathcal{D}_{m_0,0}^{(L_k)}(\omega_R t + \phi, \theta_R, 0) \sum_{m_1 = -L_k}^{L_k} \mathcal{D}_{m_1,m_0}^{(L_k)}(\alpha, \beta, \gamma) \Delta_{L_k,m_1}^{\{k\}} \right]}_{\omega_k \Xi_L^{(k)}(\Theta)} \xi^{(k)}(i,j), \tag{17}$$

where  $\mathcal{D}_{m,m'}^{(L)}(\alpha,\beta,\gamma)$  are Wigner rotation matrix elements, given by

$$\mathcal{D}_{m,m'}^{(L)}(\alpha,\beta,\gamma) = e^{-im\alpha} d_{m,m'}^{(L)}(\beta) e^{-im'\gamma},$$
 (18)

 $d_{m,m'}^{(L)}(\beta)$  are the reduced Wigner rotation matrix elements,  $\omega_R$  is the rotor frequency,  $\phi$  is the initial rotor phase,  $\theta_R$  is the rotor angle,  $(\alpha, \beta, \gamma)$  are the Euler angles relating the common frame to the rotor frame, and  $\Delta_{L_k}^{\{k\}}$ is the frequency-scaled spatial spherical (fsSST) tensor part of the  $k^{\text{th}}$  frequency contribution of rank  $L_k$  in the common frame. For frequency contributions involving a single interaction, the components of  $\boldsymbol{\Delta}_L^{\{\lambda\}}$  in the common frame are given by

$$\Delta_{L,m}^{\{\lambda\}} = \sum_{m'=-L}^{L} \mathcal{D}_{m,m'}^{(L)}(\Theta_{\text{PAS}}^{\{\lambda\}}) \varsigma_{L,m'}^{\{\lambda\}}, \tag{19}$$

where  $\varsigma_L^{\{\lambda\}}$  is an fsSST part of rank L in the PAS of the single interaction spatial tensor, and  $\Theta_{\rm PAS}^{\{\lambda\}}$  is the orientation of the PAS relative to the common frame. The components of  $\varsigma_L^{\{\lambda\}}$  for each single interaction fsSST are expanded and given in Table [].

In the Supplementary Material, we further derive the fsSST in the common frame for the second-order perturbation theory corrections involving the quadrupolar interaction of spin I, with (1) the shielding interaction of spin I, i.e.,  $(\sigma q_I)$ , (2) the weak J coupling interaction

## ACCEPTED MANUSCRIP

accepted manuscript. However, the online version of record will be different from this version once it has been copyedited and typeset This is the author's peer reviewed.

PLEASE CITE THIS ARTICLE AS DOI: 10.1063/5.0209887

TABLE I. Frequency-scaled spatial spherical tensor elements in the principal axis system for the various NMR interactions. For all interactions,  $\zeta_{L,\pm 1}^{\{\lambda\}} = \zeta_{L,\pm 3}^{\{\lambda\}} = 0$ . The  $\eta_{\lambda}$  are the asymmetry parameters for the symmetric tensor associated with each nuclear spin interaction. For the Larmor frequency,  $\omega_0 = -\gamma_I B_0$ , where  $\gamma_I$  is the magnetogyric ratio and  $B_0$  is the external static magnetic flux density. For the quadrupolar coupling,  $\omega_q = \frac{6\pi C_q}{2I(2I-1)}$  where I is the nuclear angular momentum quantum number,  $C_q = \frac{q_e Q_I}{h} \zeta_q$ ,  $q_e$  is the fundamental unit of charge,  $Q_I$  is the nuclear electric quadrupolar moment, h is the planck constant, and  $\zeta_q$  is the electric field gradient at the nucleus. For the nuclear magnetic shielding,  $\sigma'_{\rm iso} = \sigma_{\rm iso} - \sigma^{\rm ref}_{\rm iso}$ is the isotropic nuclear shielding relative to the reference nucleus, and  $\zeta_{\sigma}$  is the shielding anisotropy defined according to the Haeberlen convention. For the dipolar coupling,  $\omega_d = -\frac{\mu_0}{4\pi} \frac{\gamma_1 \gamma_2 \hbar}{r^3}$ , where  $\gamma_1$  and  $\gamma_2$  are the gyromagnetic ratios of the two coupled nuclei, r is the distance between the two nuclei,  $\hbar$  is the reduced planck constant, and  $\mu_0$  is the magnetic permeability constant. For the J coupling,  $J_{\rm iso}$  is the isotropic J coupling, and  $\zeta_J$  is the J coupling anisotropy defined according to the Haeberlen convention.

to spin S, i.e.,  $(Jq_I)$ , and (3) the weak dipolar coupling interaction to spin S, i.e.,  $(dq_I)$ . These contributions can be generically written for  $\lambda \in \{\sigma, J, d\}$ , as

$$\begin{split} \Delta_{L,m}^{\{\lambda q_I\}} &= -\frac{h_L^{\{\lambda q_I\}}}{\omega_{0,I}} \sum_{m'} \langle L \ m | 2 \ 2 \ m' \ m - m' \rangle \\ &\qquad \times \Delta_{2,m'}^{\{\lambda\}} \Delta_{2,m-m'}^{\{q_I\}}, \quad (20) \end{split}$$

where  $\langle L M | \ell_1 \ell_2 m_1 m_2 \rangle$  are the Clebsch-Gordon coefficients, and

$$h_0^{\{\lambda q_I\}} = -\sqrt{\frac{9}{5}}, \ h_2^{\{\lambda q_I\}} = \sqrt{\frac{9}{14}}, \ h_4^{\{\lambda q_I\}} = \sqrt{\frac{72}{35}}.$$
 (21)

The product of each  $\Delta_L$  with its corresponding spin transition function for each perturbation term creates a frequency tensor contribution. The transition frequency tensor contributions considered here are given in Table III. All the frequency tensor contributions of similar ranks are summed together into total transition frequency tensors of rank L, as illustrated below:

accepted manuscript. However, the online version of record will be different from this version once it has been copyedited and typeset This is the author's peer reviewed.

PLEASE CITE THIS ARTICLE AS DOI: 10.1063/5.0209887

$$\mathbf{F}_{2}(i,j) = \boldsymbol{\Delta}_{2}^{\{\sigma\}} \mathbf{p}_{u} + \boldsymbol{\Delta}_{2}^{\{J\}} (\mathbf{pp})_{u,u'} + \boldsymbol{\Delta}_{2}^{\{d_{IS}\}} (\mathbf{pp})_{u,u'} + \boldsymbol{\Delta}_{2}^{\{q\}} \mathbf{d}_{u} + \boldsymbol{\Delta}_{2}^{\{qq\}} \mathbf{c}_{2,u} + \boldsymbol{\Delta}_{2}^{\{\sigma q\}} \mathbf{d}_{u}$$

$$+ \Delta_2^{\{dq\}} (\mathbb{dp})_{u,u'} + \Delta_2^{\{Jq\}} (\mathbb{dp})_{u,u'}, \tag{23}$$

$$\mathbf{F}_{4}(i,j) = \Delta_{4}^{\{qq\}} \mathbf{c}_{4,u} + \Delta_{4}^{\{\sigma q\}} \mathbf{d}_{u} + \Delta_{4}^{\{dq\}} (\mathbf{dp})_{u,u'} + \Delta_{4}^{\{Jq\}} (\mathbf{dp})_{u,u'}. \tag{24}$$

Contributions can be included or excluded as desired during each spectral or delay event. We obtain the total transition frequency in the lab frame from the total transition frequency tensor in the common frame,  $\mathbf{F}_L$ , as

$$\Omega(t, i, j) = \sum_{L=0, 2, 4} \sum_{m=-L}^{L} e^{-im(\omega_R t + \phi)} d_{m, 0}^{(L)}(\theta_R) 
\times \sum_{m'=-L}^{L} e^{-im'\alpha} d_{m', m}^{(L)}(\beta) e^{-im\gamma} F_{L, m'}(i, j).$$
(25)

### D. Mixing Amplitudes

### 1. Pure rotations

The set of nuclei,  $\mathcal{I}$ , in a spin system can be partitioned into  $n_c$  disjoint subsets of  $\{\mathfrak{I}_1,\mathfrak{I}_2,\ldots,\mathfrak{I}_{n_c}\}$ , called *channels*, where  $\mathfrak{I}_c$  is the set of nuclei in the  $c^{\text{th}}$  subset, i.e., the  $c^{\text{th}}$  channel. This partitioning is useful for separating nuclei into subsets of nuclei of the same isotope, although it could also be used to separate nuclei into subsets for other purposes, such as selective excitation of a subset of nuclei within a specific excitation bandwidth. Following these definitions, a single-transition operator is written as the direct product

$$\hat{\chi} = \bigotimes_{c=1}^{n_c} \bigotimes_{u \in \mathcal{I}_c} |I_u, m_{u,j}\rangle \langle I_u, m_{u,i}|.$$
 (26)

Assuming that nuclei in each *channel* have the same gyromagnetic ratio, the RF Hamiltonian in Eq. (5) after transforming into the multiply rotating interaction frame of the nuclei in each channel, can be written

$$\hat{\mathcal{H}}_{RF}/\hbar = \sum_{c=1}^{n_c} \sum_{u \in \mathfrak{I}_c} \omega_{1,c} \left[ \hat{I}_{u,x} \cos \psi_c + \hat{I}_{u,y} \sin \psi_c \right], \quad (27)$$

where  $\omega_{1,c}$  and  $\psi_c$  are the RF amplitude and phase for the nuclei in the  $c^{\rm th}$  channel, respectively, and  $\hat{I}_{u,x}$  and  $\hat{I}_{u,y}$  are the x and y components of the spin operator for the  $u^{\rm th}$  nucleus. By adopting assumption III, where evolution due to all spin couplings internal to the sample is neglected during the pulse, the effect of an RF pulse of duration  $t_p$  on the density operator can be calculated

analytically as pure rotations about an axis in the x-y plane of each channel's rotating frame defined by a given rotation angle,  $\theta_c = \omega_c t_p$ , and phase,  $\psi_c$ . The mixing amplitude for the coherence transfer from  $\hat{\chi}$  to  $\hat{\chi}'$  by a rotation is given by

$$u_{\chi',\chi} = \prod_{c=1}^{n_c} \prod_{u \in \mathfrak{I}_c} d_{m'_{u,j},m_{u,j}}^{(I_u)}(\theta_c) d_{m'_{u,i},m_{u,i}}^{(I_u)}(\theta_c) e^{-i\Delta p_u \psi_c} (i)^{\Delta p_u},$$

where  $\mathbb{p}_u = m_{u,j} - m_{u,i}$  (Eq. (A2)) and  $\Delta \mathbb{p}_u = \mathbb{p}'_u - \mathbb{p}_u$ . We note two interesting and useful cases. One is that coherence transfer under a  $\pi$  rotation simplifies to

$$|I_{u}, m_{u,j}\rangle \langle I_{u}, m_{u,i}| \xrightarrow{\pi_{\psi}} |I_{u}, -m_{u,i}\rangle \langle I_{u}, -m_{u,i}| e^{-i\Delta p_{u}\psi} (i)^{\Delta p_{u}}, \quad (29)$$

i.e., a  $\pi$  rotation can make only one connection between transitions in adjacent spectral or delay events. It is also a special connection because the  $\mathbb{p}_u$  transition symmetry value for the two transitions are equal but opposite in sign. Additionally, the  $\mathbb{d}_u$  transition symmetry, given in Eq. (A3), remains unchanged ( $\Delta \mathbb{d}_u = 0$ ) for the two transitions. The other interesting case is that, while a rotation can transfer a transition into many other transitions, the  $\mathbb{d}_u$  transition symmetry value cannot remain unchanged ( $\Delta \mathbb{d}_u \neq 0$ ) between two connected transitions under a  $\pi/2$  rotation. This is similarly true for the two-spin symmetry transition function ( $\mathbb{pp}$ )<sub>u,u'</sub>, also given in Appendix A

### 2. Total Mixing

It is helpful to define an artificial total mixing operator, where selected transitions are transferred to all selected transitions in the following spectral or delay event with 100% efficiency. For example, suppose the first of two adjacent spectral or delay events has three selected transitions, and the second has two selected transitions. In that case, a total mixing operation will make  $2\times 3=6$  connections, i.e., six transition pathways passing from the first to second spectral or delay event. This total mixing assumes that every connection has a mixing amplitude of 1. While the total mixing operation is unphysical, it can be numerically efficient and, when used with caution, yields fast and accurate simulations.

## ACCEPTED MANUSCRIPT

### The Journal of Chemical Physics

accepted manuscript. However, the online version of record will be different from this version once it has been copyedited and typesel This is the author's peer reviewed.

PLEASE CITE THIS ARTICLE AS DOI: 10.1063/5.0209887

-		
Contribution	SPT	$\mathbf{F}_L(i,j)$
	order	contribution
shielding	1st	$oldsymbol{\Delta}_0^{\{\sigma\}} \mathbb{p}_u$
shielding	1st	$oldsymbol{\Delta}_2^{\{\sigma\}} \mathbb{p}_u$
weak J	1st	${f \Delta}_0^{\{J\}}({\mathbb p}{\mathbb p})_{u,u'}$
weak J	1st	${f \Delta}_2^{\{J\}}({\mathbb p}{\mathbb p})_{u,u'}$
weak dipolar	1st	$oldsymbol{\Delta}_2^{\{d_{IS}\}}(\mathbb{pp})_{u,u'}$
quadrupolar	1st	$oldsymbol{\Delta}_2^{\{q\}} \mathbb{d}_u$
quadrupolar	2nd	$oldsymbol{\Delta}_0^{\{qq\}} \mathbb{c}_{0,u}$
quadrupolar	2nd	${\bf \Delta}_2^{\{qq\}}\mathbb{c}_{2,u}$
quadrupolar	2nd	$\mathbf{\Delta}_{4}^{\{qq\}}\mathbb{c}_{4,u}$
quadrupolar-shielding	2nd	$\mathbf{\Delta}_0^{\{\sigma q\}}\mathbb{d}_u$
quadrupolar-shielding	2nd	$\mathbf{\Delta}_2^{\{\sigma q\}} \mathbb{d}_u$
quadrupolar-shielding	2nd	$\boldsymbol{\Delta}_{4}^{\{\sigma q\}}\mathbb{d}_{u}$
quadrupolar-weak dipole	2nd	$oldsymbol{\Delta}_0^{\{dq\}}( exttt{dp})_{u,u'}$
quadrupolar-weak dipole	2nd	$\mathbf{\Delta}_2^{\{dq\}}( exttt{dp})_{u,u'}$
quadrupolar-weak dipole	2nd	${f \Delta}_4^{\{dq\}}({ m dp})_{u,u'}$
quadrupolar-weak J	2nd	$\mathbf{\Delta}_0^{\{Jq\}}( exttt{dp})_{u,u'}$
quadrupolar-weak J	2nd	$\mathbf{\Delta}_2^{\{Jq\}}( exttt{dp})_{u,u'}$
quadrupolar-weak J	2nd	$oldsymbol{\Delta}_4^{\{Jq\}}( exttt{dp})_{u,u'}$

TABLE II. Frequency tensor contributions from the first- and second-order perturbation terms. Here, SPT is the static perturbation theory order. The  $\Delta_L^{\{k\}}$  are the  $L^{\rm th}$ -rank frequency-scaled spatial spherical (fsSST) tensor part of the contribution defined in section IIC. The  $\mathbb{p}_u$  and  $\mathbb{d}_u$  are the single-spin transition symmetry functions defined in Eq. (A7). The  $\mathbb{c}_{L,u}$  are the single-spin transition symmetry functions of rank L defined in Eqs. (A5). The  $(\mathbb{pp})_{u,u'}$  and  $(\mathbb{dp})_{u,u'}$  are the two-spin transition symmetry functions defined in Eq. (A8).

### E. Selecting Transition Pathways

In a coupled spin system, it is helpful to define the transition symmetry functions for the channel as

$$\mathbf{p}_c = \sum_{u \in \mathfrak{I}_c} \mathbf{p}_u, \quad \text{and} \quad \mathbf{d}_c = \sum_{u \in \mathfrak{I}_c} \mathbf{d}_u,$$
 (30)

where  $\mathbf{p}_u$  and  $\mathbf{d}_u$  are the transition symmetry functions evaluated on the uth spin, and  $\mathfrak{I}_c$  is the subset of spins in the cth channel. Furthermore, we define the transition symmetry functions for the entire spin system as

$$p_T = \sum_{c=1}^{n_c} p_c$$
, and  $d_T = \sum_{c=1}^{n_c} d_c$ . (31)

While these functions are not used in evaluating frequency contributions, they can be useful for selecting sets of transitions. In designing an experimental NMR pulse sequence, NMR spectroscopists use RF phase cycling to select a set of transition pathways based on the  $p_c$  symmetry pathways. In a numerical simulation of the same NMR pulse sequence, one can select the same transition pathways by retaining only the density matrix elements in each evolution period that follow the desired  $p_c$  symmetry pathways. That is, it is unnecessary to simulate the RF phase cycling used in an experiment when modeling its spectrum.

Identifying a specific transition by its row and column index in a density matrix requires a detailed description of the spin system and how the eigenstates are assigned to the indexes. Alternatively, the transition symmetry functions can identify transitions without such details. For example, a single-spin transition in a spin I > 1/2 nucleus can be identified from its  $\mathbb{p}_u$  and  $\mathbb{d}_u$  values. This is illustrated in Fig. S2 of the Supplementary Material for the transitions of integral and half-integral spin nuclei. Note, for simplifying notation in this section's discussion, we use the integer-scaled transition symmetry functions, defined by Eqs. (A9) and  $(\overline{A10})$ . Among the set of  $p_u = -1$  transitions, a transition will be uniquely identified with a  $d_u$  value that is one of  $d_u = 0, \pm 2, \pm 4, \dots, \pm (2I_u - 1)$  for half-integral spins, or  $d_u = \pm 1, \pm 3, \dots, \pm (2I_u - 1)$  for integral spins. One can also identify whether the nucleus has an integral or half-integral spin by the  $p_u$  and  $d_u$  values of any transition.

As a simple illustration of this approach, consider the four different NMR "methods," in Fig. 2, which are distinguished by their different  $p_u$  and  $d_u$  symmetry pathways. Designing a numerical method to simulate the Hahn echo experiment in Fig. 2A and not the Hahn-solid echo experiment in Fig. 2B, requires selecting the symmetry pathways

$$(\mathbf{p}_{u}, \mathbf{d}_{u}) = \begin{cases} (+1, +1) \xrightarrow{\theta_{2}} (-1, +1), & \text{Hahn Echo} \\ (+1, -1) \xrightarrow{\theta_{2}} (-1, -1). & \end{cases}$$
(32)

As mentioned in the previous section, coherence transfer with  $\Delta d_u = 0$  between the first and second evolution periods can be enforced by using  $\theta_2 = \pi$ . Similarly, designing a numerical method to simulate the solid echo experiment in Fig. 2C and not the solid anti-echo experiment

This is the author's peer reviewed, accepted manuscript. However, the online version of record will be different from this version once it has been copyedited and typeset. PLEASE CITE THIS ARTICLE AS DOI: 10.1063/5.0209887

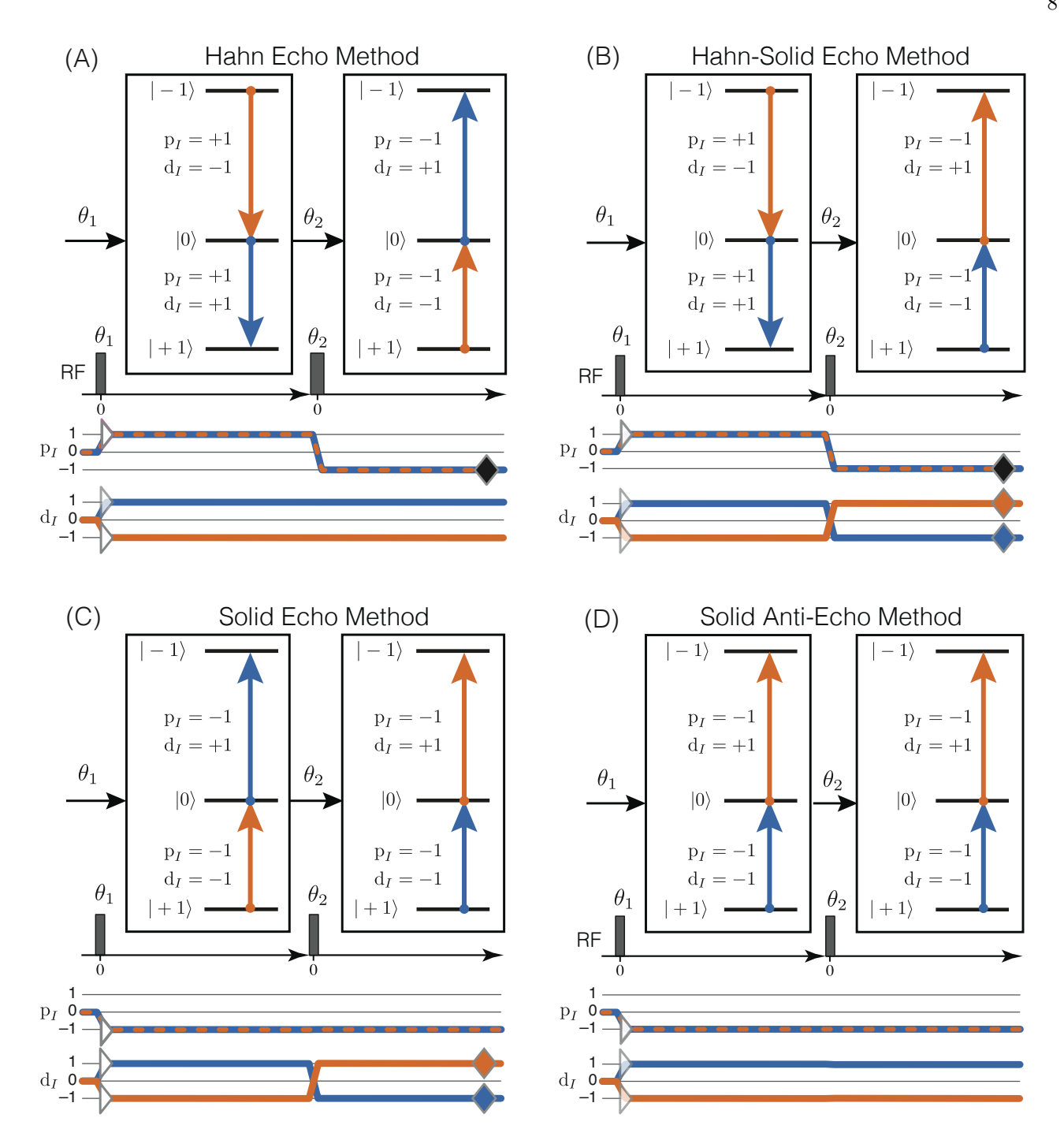


FIG. 2. Two-pulse methods on an I=1 spin system, which are distinguished by their  $p_I$  and  $d_I$  pathways. These are (A) the Hahn echo experiment, (B) the Hahn-solid echo experiment, (C) the solid echo experiment, and (D) the solid anti-echo experiment. A filled diamond represents a contribution to a directly observable echo. An open triangle represents a contribution to an indirectly observable free induction decay.

in Fig. 2D, requires selecting the symmetry pathways

$$(\mathbf{p}_{u}, \mathbf{d}_{u}) = \begin{cases} (-1, +1) \xrightarrow{\theta_{2}} (-1, -1), \\ (-1, -1) \xrightarrow{\theta_{2}} (-1, +1). \end{cases}$$
 Solid Echo (33)

Here, coherence transfer with  $\Delta d_u \neq 0$  between the first

and second evolution periods can be enforced by using  $\theta_2 = \pi/2.$ 

A transition in a multi-site system can also be identified by its transition symmetry function values. For example, one can readily verify that a transition in a two weakly coupled spin 1/2 nuclei (AX) system can be identified by its  $p_A$ ,  $p_X$ ,  $(pp)_{AX}$  values, as illustrated

This is the author's peer reviewed.

in Fig. S3 of the Supplementary Material. This is similarly illustrated in a three weakly coupled spin 1/2 nuclei (AMX) system, where a transition can be identified by its  $\mathbf{p}_A$ ,  $\mathbf{p}_M$ ,  $\mathbf{p}_X$ ,  $(\mathbf{pp})_{AX}$ ,  $(\mathbf{pp})_{AM}$ , and  $(\mathbf{pp})_{MX}$  values, as illustrated in Tables S4, S5 and S6 of the Supplementary Material.

For example, for the subset of nuclei in a given channel,  $u \in \mathfrak{I}_c$ , one can use the channel symmetry function,  $\mathbf{p}_c$ , defined in Eq. (30), to select the subset of single-spin transitions with  $\mathbf{p}_u = -1$  for all nuclei in a channel with the additional constraint that  $\mathbf{p}_c = -1$ , i.e.,

$$p_u = -1 \quad \text{while} \quad p_{u'} = 0 \quad \forall u' \neq u. \tag{34}$$

In another example, the subset of homonuclear three-spin single-quantum transitions in a channel are selected with the constraints that  $\mathbf{p}_c=-1$  and

$$p_u = +1, \quad p_{u'} = -1, \quad p_{u''} = -1,$$
  
while  $p_{u'''} = 0 \quad \forall u''' \neq u, u', u''.$  (35)

One can also identify heteronuclear multi-spin transitions using multiple channels. For example, a two-spin heteronuclear coherence with  $\mathbf{p}_T=-3$  is identified by the transition symmetry functions

$$p_c = -1, \quad p_{c'} = -2, \quad \text{while} \quad p_{c''} = 0, \quad \forall c'' \neq c, c',$$
(36)

and

accepted manuscript. However, the online version of record will be different from this version once it has been copyedited and typeset

PLEASE CITE THIS ARTICLE AS DOI: 10.1063/5.0209887

$$p_u = -1, \quad p_{u'} = -2,$$
  
while  $p_{u''} = 0 \quad \forall u'' \neq u, u', \quad u \in \mathfrak{I}_c, u' \in \mathfrak{I}_{c'}.$  (37)

For coupled nuclei with spin I > 1/2, the  $d_u$  transition symmetry can be employed to distinguish subsets of transitions further.

### F. Transition Pathway Spectrum in a Rotating Solid

The time-dependent frequency for a transition  $\hat{\chi}=|j\rangle\langle i|$  due to rotor modulation in Eq. (25) can be separated into static and rotor-modulated frequency contributions as

$$\Omega_{\chi}(t,i,j) = \sum_{\substack{L=0,2,4\\ m \neq 0}} \left[ \varpi_{L,0}(\theta_R,\alpha,\beta) + \sum_{\substack{m=-L\\ m \neq 0}}^{L} \varpi_{L,m}(\theta_R,\alpha,\beta) e^{-im(\omega_R t + \phi + \gamma)} \right], \quad (38)$$

where

$$\varpi_{L,m}(\theta_R, \alpha, \beta) = d_{m,0}^{(L)}(\theta_R) 
\times \sum_{m'=-L}^{L} e^{-im'\alpha} d_{m',m}^{(L)}(\beta) F_{L,m'}(i,j). \quad (39)$$

Using this expression, we write the accumulated phase of the  $\hat{\chi}$  transition coherence during a free evolution period as given by

$$\Phi(t_1, t_0) = \int_{t_0}^{t_1} \Omega_{\chi}(s) ds = W_{\chi}(\theta_R, \alpha, \beta)(t_1 - t_0) 
+ \sum_{\substack{m = -4 \\ m \neq 0}}^{4} W_{m,\chi}(\theta_R, \alpha, \beta) e^{-im(\gamma + \phi)} \left\{ e^{-im\omega_R t_1} - e^{-im\omega_R t_0} \right\},$$
(40)

where

$$W_{\chi}(\theta_R, \alpha, \beta) = \sum_{L=0,2,4} \varpi_{L,0}(\theta_R, \alpha, \beta), \qquad (41)$$

and

$$W_{m,\chi}(\theta_R, \alpha, \beta) = \sum_{L=2.4} \frac{\varpi_{L,m}(\theta_R, \alpha, \beta)}{im\omega_R}.$$
 (42)

With our theoretical assumptions, the signal for an individual crystallite with orientation  $(\alpha, \beta, \gamma)$  from a transition pathway through n transitions can be written as

$$s(\mathbf{t}, \alpha, \beta, \gamma) = \prod_{\varepsilon=1}^{n} u_{\varepsilon}(t_{\varepsilon}, t_{\varepsilon-1}, \alpha, \beta, \gamma) u_{\varepsilon, \varepsilon-1}(\alpha, \beta, \gamma),$$
(43)

where  $\mathbf{t} = (t_0, t_1, \dots, t_n)$ ,  $u_{\varepsilon, \varepsilon - 1}(\alpha, \beta, \gamma)$  is the complex amplitude of the  $\hat{\chi}_{\varepsilon - 1} \to \hat{\chi}_{\varepsilon}$  coherence transfer, and  $u_{\varepsilon}(t_{\varepsilon}, t_{\varepsilon - 1}, \alpha, \beta, \gamma)$  is the free evolution "propagator" for the  $\hat{\chi}_{\varepsilon}$  transition, given by

$$u_{\varepsilon}(t_{\varepsilon}, t_{\varepsilon-1}) = \sum_{N,N'} A_{\varepsilon}(N) A_{\varepsilon}^{*}(N') e^{i(N'-N)(\gamma+\phi)} \times e^{i(N'-N)\omega_{R}t_{\varepsilon-1}} e^{-i(W_{\varepsilon}+N\omega_{R})\Delta t_{\varepsilon}}.$$
(44)

Here,  $\phi$  is the rotor phase at the beginning of the sequence, and  $A_{\varepsilon}(N)$  is the spinning sideband amplitude. In this and the following expressions, we have dropped the explicit dependences on rotor angle, rotor frequency, and orientation, i.e.,  $A_{\varepsilon}(N_{\varepsilon}) \equiv A_{\varepsilon}(N_{\varepsilon}|\theta_R, \omega_R, \alpha, \beta)$ , and  $W_{\varepsilon} \equiv W_{\varepsilon}(\theta_R, \alpha, \beta)$ .

There is a discrete Fourier relationship between the amplitude of the spinning sideband and the rotor pitch, which is given by

$$A(N) = \frac{1}{2\pi} \int_{-\pi}^{\pi} a(\Phi)e^{iN\Phi}d\Phi. \tag{45}$$

Thus, the sideband amplitude,  $A_{\varepsilon}(N_{\varepsilon})$ , is obtained from

$$a_{\varepsilon}(\Phi) = \exp\left\{-i\sum_{\substack{m=-4\\m\neq 0}}^{4} W_{m,\varepsilon}(\theta_R, \alpha, \beta)e^{im\Phi}\right\}$$
 (46)

PLEASE CITE THIS ARTICLE AS DOI: 10.1063/5.020988

This is the author's peer reviewed.

with respect to  $\Phi$ , the rotor pitch. For a given value of  $\alpha$  and  $\beta$ , this function is numerically evaluated from  $\Phi=0$  to  $2\pi$  with a  $\Delta\Phi$  increment, and Fourier transformed into  $A(N|\alpha,\beta)$ . To avoid aliasing of signals in the sideband order dimension, the  $\Delta\Phi$  increment must be smaller than  $\pi/|N_{\rm band}|$ , where  $|N_{\rm band}|$  is the highest order sideband present in the sideband pattern.

We assume that  $u_{\varepsilon,\varepsilon-1}(\alpha,\beta,\gamma)=u_{\varepsilon,\varepsilon-1}$  are independent of orientation, substitute the above equations in Eq. (43), and perform a partial integration over  $\gamma$ , to obtain the n-dimensional signal from free evolution through n transitions as given by

$$\langle s(\mathbf{t}) \rangle_{\gamma} = \langle s(\mathbf{0}) \rangle_{\gamma} \sum_{N_{1}} \cdots \sum_{N_{n}} \sum_{N'_{2}} \cdots \sum_{N'_{n}} I(\mathbf{N}, \mathbf{N}')$$

$$\times \exp \left\{ -i \sum_{\varepsilon=1}^{n} \left[ W_{\varepsilon} + \left( N_{\varepsilon} - \sum_{\varepsilon' = \varepsilon + 1}^{n} (N'_{\varepsilon'} - N_{\varepsilon'}) \right) \omega_{R} \right] \Delta t_{\varepsilon} \right\},$$
(4)

where 
$$N_1' = N_1 - \sum_{\varepsilon=2}^n (N_\varepsilon' - N_\varepsilon)$$
, and

$$I(\mathbf{N}, \mathbf{N}') = 2\pi \prod_{\varepsilon=1}^{n} A_{\varepsilon}(N_{\varepsilon}|\theta_{R}, \omega_{R}) A_{\varepsilon}^{*}(N_{\varepsilon}'|\theta_{R}, \omega_{R}), \quad (48)$$

with 
$$\mathbf{N} = (N_1, N_2, \dots, N_n)$$
 and  $\mathbf{N}' = (N_1', N_2', \dots, N_n')$ .

The total number of free evolution events (i.e., delay and spectral events) is given by  $n = \sum_{v=1}^{n_{\text{dim}}} (n_v^{\text{de}} + n_v^{\text{se}})$ . The free evolution events, ordered by time and indexed by  $\varepsilon = 1 \dots n$ , are partitioned into disjoint subsets of delay events,  $\mathfrak{D}_1, \mathfrak{D}_2, \dots, \mathfrak{D}_{n_{\text{dim}}}$  and spectral events,  $\mathfrak{S}_1, \mathfrak{S}_2, \dots, \mathfrak{S}_{n_{\text{dim}}}$ . The total number of mixing events is given by  $m = \sum_{v=1}^{n_{\text{dim}}} n_v^{\text{mx}}$ , and are similarly ordered by time and indexed by  $\mu = 1 \dots m$ . We assume that mixing events occur instantaneously, with no rotor phase advance and no free evolution of transitions. Furthermore, we assume that mixing events are independent of  $\alpha$ ,  $\beta$ , and  $\gamma$ , and thus define

$$\langle s(\mathbf{0}) \rangle_{\gamma} = \prod_{j=1}^{n} u_{j,j-1} = \prod_{\mu=1}^{m} u_{\mu}.$$
 (49)

Reexpressing Eq. (47) in terms of delay and spectral event durations and taking the  $n_{\rm dim}$ -dimensional Fourier transform with respect to  $\Delta t$  gives

$$\langle s(\boldsymbol{\omega}, \boldsymbol{\tau}) \rangle_{\gamma} = \langle s(\mathbf{0}) \rangle_{\gamma} \sum_{N_{1}} \cdots \sum_{N_{n}} \sum_{N_{2}'} \cdots \sum_{N_{n}'} I(\mathbf{N}, \mathbf{N}') \exp \left\{ -i \sum_{\mathbf{v}=1}^{n_{\text{dim}}} \sum_{\varepsilon \in \mathfrak{D}_{\mathbf{v}}} \left( W_{\varepsilon} - \left( N_{\varepsilon} - \sum_{\varepsilon'=\varepsilon+1}^{n} (N_{\varepsilon'}' - N_{\varepsilon'}) \right) \omega_{R} \right) \tau_{\varepsilon} \right\}$$

$$\times \prod_{\mathbf{v}=1}^{n_{\text{dim}}} \delta \left( \sum_{\varepsilon \in \mathfrak{S}_{\mathbf{v}}} \left( x_{\varepsilon} W_{\varepsilon} - \left( N_{\varepsilon} - \sum_{\varepsilon'=\varepsilon+1}^{n} (N_{\varepsilon'}' - N_{\varepsilon'}) \right) x_{\varepsilon} \omega_{R} \right) - \omega_{\mathbf{v}} \right), \quad (50)$$

where  $\boldsymbol{\omega}=(\omega_1,\ldots,\omega_{n_{\mathrm{dim}}})$  and  $x_\varepsilon$  is assigned to the corresponding fraction  $x_{\mathrm{v},k}$  for the  $k^{\mathrm{th}}$  propagator in the v<sup>th</sup> spectral dimension. Only a numerical integration over the angles  $\alpha$  and  $\beta$  remains to obtain the transition pathway spectrum from a polycrystalline sample. From Eq. (50), one also sees for evolution periods divided among multiple spectral events that a complex sideband pattern can emerge with sidebands flanking the centerband at non-integer multiples of the rotor frequency, depending on the values of  $x_\varepsilon$ .

### G. Numerical integration over polycrystalline orientations

An n-dimensional anisotropic NMR spectrum of a polycrystalline sample is obtained by the integral

$$\langle s(\boldsymbol{\nu}) \rangle = \int_{U} \langle s(\boldsymbol{\nu}, \alpha, \beta) \rangle_{\gamma} d\sigma,$$
 (51)

where U is the unit sphere in  $\mathbb{R}^3$  and  $\boldsymbol{\nu} = \boldsymbol{\omega}/(2\pi)$ . This integral is approximated using a finite element integration,

$$\langle s(\boldsymbol{\nu}) \rangle = \sum_{r=1}^{M_{\Delta}} \int_{\Delta_r} \langle s(\boldsymbol{\nu}, \alpha, \beta) \rangle_{\gamma} d\sigma_r = \sum_{r=1}^{M_{\Delta}} s_{\Delta_r}(\boldsymbol{\nu}), \quad (52)$$

where  $\{\Delta_1, \ldots, \Delta_{M_{\Delta}}\}$  is a triangulation of U into  $M_{\Delta}$  triangles with vertices

$$\Delta_r = \{\vec{e}_{r,A}, \vec{e}_{r,B}, \vec{e}_{r,C}\} = \{(\alpha_{r,A}, \beta_{r,A}), (\alpha_{r,B}, \beta_{r,B}), (\alpha_{r,C}, \beta_{r,C})\}, \quad (53)$$

and  $s_{\Delta_r}(\boldsymbol{\nu})$  is the spectrum obtained after integration over the solid angle of the  $r^{\rm th}$  finite element.

As described by Alderman, Solum, and Grant (ASG)<sup>20</sup>, the triangulation of U is approximated by first inscribing an octahedron inside a unit sphere. The equilateral triangle faces of the octahedron are further triangulated into  $M_{\Delta}=\mathfrak{N}^2$  equilateral triangles as illustrated

This is the author's peer reviewed, accepted manuscript. However, the online version of record will be different from this version once it has been copyedited and typeset

PLEASE CITE THIS ARTICLE AS DOI: 10.1063/5.0209887

in Fig. 3 of the ASG paper<sup>20</sup>. The total number of orientations,  $N_{\Theta}$ , is defined as,

$$N_{\Theta} = \mathcal{F}(\mathfrak{N}+1)(\mathfrak{N}+2)/2,\tag{54}$$

where  $\mathcal{F}$  is the number of octant faces.

In a one-dimensional anisotropic spectrum, the frequencies and amplitudes evaluated at the three vertices of a triangle are denoted as  $(f_A, a_A)$ ,  $(f_B, a_B)$ ,  $(f_C, a_C)$ . For this case, ASG<sup>[20]</sup> developed a finite element interpolation algorithm. In this approach, the frequencies are labeled in ascending order and assigned to  $f_{\min}$ ,  $f_{\min}$ , and  $f_{\max}$ , respectively, and the finite element spectrum is approximated as

$$s_{\Delta_r}(\nu) = f(a_A, a_B, a_c, \Delta_r) \operatorname{tri}(\nu, f_{\min}, f_{\min}, f_{\max}), \quad (55)$$

where  $tri(\nu, f_{min}, f_{mid}, f_{max})$  is a normalized triangular distribution function given by

$$\begin{split} & \operatorname{tri}(\nu, f_{\min}, f_{\operatorname{mid}}, f_{\max}) = \frac{2}{(f_{\max} - f_{\min})} \\ & \times \begin{cases} (\nu - f_{\min})/(f_{\operatorname{mid}} - f_{\min}), & f_{\min} \leq \nu < f_{\operatorname{mid}}, \\ (f_{\max} - \nu)/(f_{\max} - f_{\operatorname{mid}}), & f_{\min} \leq \nu < f_{\max}, \\ 0, & \text{otherwise.} \end{cases} \tag{56} \end{split}$$

and  $f(a_A, a_B, a_c, \Delta_r)$  is a scaling factor that accounts for the area of the planar triangle projected onto the surface of the sphere. The triangular line shape assumes that the transition frequencies vary linearly across the triangle's surface and that the differences in amplitude at the vertices are minor. This approximation becomes valid in the limit of large  $M_{\Delta}$ .

Recently, Srivastava et al. developed an algorithm for the finite element integration of 2D NMR spectra correlating dimensions with anisotropic frequency contributions. In the finite-element integration of a 2D spectrum, the correlated frequency pairs and amplitudes evaluated at the three vertices of a triangle are  $(f_{1A}, f_{2A}, a_A)$ ,  $(f_{1B}, f_{2B}, a_B)$ ,  $(f_{1C}, f_{2C}, a_C)$ . In this approach, the 2D spectrum is obtained by applying the ASG 1D algorithm to each one-dimensional cross-section, represented as the sum of two triangular line shapes. This algorithm can be used for the finite element integration of 2D spectra. It is possible to extend the approach of Srivastava et al. to higher dimensional NMR spectra correlating anisotropic dimension.

### H. Affine Transformation of Spectrum

The ability to refocus different spatial and transition symmetries into echoes with different paths in time-resolved NMR experiments creates opportunities for generating multi-dimensional spectra that correlate different interactions. These spectra can be made easier to interpret through similarity transformations. Most similarity transformations in NMR are affine transformations, as

they preserve the colinearity of points and ratios of distances. An active affine transformation of the signal can be performed according to

$$S(\boldsymbol{\omega}') = S(\boldsymbol{\mathcal{A}}\,\boldsymbol{\omega}),\tag{57}$$

where  $\mathcal{A}$  is a  $n_{\text{dim}} \times n_{\text{dim}}$  matrix representing the affine transformation. In some cases, simulating  $S(\boldsymbol{\omega})$  and obtaining  $S(\boldsymbol{\omega}')$  through application of the affine transformation in Eq. (57) can reduce the number of spectral event propagators that would have been needed to simulate  $S(\boldsymbol{\omega}')$  directly.

### III. RESULTS AND DISCUSSION

A major motivation for the approach presented here is to provide a theoretical framework for rapidly simulating one- and higher-dimensional NMR spectra of complex materials in the solid state, i.e., structurally disordered, amorphous, and heterogenous samples. Depending on the NMR method and the relative sizes of the different interaction tensors, the nuclear spin network of the material's full structure can often be described by a distribution of smaller spin subsystems, each described by a set of interaction tensor parameters,  $\mathbf{R}$ . This set of reduced spin subsystems can be used to generate a subspectra basis,  $\mathcal{K}(\omega, \mathbf{R})$ , for a given NMR method. Taken together with the spin subsystem populations,  $f(\mathbf{R})$ , the predicted spectrum,  $S(\omega)$ , is given by

$$S(\omega) = \int_{\mathbf{R}} f(\mathbf{R}) \, \mathcal{K}(\omega, \mathbf{R}) \, d\mathbf{r}. \tag{58}$$

The spin subsystem populations,  $f(\mathbf{R})$ , are often obtained from a structural hypothesis for the material, such as a molecular cluster model, a crystallographic model, or a molecular dynamics (MD) simulation. Alternatively, with a limited number of parameters in  $\mathbf{R}$ , it is possible to perform a direct inversion of the spectrum to obtain  $f(\mathbf{R})$ . In either case, it is essential to have efficient numerical algorithms for the simulation of large subspectra bases,  $\mathcal{K}(\omega, \mathbf{R})$ , for the NMR method from the desired transition pathways of the spin subsystem.

To demonstrate the significance of our approach for such purposes, we present a few examples of spectra predicted using the Czjzek and extended-Czjzek tensor parameter distributions for  $f(\mathbf{R})$ . The Czjzek distribution originally developed to model random distributions of electric field gradient (EFG) tensors in glasses—is a general model for simulating anisotropic line shapes arising from a random distribution of second-rank NMR tensors deviating from a mean anisotropy of zero.

PLEASE CITE THIS ARTICLE AS DOI: 10.1063/5.0209887

This is the author's peer reviewed.

It is given by

$$f(\zeta, \eta | \sigma_{\zeta}) = \frac{\zeta^{4} \eta}{\sqrt{2\pi} \sigma_{\zeta}^{5}} \left( 1 - \frac{\eta^{2}}{9} \right)$$

$$\times \exp \left\{ -\frac{\zeta^{2} \left( 1 + \frac{\eta^{2}}{3} \right)}{2\sigma_{\zeta}^{2}} \right\}, \quad (59)$$

where  $\zeta$  and  $\eta$  are the two independent parameters of the second-rank traceless symmetric tensor, and  $\sigma_{\zeta}$  is the width parameter. The Czjzek distribution assumes uncorrelated Gaussian distributions of second-rank spherical tensor components with a single width parameter. See the recent work of Werner-Zwanziger et al. [53] for its mathematical derivation and more illustrative experimental examples.

In modeling the magic-angle spinning spectrum from a sample with a Czjzek distribution of 2nd-rank tensors, we further assume an uncorrelated Gaussian distribution of isotropic chemical shifts,  $\delta_{\rm cs}^{\rm iso}$ ,

$$f(\delta_{\rm cs}^{\rm iso}|\delta_0, \sigma_\delta) = \frac{1}{\sqrt{2\pi}\sigma_\delta} \exp\left\{-\frac{(\delta_{\rm cs}^{\rm iso} - \delta_0)^2}{2\sigma_\delta^2}\right\}, \quad (60)$$

where  $\delta_0$  is the mean isotropic chemical shift, and  $\sigma_{\delta}$  is the standard deviation of the isotropic chemical shift. Taken together, the full distribution of spin system parameters is given by

$$f(\delta_{\rm cs}^{\rm iso}, \zeta, \eta | \sigma_{\zeta}, \delta_{0}, \sigma_{\delta}) = f(\zeta, \eta | \sigma_{\zeta}) f(\delta_{\rm cs}^{\rm iso} | \delta_{0}, \sigma_{\delta}).$$
 (61)

The distribution in Eq. (61) is often used when modeling the distribution of EFG tensors of tetrahedrally and octahedrally coordinated aluminum sites in oxide glasses. <sup>54</sup> An example of such a distribution is illustrated in Fig. 3. In presenting this distribution, we have reparameterized the  $C_q$  and  $\eta_q$  coordinate values onto the more numerically stable grid of  $x_q$  and  $y_q$  coordinates, following Srivastava et al. Further details on the  $x_q$  and  $y_q$  definitions are given in the Supplementary Material. From this distribution, the spin interaction parameters for  $N_{\rm sys}=3\,667$  unique spin systems for <sup>27</sup>Al are extracted, i.e., only those whose probability exceeds a minimum threshold of 0.1% are accepted. This spin system set is used to simulate the <sup>27</sup>Al MAS spectrum presented in Fig. 4A, following the numerical approach outlined in the previous section. The spectrum of each spin system is numerically integrated and interpolated over  $M_{\Delta} = 4\,900$  triangular elements, i.e.,  $\mathfrak{N} = 70$  in section  $\overline{\mathbf{IIG}}$ . The full simulation, required  $N_{\Theta} \times 2N_{\text{band}} \times N_{\text{sys}} = (2556)(8)(3667) = 74,982,816 \text{ fre-}$ quency and amplitude calculations, and was completed in 2.5 s on a laptop computer (Apple MacBook Air, 3.49) GHz M2 processor with eight cores and 24 GB RAM).

Using the same set of spin systems, we also simulate the <sup>27</sup>Al 3Q-MAS NMR correlation spectrum of an amorphous sample, presented in Fig. 4B, using our numerical

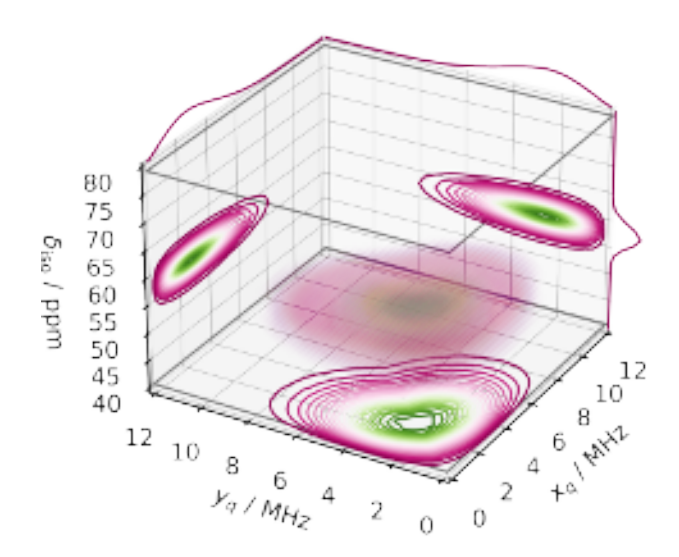


FIG. 3. The 3D probability distribution of <sup>27</sup>Al spin system parameters,  $\mathbf{R} = (\delta_{\mathrm{cs}}^{\mathrm{iso}}, x_q, y_q)$ , obtained from Eqs. (59), (60), and (61). The second-rank EFG tensor anisotropy parameters  $x_q$  and  $y_q$  are distributed according to the Czjzek distribution with a width parameter of  $\sigma_{C_q} = 2.5$  MHz (see Eq. S343 in the Supplementary Material). The isotropic chemical shift parameter,  $\delta_{\mathrm{cs}}^{\mathrm{iso}}$ , is distributed normally with a mean of  $\delta_0 = 58$  ppm and a standard deviation of  $\sigma_\delta = 2$  ppm. From this 3D distribution, the spin interaction parameters of unique spin systems are extracted and used for the simulations presented in Fig. [4]

approach. This simulation required 3.2 s on the same laptop computer. We present this simulation with the caveat that it assumes a uniform excitation and mixing of triple-quantum transitions for all crystallite orientations. Thus, it gives an approximate representation of the distribution of 3Q-MAS NMR spectral amplitudes. While this is a consequence of Assumption III, it is not a strict limitation, and our approach could be adapted to include the effects of non-uniform excitation and mixing of transitions.

Another example of a spin system distribution for modeling disorder in materials is the extended-Czjzek distribution. The extended-Czjzek distribution is a generalization of the Czjzek distribution and is given by

$$\mathbf{S}_T = \mathbf{S}(0) + \rho \mathbf{S}_c(\sigma_c = 1), \tag{62}$$

where  $\mathbf{S}_T$  is the total tensor,  $\mathbf{S}(0)$  is the dominant tensor,  $\mathbf{S}_c(\sigma_c = 1)$  is the Czjzek random model attributing to the random perturbation of the tensor about the dominant tensor,  $\mathbf{S}(0)$ . Here  $\sigma_c$  is not the Czjzek width from Eq. (60) but the standard deviation of the underlying 5D multi-variate normal distribution. In the extended-Czjzek distribution, the size of the random perturbations

accepted manuscript. However, the online version of record will be different from this version once it has been copyedited and typeset This is the author's peer reviewed.

PLEASE CITE THIS ARTICLE AS DOI: 10.1063/5.0209887

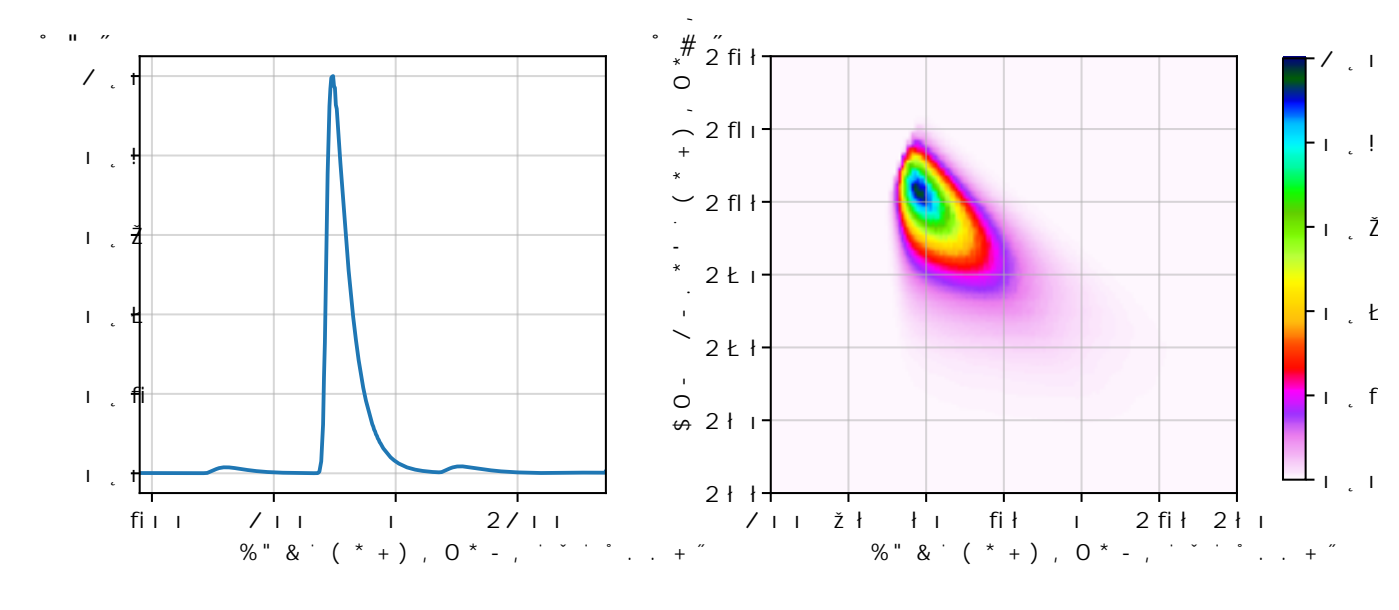


FIG. 4. (A) Simulation of an  $^{27}$ Al NMR spectrum at  $B_0=9.4\,\mathrm{T}$  undergoing magic-angle spinning at  $\omega_R/(2\pi)=10\,\mathrm{kHz}$ . The spectrum is simulated from  $N_{\mathrm{sys}}=3\,667$  spin systems with the distribution of  $x_q,\,y_q,\,$  and  $\delta_{\mathrm{cs}}^{\mathrm{iso}},\,$  shown in Fig. 3. No additional convolutional broadening was applied to the spectrum. The total computation time was 2.56 s. (B) Simulation of the  $^{27}$ Al 3Q-MAS NMR correlation spectrum at  $B_0=9.4\,\mathrm{T},\,$  assuming an infinite spinning speed. The spectrum is simulated from 3,667 spin systems with the distribution shown in Fig. 3. For each orientation, two correlated frequencies and one sideband amplitude were calculated. The spectrum of each spin system is numerically integrated and interpolated over  $M_\Delta=4\,900$  triangular elements, i.e.,  $\mathfrak{N}=70$ . This was repeated for each of the 3 667 unique spin systems. The total computation time was 3.2 s. No additional convolutional broadening was applied to the spectrum. Note this 3Q-MAS simulation assumes uniform excitation and mixing of triple-quantum coherence for all crystallite orientations.

is determined by the factor  $\rho$ , given by

$$\rho = \frac{||\mathbf{S}(0)||\epsilon}{\sqrt{30}},\tag{63}$$

where  $||\mathbf{S}(0)||$  is the 2-norm of the dominant tensor, and  $\epsilon$  is a fraction. Further details on the numerical implementation of the extended-Czjzek distribution are given in Appendix  $\boxed{\mathbf{B}}$ .

An example of an extended Czjzek distribution is illustrated in Fig. 5A for the case of a <sup>29</sup>Si sites with dominant nuclear shielding tensor parameters of  $\zeta_{\sigma} = 80 \text{ ppm}$  and  $\eta_{\sigma} = 0.15 \text{ ppm}$  and an extended Czjzek perturbation fraction of  $\epsilon = 0.125$ . In presenting this distribution, we have similarly reparameterized the  $\zeta_{\sigma}$  and  $\eta_{\sigma}$  coordinate values in terms of  $x_{\sigma}$  and  $y_{\sigma}$  coordinates. In this example, we also assume an uncorrelated Gaussian distribution of isotropic chemical shifts. However, instead of creating a 3D probability distribution using Eq. (61), it is more efficient to model the isotropic chemical shift through a Gaussian convolution of the MAS spectrum simulated using the mean isotropic chemical shift. In this example, the isotropic chemical shift parameter,  $\delta_{cs}^{iso}$ , is distributed normally with a mean of  $\delta_0 = -100$  ppm and a standard deviation of  $\sigma_{\delta} = 2$  ppm. From the distribution in Fig. 5A, the spin interaction parameters for  $N_{\text{sys}} = 382$ unique spin systems are extracted and used to simulate the <sup>29</sup>Si MAS spectrum presented in Fig. 5B. As before, the spectrum of each spin system is numerically integrated and interpolated over  $M_{\Delta}=4\,900$  triangular elements ( $\mathfrak{N}=70$ ). The full simulation, required  $N_{\Theta}\times 2N_{\rm band}\times N_{\rm sys}=(2\,556)(20)(382)=19,527,840$  frequency and amplitude calculations, and was completed 543 ms on the same laptop computer as the previous simulations.

Finally, to illustrate a two-dimensional frequencydomain simulation of correlated spinning sidebands, we examine the 2D Phase Adjusted Spinning Sideband 56-60 (PASS) spectrum of a  ${}^{2}$ H (I=1) nucleus. As shown by Aleksis et al. 61, when applied to a spin I=1 system, a 2D PASS spectrum can be sheared to produce a correlation of spinning sidebands produced by pure shift anisotropy to those produced by first-order quadrupolar frequency anisotropy. Additional details on the simulation of the 2D-PASS sequence and its application to spin I=1 systems are given in Section S8 of the Supplementary Material. Using the expressions of Section IIF, a series of 2D PASS spectra, shown in Fig. 6, were simulated for a <sup>2</sup>H nucleus with  $C_q = 50 \text{ kHz}$ ,  $\eta_q = 0.9 \text{ and}$  $\zeta_{\sigma} = 150 \text{ ppm}$  and  $\eta_{\sigma} = 0.7$  at various relative orientations of the shielding to EFG tensor while spinning at  $\omega_R/(2\pi) = 2$  kHz. Each simulation was completed in approximately 50 ms on the same laptop computer as the previous simulations. These spectra agree with the density matrix simulations of the 2D PASS sequence presented in Fig. S9 of the Supplementary Material.

This is the author's peer reviewed, accepted manuscript. However, the online version of record will be different from this version once it has been copyedited and typeset

PLEASE CITE THIS ARTICLE AS DOI: 10.1063/5.0209887

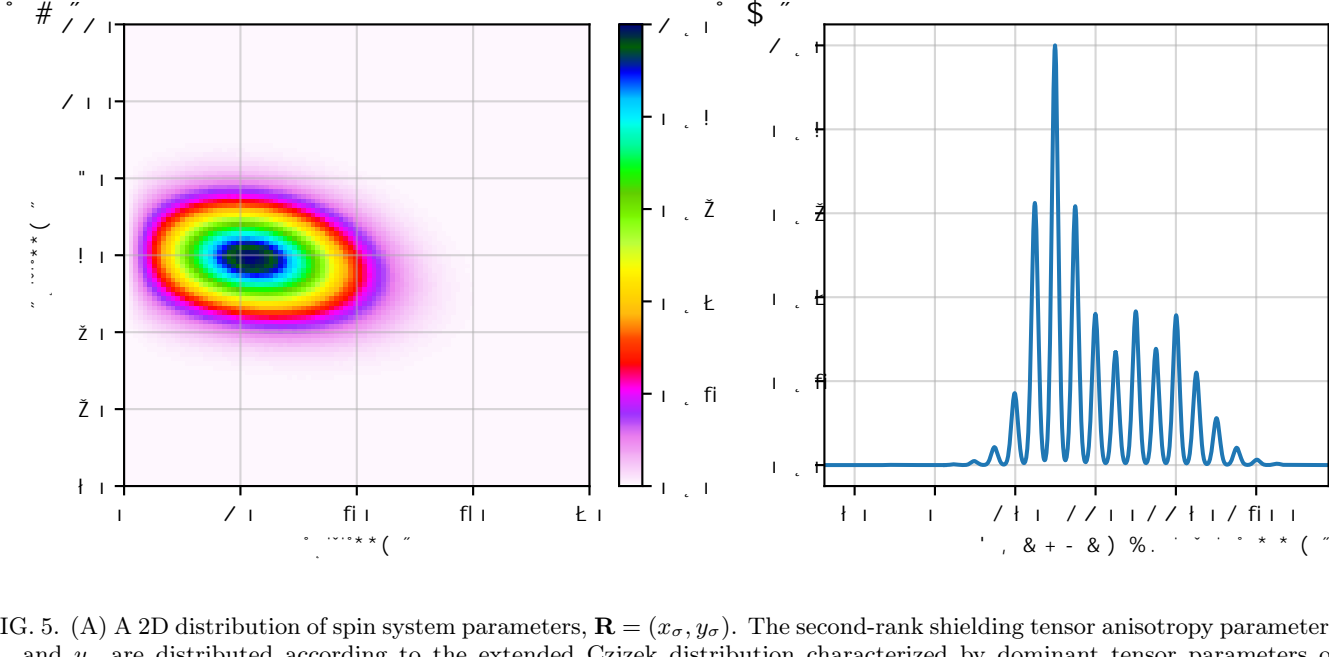


FIG. 5. (A) A 2D distribution of spin system parameters,  $\mathbf{R} = (x_{\sigma}, y_{\sigma})$ . The second-rank shielding tensor anisotropy parameters  $x_{\sigma}$  and  $y_{\sigma}$  are distributed according to the extended Czjzek distribution characterized by dominant tensor parameters of  $\zeta_{\sigma}=80~\mathrm{ppm}$  and  $\eta_{\sigma}=0.15~\mathrm{ppm}$  and a perturbation fraction of  $\epsilon=0.125$ . (B) Simulation of an <sup>29</sup>Si NMR spectrum at  $B_0 = 9.4 \,\mathrm{T}$  undergoing magic-angle spinning at  $\omega_R/(2\pi) = 1 \,\mathrm{kHz}$ . The spectrum is simulated from  $N_{\mathrm{sys}} = 382 \,\mathrm{spin}$  systems with the distribution of nuclear shielding tensor parameters shown in (A). The isotropic chemical shift parameter,  $\delta_{cs}^{iso}$ , is distributed normally with a mean of  $\delta_0 = -100$  ppm and a standard deviation of  $\sigma_{\delta} = 2$  ppm. It is modeled using a Gaussian convolution of the simulated spectrum. For each orientation, a single frequency and  $2N_{\rm band}=20$  sideband amplitudes were calculated. The spectrum of each spin system is numerically integrated and interpolated over  $M_{\Delta} = 4\,900$  triangular elements, i.e.,  $\mathfrak{N} = 70$ . The total computation time was 543 ms.

### IV. SUMMARY

We have outlined a theoretical approach supporting algorithms for the frequency domain simulation of multipulse multi-dimensional NMR spectra of polycrystalline solids. While this approach relies on a set of theoretical assumptions common to many solid-state NMR density matrix simulations, such as the high-field approximation and the neglect of relaxation processes, it gains significant computational efficiency by further assuming that there are no degeneracies in the energy eigenstates, i.e., all dipolar couplings are in the weak limit and that there are no rotational resonances during evolution periods. Under these assumptions, the symmetry pathway formalism<sup>28</sup> is exploited to reduce an NMR method applied to a spin system into a sum of individual transition pathways, whose signals are more efficiently calculated individually than as part of a full-density matrix simula-

To increase numerical efficiencies further, our approach restricts coherence transfer among transitions to pure rotations about an axis in the x-y plane of the rotating frame or through an artificial total mixing operation between selected transitions of adjacent free evolution periods. The assumptions used in this approach are valid for most commonly used solid-state NMR methods. While a more general treatment of the spin system's evolution

during mixing periods is possible, it would require a more sophisticated treatment and come at the cost of increased numerical complexity and reduced numerical efficiencies.

The algorithms outlined here have been incorporated into MRSimulator, an open-source Python package for simulating multi-dimensional NMR spectra of polycrystalline solids and will be described elsewhere. MRSimulator is also used in the open-source Python package, MRInversion, 50 for the linear inversion of experimental NMR spectra of amorphous samples. Examples of the linear inversion of experimental NMR spectra of amorphous samples using the algorithms described here can be found in Srivastava et al. 50.

### **ACKNOWLEDGEMENTS**

This material is based upon work supported by the Chemical Measurement and Imaging program in the National Science Foundation Division of Chemistry under Grant No. CHE-2107636 (with partial co-funding from the Ceramics program in the Division of Materials Research). P.J.G. also acknowledges support from the Fulbright Scholar Program, sponsored by the U.S. Department of State, the U.S.-Italy Fulbright Commission, and the Centro Risonanze Magnetiche, Universitá degli Studi, Firenze.

PLEASE CITE THIS ARTICLE AS DOI: 10.1063/5.020988

This is the author's peer reviewed.

### °! ž/~″!/~į!/ °! Ł/ ` ″! / ` ॄ! / ) Ł/ 3753 ) fl/ fi / . 4 . 4 fi/ -l #. fl/ °!/~″! Ž/~ ॄ! ž/ °!/~″! ž/~ ॄ! ž/ Ł/ ო -3753 fl/ fi / . 4 0 4 $\alpha$ . fi/ \_ fl/ °! ž/ ~ ″! ž/ ~ į! Ł/ °! ž/`″! ž/`ृ! Ž/ °! ž/`″! ž/`ॄ! ž/ Ł/ ) fl/ 375; fi / 9 ~ fi/ fl/ ) fl+)+/+/ fl+ / ) fl+)+/+/ fl+ / ) fl+)+/+/ fl+

FIG. 6. Simulation of the 2D PASS spectra for a  $^2$ H nucleus at  $B_0 = 9.395$  T with  $C_q = 50$  kHz,  $\eta_q = 0.9$  and  $\zeta_{\sigma} = 150$  ppm and  $\eta_{\sigma} = 0.7$  for various relative orientations of the shielding to EFG tensor while spinning at  $\omega_R/(2\pi) = 2$  kHz, in agreement with the full density matrix simulations in Fig. [S9]. These simulations employ the two transition pathways  $|-1\rangle\langle 0| \to |-1\rangle\langle 0|$  and  $|0\rangle \langle +1| \rightarrow |0\rangle \langle +1|$ , which map to the transition symmetry pathways  $p_I = -1 \rightarrow -1$  and  $d_I = \pm 1 \rightarrow \pm 1$ . For each orientation, a single frequency and  $2N_{\rm band}=64$  sideband amplitudes were calculated. The spectrum of each spin system is numerically integrated over 377 orientations. Each simulation was completed in approximately 50 ms.

### SUPPLEMENTARY MATERIAL

The supplementary material presents the derivations, definitions, and conventions supporting the expressions given in the main text. Additionally, Python scripts for simulating the figures in section III are provided.

### CODE AND DATA AVAILABILITY STATEMENT

The open-source Python package, MRSimulafor implementing the algorithms described here along with documentation for its installation and use, is made available in GitHub at https://github.com/deepanshs/mrsimulator. The MRSimulator, documentation for available

https://mrsimulator.readthedocs.io also includes example scripts for obtaining simulations and least-squares analyses of experimental datasets presented in this work, as well as numerous other examples.

### Appendix A: Spin Transition Symmetry Functions

The spin transition symmetry functions, 28 arising from the irreducible spherical tensor operators,  $\hat{T}_{\ell,0}$ , are given by

$$\xi_{\ell}(i,j) = \langle j|\hat{T}_{\ell,0}|j\rangle - \langle i|\hat{T}_{\ell,0}|i\rangle. \tag{A1}$$

Besides their use in calculating transition frequency contributions, these functions help identify the transition pathways in a spin-system agnostic manner. They also

# accepted manuscript. However, the online version of record will be different from this version once it has been copyedited and typeset This is the author's peer reviewed,

PLEASE CITE THIS ARTICLE AS DOI: 10.1063/5.0209887

aid in pulse sequence design by identifying how different frequency contributions refocus through the transition pathways. We emphasize spin transition function symmetries by replacing the symbol  $\xi_{\ell}(i,j)$  for irreducible spherical tensor operators of rank  $\ell=1,2,3,\ldots$  with the lower-case symbols  $\mathfrak{p}(i,j), \mathfrak{d}(i,j), \mathfrak{f}(i,j),\ldots$ , i.e., we follow the spectroscopic sub-shell letter designations. The  $\ell=0$  function is dropped as it evaluates to zero.

For a single spin, I, a complete set of spin-transition symmetry functions is defined up to  $\ell=2I$ . In the case of a single spin system,  $\{I\}$ , the first three integer-scaled transition symmetry functions evaluate to

$$p_I(m_i, m_j) = m_j - m_i, \tag{A2}$$

$$d_I(m_i, m_j) = \sqrt{\frac{3}{2}} (m_j^2 - m_i^2),$$
 (A3)

$$f_I(m_i, m_j) = \frac{1}{\sqrt{10}} \left[ 5(m_j^3 - m_i^3) + (1 - 3I(I+1))(m_j - m_i) \right].$$
 (A4)

For 2nd-order quadrupolar coupling frequency contributions, it is convenient to define "hybrid" spin transition functions as linear combinations of the spin transition functions

$$c_0 = \frac{4}{\sqrt{125}} [I(I+1) - 3/4] \, \mathbb{p}_I + \sqrt{\frac{18}{25}} \, \mathbb{f}_I,$$

$$c_2 = \frac{2}{\sqrt{175}} [I(I+1) - 3/4] \, \mathbb{p}_I - \frac{6}{\sqrt{35}} \, \mathbb{f}_I,$$

$$c_4 = -\frac{184}{\sqrt{875}} [I(I+1) - 3/4] \, \mathbb{p}_I - \frac{17}{\sqrt{175}} \, \mathbb{f}_I.$$
(A5)

For  $n_{\mathcal{I}}$  weakly coupled nuclei, we define the transition symmetry functions

$$\xi_{\ell_1,\ell_2,\dots,\ell_{n_{\mathcal{I}}}}(i,j) = \langle j | \hat{T}_{\ell_1,0}(\vec{I}_1) \, \hat{T}_{\ell_2,0}(\vec{I}_2) \, \dots \, \hat{T}_{\ell_n,0}(\vec{I}_{n_{\mathcal{I}}}) \, | j \rangle - \langle i | \, \hat{T}_{\ell_1,0}(\vec{I}_1) \, \hat{T}_{\ell_2,0}(\vec{I}_2) \, \dots \, \hat{T}_{\ell_n,0}(\vec{I}_{n_{\mathcal{I}}}) \, | i \rangle . \quad (A6)$$

Replacing the symmetry function symbol using sub-shell letter designations becomes more cumbersome in this case. When the  $\ell$  values are zero on all nuclei except one, we identify these single-spin functions as

$$\mathbb{p}_{1} = \xi_{1,0,\dots,0}(i,j), \quad \mathbb{p}_{2} = \xi_{0,1,\dots,0}(i,j), \quad \dots, \quad \mathbb{p}_{n_{\mathcal{I}}} = \xi_{0,0,\dots,1}(i,j), 
d_{1} = \xi_{2,0,\dots,0}(i,j), \quad d_{2} = \xi_{0,2,\dots,0}(i,j), \quad \dots, \quad d_{n_{\mathcal{I}}} = \xi_{0,0,\dots,2}(i,j), 
f_{1} = \xi_{3,0,\dots,0}(i,j), \quad f_{2} = \xi_{0,3,\dots,0}(i,j), \quad \dots, \quad f_{n_{\mathcal{I}}} = \xi_{0,0,\dots,3}(i,j), 
\vdots \qquad \vdots \qquad \vdots \qquad \vdots$$
(A7)

When the  $\ell$  values are zero on all nuclei except two,

then we identify these two-spin functions using a concatenation of sub-shell letter designations, e.g.,

$$(\mathbb{pp})_{1,2} = \xi_{1,1,0,\dots,0}(i,j), \quad (\mathbb{pp})_{1,3} = \xi_{1,0,1,\dots,0}(i,j), \quad \dots, \quad (\mathbb{pp})_{1,n_{\mathcal{I}}} = \xi_{1,0,0,\dots,1}(i,j),$$
 
$$(\mathbb{pd})_{1,2} = \xi_{1,2,0,\dots,0}(i,j), \quad (\mathbb{pd})_{1,3} = \xi_{1,0,2,\dots,0}(i,j), \quad \dots, \quad (\mathbb{pd})_{1,n_{\mathcal{I}}} = \xi_{1,0,\dots,2}(i,j),$$
 
$$(\mathbb{dp})_{1,2} = \xi_{2,1,0,\dots,0}(i,j), \quad (\mathbb{dp})_{1,3} = \xi_{2,0,1,\dots,0}(i,j), \quad \dots, \quad (\mathbb{dp})_{1,n_{\mathcal{I}}} = \xi_{2,0,\dots,1}(i,j),$$
 
$$\vdots \qquad \qquad \vdots \qquad \qquad \vdots$$

Two-spin functions are needed for frequency contributions arising from cross-terms involving dipolar couplings in a second-order perturbation theory treatment of a sizeable quadrupolar coupling. Three- or higher-spin functions occur in higher-order perturbation theory crossterms, which are not considered here.

For the sole purpose of simplifying notation in discussions and figures, we scale the single-spin transition sym-

(A11)

accepted manuscript. However, the online version of record will be different from this version once it has been copyedited and typeset

PLEASE CITE THIS ARTICLE AS DOI: 10.1063/5.0209887

This is the author's peer reviewed,

metry functions to integer values according to

$$\mathbf{p}_{u} = \mathbf{p}_{u}, \ \mathbf{d}_{u} = \sqrt{\frac{2}{3}} \, \mathbf{d}_{u}, \ \mathbf{f}_{u} = \sqrt{\frac{10}{9}} \, \mathbf{f}_{u}, \ \cdots \tag{A9}$$

and scale the two-spin transition symmetry functions to

integer values according to

$$({\rm pp})_{u,u'} = \, 2({\rm pp})_{u,u'}, \ ({\rm dp})_{u,u'} = \, 2\sqrt{6} \, ({\rm dp})_{u,u'}. \ ({\rm A}10)$$

Setting  $u \equiv I$  and  $u' \equiv S$ , the scaled two-spin functions are given by

$$(pp)_{IS}(m_{I,i}, m_{S,i}, m_{I,j}, m_{S,j}) = 2m_{I,j}m_{S,j} - 2m_{I,i}m_{S,i}$$
 for  $I \ge \frac{1}{2}$ ,  $S \ge \frac{1}{2}$ ,

$$(\mathrm{dp})_{IS}(m_{I,i}, m_{S,i}, m_{I,j}, m_{S,j}) = 6\left(m_{I,j}^2 m_{S,j} - m_{I,i}^2 m_{S,i}\right) - 2I(I+1)(m_{S,j} - m_{S,i}), \quad \text{for } I \ge 1, \ S \ge \frac{1}{2}, \quad (A12)$$

$$(\mathrm{pd})_{IS}(m_{I,i}, m_{S,i}, m_{I,j}, m_{S,j}) = 6\left(m_{S,j}^2 m_{I,j} - m_{S,i}^2 m_{I,i}\right) - 2S(S+1)(m_{I,j} - m_{I,i}). \quad \text{for } I \ge \frac{1}{2}, S \ge 1. \quad (A13)$$

Section IIC gives the analytical expressions for the frequency contributions obtained from perturbation theory. These expressions, given in Table II are defined in terms of the unscaled symmetry functions, which we consistently denote using a lower-case blackboard bold font.

### Appendix B: Extended Czjzek Distribution Computation

The tensor distribution of the extended Czjzek model is given in Eq. 62, where

$$\mathbf{S}(0) = \begin{bmatrix} -\zeta (\eta + 1)/2 & 0 & 0\\ 0 & \zeta (\eta - 1)/2 & 0\\ 0 & 0 & \zeta \end{bmatrix}$$
(B1)

and

$$\mathbf{S}_{c} = \begin{bmatrix} -U_{1} + \sqrt{3}U_{5} & \sqrt{3}U_{4} & \sqrt{3}U_{2} \\ \sqrt{3}U_{4} & -U_{1} - \sqrt{3}U_{5} & \sqrt{3}U_{3} \\ \sqrt{3}U_{2} & \sqrt{3}U_{3} & 2U_{1} \end{bmatrix}.$$
(B2)

Here,  $U_i$  is a random number sampled from a normal distribution with a unit standard deviation. To determine the extended Czjzek distribution,  $f_{\rm ext}(\zeta,\eta)$ , the eigenvalues,  $\lambda_k$  (k=0,1,2), of  $\mathbf{S}_T$  are first evaluated using numerical diagonalization. Next, the eigenvalues are sorted according to the Haeberlen convention,  $|\lambda_0| \geq |\lambda_1| \geq |\lambda_2|$ , to determine  $\zeta = \lambda_0$  and  $\eta = (\lambda_1 - \lambda_2)/\lambda_0$ . This process is repeated over millions of random tensors,  $\mathbf{S}_T$ , and the resulting  $(\zeta,\eta)$  coordinates are binned over a pre-determined grid.

Numerical diagonalizations can be computationally intensive, particularly in iterative algorithms like the least-squares minimization. An alternative is to find the analytical eigenvalues of  $\mathbf{S}_T$  by determining the roots of the determinant,

$$|\mathbf{S}_T - \lambda I| = 0. \tag{B3}$$

This determinant is a cubic equation of the form

$$\lambda^3 + a\lambda + b = 0, (B4)$$

and its analytical roots are given as

$$\lambda_k = 2\sqrt{a'}\cos\left[\theta_{ab} - \frac{2\pi k}{3}\right],$$
 (B5)

where a' = -a/3, b' = -b/2, k = (0, 1, 2), and

$$\theta_{ab} = \frac{1}{3} \arccos\left(\frac{b'}{a'\sqrt{a'}}\right).$$
 (B6)

For the Eq. (B4), the values of a and b are given as the scalar dot product,

$$a = a_{\text{coeff}} \cdot a_{\text{basis}}$$
 (B7)

$$b = b_{\text{coeff}} \cdot b_{\text{basis}}.$$
 (B8)

We define the vectors  $a_{\text{coeff}}$  and  $b_{\text{coeff}}$  as the *coefficients*, which are listed in the first column of Table III and Table IV, respectively. Similarly, we define the vectors  $a_{\text{basis}}$  and  $b_{\text{basis}}$  as the *basis*, which are listed in the second column of Table III and Table IV respectively. Note that the *basis* is composed purely of  $U_i$  and only requires a one-time computation in an iterative algorithm, while the *coefficients* update at each iteration.

For the Haeberlen convention,  $\zeta$  is the maximum absolute eigenvalue. By analyzing the three roots, we can determine that when  $0 \le \theta_{ab} < \pi/6$ , the  $(\zeta, \eta)$  coordinates are

$$\zeta = \lambda_0 = 2\sqrt{a'}\cos\theta_{ab},\tag{B9}$$

$$\eta = (\lambda_1 - \lambda_2)/\lambda_0 = \sqrt{3} \tan \theta_{ab},$$
(B10)

and for  $\pi/6 \le \theta_{ab} \le \pi/3$ , the coordinates are

$$\zeta = \lambda_2 = -2\sqrt{a'}\sin(\theta_{ab} + \pi/6), \tag{B11}$$

$$\eta = (\lambda_1 - \lambda_0)/\lambda_2 = \frac{\sqrt{3}}{\tan(\theta_{ab} + \pi/6)},$$
 (B12)

which reduces the computational cost of sorting the eigenvalues. Figure 7 compares the numerical diagonalization method to the algorithm proposed in this work,

PLEASE CITE THIS ARTICLE AS DOI: 10.1063/5.0209887

This is the author's peer reviewed,

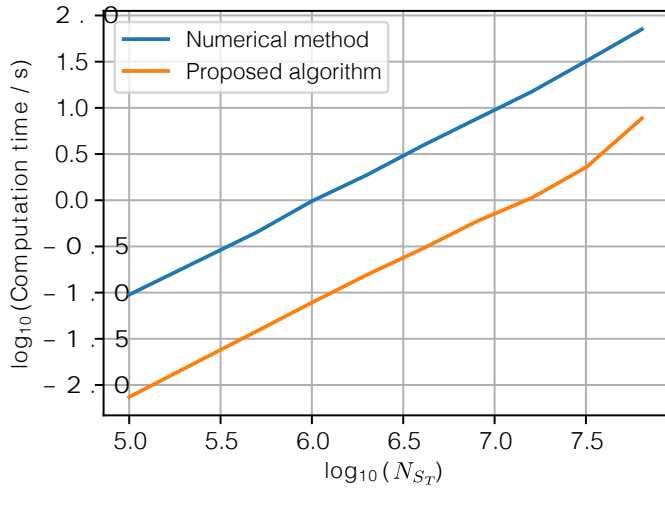


FIG. 7. Comparison between computation time for generating Extended Czizek distribution via random sampling of  $N_{S_T}$ tensors using conventional numerical approach vs. proposed algorithm. The proposed algorithm is over 10x faster.

TABLE III. Coefficients and basis for a in the cubic equation in Eq. (B4).

$a_{\text{coeff}}$	$a_{ m basis}$
$\rho^2$	$-3(U_1^2 + U_2^2 + U_3^2 + U_4^2 + U_5^2)$
$\zeta \rho$	$-3U_{1}$
$\zeta\eta\rho$	$\sqrt{3}U_5$
$\zeta^2(3+\eta^2)$	-1/4

demonstrating that the proposed algorithm is an order of magnitude faster than the conventional numerical method.

<sup>1</sup>A. Abragam, Principles of Nuclear Magnetism (Oxford University Press, Oxford, 1961).

<sup>2</sup>C. P. Slichter, Principles of Magnetic Resonance Verlag, Berlin, 1980).

<sup>3</sup>R. R. Ernst, G. Bodenhausen, and A. Principles of Nuclear Magnetic Resonance in One and Two Dimensions A. Wokaun and R. R. Ernst, Chem. Phys. Lett. 52, 407 (1977). (Oxford University Press, Oxford, 1987).

 $^4\mathrm{\dot{M}}.$  H. Levitt, Spin Dynamics: Basics of Nuclear Magnetic Resonance (Wiley, New  $\overline{\text{York}, 2001}$ ).

<sup>5</sup>P. T. Callaghan, Principles of Nuclear Magnetic Resonance Microscopy; **58**, 370 (1984). Oxford science publications (Clarendon Press, 1993)

<sup>6</sup>U. Haeberlen, High Resolution NMR in Solids: Selective Averaging, Advances in Magnetic Resonance (Academic Press, New York, 1976).

 $^7$ M. Principles of High Resolution NMR in Solids, Mehring, Vol. 11 (Springer-Verlag, Berlin, 1983).

Schmidt-Rohr Η. W. and Spiess, Multidimensional Solid-State NMR and Polymers (Academic Press, London, 1994).

<sup>9</sup>F. de Bouregas and J. Waugh, J. Magn. Reson. **96**, 280 (1992). <sup>10</sup>S. Smith, T. Levante, B. Meier, and R. Ernst, J. Magn. Reson. A **106**, 75 (1994)

<sup>11</sup>M. Edén, Y. K. Lee, and M. H. Levitt, J. Magn. Reson. A 120, 56 (1996)

<sup>12</sup>M. Hohwy, H. Bildsøe, H. Jakobsen, and N. Nielsen, J. Magn. Reson. **136**, 6 (1999).

<sup>13</sup>M. Bak, J. T. Rasmussen, and N. C. Nielsen, J. Magn. Reson. **147**, 296 (2000)

<sup>14</sup>W. B. Blanton, J. Magn. Reson. **162**, 269 (2003).

<sup>15</sup>M. Veshtort and R. G. Griffin, J. Magn. Reson. 178, 248 (2006) <sup>16</sup>H. Hogben, M. Krzystyniak, G. Charnock, P. Hore,

I. Kuprov, J. Magn. Reson. 208, 179 (2011).

<sup>17</sup>Z. Tošner, R. Andersen, B. Stevensson, M. Edén, N. C. Nielsen, and T. Vosegaard, J. Magn. Reson. 246, 79 (2014).

<sup>18</sup>C. Bengs and M. H. Levitt, Magnetic Resonance in Chemistry **56**, 374 (2018)

<sup>19</sup>D. W. Juhl, Z. Tošner, and T. Vosegaard, Annual Reports on NMR Spectroscopy **100**, 1 (2020).

<sup>20</sup>D. W. Alderman, M. S. Solum, and D. M. Grant, J. Chem. Phys. 84, 3717 (1986)

<sup>21</sup>N. K. Sethi, D. W. Alderman, and D. M. Grant, Mol. Phys. **71**, 217 (1990)

<sup>22</sup>Z. Zheng, Z. H. Gan, N. K. Sethi, D. W. Alderman, and D. M. Grant, J. Magn. Reson. 95, 509 (1991).

<sup>23</sup>D. Massiot, F. Fayon, M. Capron, I. King, S. Le Calvé, B. Alonso, J.-O. Durand, B. Bujoli, Z. Gan, and G. Hoatson, Magn. Reson. Chem. **40**, 70 (2002).

<sup>24</sup>T. Kemp and M. Smith, Solid State NMR **35**, 243 (2009)

<sup>25</sup>F. A. Perras, C. M. Widdifield, and D. L. Bryce, Solid State NMR **45-46**, 36 (2012).

<sup>26</sup>S. van Meerten, W. Franssen, and A. Kentgens, J. Magn. Reson. **301**, 56 (2019)

<sup>27</sup>F. A. Perras and A. L. Paterson, Solid State NMR **131**, 101935 (2024)

<sup>28</sup>P. J. Grandinetti, J. T. Ash, and N. M. Trease, Prog. Nucl. Mag. Res. Sp. **59**, 121 (2011).

<sup>29</sup>M. H. Levitt, J. Magn. Reson. **82**, 427 (1989).

<sup>30</sup>D. Manzano, AIP Advances 10, 025106 (2020).

<sup>31</sup>C. Bengs and M. H. Levitt, J. Magn. Reson. **310**, 106645 (2020).

<sup>32</sup>T. M. Barbara, Magnetic Resonance **2**, 689 (2021).

<sup>33</sup>R. Andrew, A. Bradbury, and R. G. Eades, Nature **182**, 1659 (1958).

<sup>34</sup>E. R. Andrew, A. Bradbury, and R. G. Eades, Nature **183**, 1802 (1958).

<sup>35</sup>S. Ganapathy, S. Schramm, and E. Oldfield, J. Chem. Phys. **77**, 4360 (1982).

<sup>36</sup>T. Terao, T. Fujii, T. Onodera, and A. Saika, Chem. Phys. Lett. **107**, 145 (1984).

<sup>37</sup>M. Goldman, P. J. Grandinetti, A. Llor, Z. Olejniczak, J. R. Sachleben, and J. W. Zwanziger, J. Chem. Phys. 97, 8947 (1992).

<sup>38</sup>E. Andrew, A. Bradbury, R. Eades, and V. Wynn, Phys. Lett. **4**, 99 (1963)

<sup>39</sup>D. Raleigh, M. Levitt, and R. Griffin, Chem. Phys. Lett. **146**, 71 (1988)

<sup>40</sup>M. H. Levitt, D. P. Raleigh, F. Creuzet, and R. G. Griffin, J. Chem. Phys. 92, 6347 (1990).

<sup>42</sup>G. P. Drobny, A. Pines, S. Sinton, D. Weitekamp, and D. E.

Wemmer, Faraday Symp. Chem. Soc. 13, 93 (1978)

<sup>43</sup>G. Bodenhausen, H. Kogler, and R. R. Ernst, J. Magn. Reson.

<sup>44</sup>For crystalline samples, the crystal frame is typically used as the common frame.

 $^{45}\mathrm{G.}$  Bodenhausen, S. P. Kempsell, R. Freeman,  $% \mathrm{G}$  and H. D. Hill, J. Magn. Reson. 35, 337 (1979).

<sup>46</sup>A. C. Kolbert, D. P. Raleigh, M. H. Levitt, and R. G. Griffin, J. Chem. Phys., 679 (1989).

<sup>47</sup>P. J. Grandinetti, Y. K. Lee, J. H. Baltisberger, B. Q. Sun, and A. Pines, J. Magn. Reson. A 102, 195 (1993).

<sup>48</sup>K. Atkinson, J. Austral. Math. Soc. (Series B) **23**, 332–347

<sup>49</sup>D. J. Srivastava, J. H. Baltisberger, and P. J. Grandinetti, J. Chem. Phys. **160** (2024), 10.1063/5.0200042.

<sup>50</sup>D. J. Srivastava and P. J. Grandinetti, J. Chem. Phys. **153**, 134201 (2020).

<sup>51</sup>G. Czjzek, J. Fink, F. Götz, H. Schmidt, J. M. D. Coey, J.-P. Rebouillat, and A. Liénard, Phys. Rev. B 23, 2513–2530 (1981).

<sup>52</sup>G. Czjzek, Hyperfine Interactions **14**, 189 (1983)

PLEASE CITE THIS ARTICLE AS DOI: 10.1063/5.0209887

This is the author's peer reviewed,

TABLE IV. Coefficients and basis for b in the cubic equation in Eq. (B4).

$b_{\mathrm{coeff}}$	$b_{ m basis}$	
$\overline{ ho^3}$	$-2U_1^3 - 3U_1(U_2^2 + U_3^2 - 2U_4^2 - 2U_5^2) - 3\sqrt{3}(U_2^2U_5 + 2U_2U_3U_4 - U_3^2U_5)$	
$\zeta  ho^2$	$-3(U_1^2 + U_2^2/2 + U_3^2/2 - U_4^2 - U_5^2)$	
$\zeta\eta ho^2$	$-2\sqrt{3}U_1U_5 + 3U_2^2/2 - 3U_3^2/2$	
$\zeta^2 \rho(-3 + \eta^2)$	$U_1/2$	
$\zeta^2\eta ho$	$-\sqrt{3}U_5$	
$\zeta^3(1-\eta^2)$	-1/4	

- <sup>53</sup>U. Werner-Zwanziger, A. Paterson, and J. Zwanziger, J. Non-Cryst. Solids **550**, 120383 (2020)
- <sup>54</sup>J.-B. d'Espinose de Lacaillerie, C. Fretigny, and D. Massiot, J. Magn. Reson. **192**, 244 (2008)
- <sup>55</sup>G. L. Caër, B. Bureau, and D. Massiot, J. Phys.: Condens. Matter **22** (2010), doi:10.1088/0953-8984/22/6/065402
- <sup>56</sup>W. T. Dixon, J. Magn. Reson. 44, 220 (1981).
- <sup>57</sup>W. T. Dixon, J. Chem. Phys. **77**, 1800 (1982)
- <sup>58</sup>O. N. Antzutkin, S. C. Shekar, and M. H. Levitt, J. Magn. Reson. A **115**, 7 (1995)
- <sup>59</sup>O. N. Antzutkin, Prog. NMR Spect. **35**, 203 (1999).
- $^{60}\mathrm{B.~J.~Walder,~K.~K.~Dey,~D.~C.~Kaseman,~J.~H.~Baltisberger,~}$  and P. J. Grandinetti, J. Chem. Phys. 138 (2013), 10.1063/1.4803142

- <sup>61</sup>R. Aleksis and A. J. Pell, J. Chem. Phys. **155** (2021), 10.1063/5.0061611.
- <sup>62</sup>J. T. Ash, N. T. Trease, and P. J. Grandinetti, J. Am. Chem. Soc. **130**, 10858 (2008)
- <sup>63</sup>I. Hung, A. Wong, A. P. Howes, T. Anupold, A. Samoson, M. E. Smith, D. Holland, S. P. Brown, and R. Dupree, J. Magn. Reson. **197**, 229 (2009).
- <sup>64</sup>B. J. Walder, K. K. Dey, M. C. Davis, J. H. Baltisberger, and P. J. Grandinetti, J. Chem. Phys. 142, 014201 (2015).
- 65D. Srivastava, J. Baltisberger, P. Florian, F. Fayon, R. Shakhovoy, M. Deschamps, N. Sadiki, and P. Grandinetti, Phys. Rev. B **98**, 134202 (2018).
- <sup>66</sup>J. P. Carvalho, A. Jaworski, M. J. Brady, and A. J. Pell, Magn. Reson. Chem. **58**, 1055 (2020).

### Supplementary Material for Simulating Multipulse NMR Spectra of Polycrystalline Solids in the Frequency Domain, Derivations, Definitions, and Conventions

### Deepansh J. Srivastava, Philip J. Grandinetti

June 18, 2024

### Contents

	ian Tensor Definitions and Conventions	S3
	educible spherical tensors	
S1.2 Pri	ncipal Axis System Conventions For Cartesian Tensors	
S1.2.1	Haeberlen Convention	
S1.2.2	Mehring Convention	
S1.3 Spł	herical tensor products	S8
	1 / 1 /	<b>S1</b> 0
	educible spherical tensor operators	
	educible spherical tensor operator products	
S2.3 Irre	educible spherical tensor operator commutators	S11
		S13
S3.1 Sin	gle-spin transition symmetry functions	S13
S3.2 Mu	llti-spin transition symmetry functions	S15
S3.2.1	Single-spin transition functions	S15
S3.2.2	Two-spin transition functions	S19
S4 Pertur	bation theory	S20
S5 Hamilt	conians and Transition Frequency Contributions	<b>S2</b> 1
S5.1 Zee	eman	S21
S5.2 Ele	ectric quadrupole coupling	S21
S5.2.1	First-order electric quadrupole coupling correction	
S5.2.2	Second-order electric quadrupole coupling correction	S23
S5.3 Nu	clear shielding	S25
S5.3.1	First-order nuclear shielding correction	S25
S5.3.2	Nuclear Shielding - Electric Quadrupole Cross Term	S26
S5.4 $J$ c	coupling	S26
S5.4.1	First-Order J-Coupling Correction	S27
S5.4.2	J-Coupling Quadrupolar Cross Term	S27
S5.5 Ma	gnetic dipole coupling	S29
S5.5.1	First-Order Magnetic Dipole Coupling Correction	S29
S5.5.2	Magnetic Dipole-Electric Quadrupole Coupling Cross Term in Weak Dipole Coupling Limit	S30
S6 Transit	tion Frequency Tensor Contributions	<b>S31</b>
S6.1 Sin	gle interaction frequency scaled spatial tensor parts	S31
	oss-term interaction frequency scaled spatial tensor parts	
S6.2.1	Quadrupolar-Quadrupolar 2nd-order Contributions	
S6 2 2		S3/

S6.2.3 Quadrupolar-weak $J$ 2nd-order Contributions	S34
S6.2.4 Quadrupolar-Dipolar 2nd-order Contributions	
S6.3 Total Transition Frequency Tensor in the Common Frame	S36
S7 Single Transition Coherence Transfer in High $\omega_1$ Limit	S37
S8 Transition Pathway Signal in a Rotating Sample	S39
S8.1 Evolution through one transition - The $\hat{\chi}$ spectrum	S42
S8.2 Free evolution through two transitions - The $\hat{\chi}_A \to \hat{\chi}_B$ spectrum	S42
S8.2.1 <sup>2</sup> H 2D PASS	S43
S8.2.2 Stroboscopic sampling during one time domain	
S8.2.3 Skew projection	
S8.2.4 Rotor phase advance during $u_{BA}(\alpha, \beta, \gamma)$	S49
S8.3 Free evolution through $n$ transitions	
S8.3.1 Simplifying the frequency expression	
S9 Czjzek Distribution	S53

### S1 Cartesian Tensor Definitions and Conventions

A real second-rank Cartesian tensor  $R_{ik}^{\{\lambda\}}$  can be decomposed into irreducible representations with respect to the full three-dimensional rotation group O(3) according to

$$R_{ik} = E\delta_{ik} + A_{ik} + S_{ik},\tag{S.1}$$

where

$$E = \frac{1}{3}kj\{\mathbf{R}\}, \qquad A_{ik} = \frac{1}{2}(R_{ik} - R_{ki}), \qquad S_{ik} = \frac{1}{2}(R_{ik} + R_{ki}) - \frac{1}{3}kj\{\mathbf{R}\}\delta_{ik}.$$
 (S.2)

Here E is invariant, and  $A_{ik}$  and  $S_{ik}$  are equivariant under rotations of the system.<sup>1</sup> The **A** tensor is the traceless anti-symmetric part and is equivalent to an axial (or pseudo-) vector and **S** tensor is the traceless symmetric part of the tensor. Unlike a polar (or true) vector, the components of the axial vector, **A**, do not change sign under an inversion of the coordinate system, i.e., the parity operator.

The second-rank Cartesian tensor,  $\mathbf{R}$ , cannot be diagonalized if it is not symmetric. While the anti-symmetric part of a second-rank interaction tensor can play a role in NMR relaxation, it rarely contributes to any observable NMR frequency shifts. We will use the notation

$$\{ES\}_{ik} = E\delta_{ik} + S_{ik},\tag{S.3}$$

to denote the symmetric part of the tensor that includes the invariant contribution. Both  $(\mathbf{ES})$  and  $(\mathbf{S})$  can be diagonalized, i.e., there is a coordinate transformation (rotation) that will make the tensor diagonal.

We adopt the convention that our coordinate systems and rotations follow the right-hand rule. For right-handed coordinates, your right thumb points along the z axis in a positive z direction, and the curl of your fingers represents a motion from the x axis to the y axis. A right-handed rotation about the z-axis carries the x-axis into the original position of the y-axis. Throughout this document, we attempt to follow the rotation conventions summarized in the text  $Quantum\ Theory\ of\ Angular\ Momentum\ by\ Varshalovich\ et\ al.[38].$ 

### S1.1 Irreducible spherical tensors

The second-rank Cartesian tensor,  $R_{ik}^{\{\lambda\}}$ , can be decomposed into irreducible spherical tensor components given by [8]

$$R_{0,0} = -\frac{1}{\sqrt{3}}[R_{xx} + R_{yy} + R_{zz}], \tag{S.4}$$

$$R_{1,0} = -\frac{i}{\sqrt{2}}[R_{xy} - R_{yx}], \quad R_{1,\pm 1} = -\frac{1}{2}[R_{zx} - R_{xz} \pm i(R_{zy} - R_{yz})], \tag{S.5}$$

$$R_{2,0} = \frac{1}{\sqrt{6}} [3R_{zz} - (R_{xx} + R_{yy} + R_{zz})], \quad R_{2,\pm 1} = \mp \frac{1}{2} [R_{xz} + R_{zx} \pm i(R_{yz} + R_{zy})],$$

$$R_{2,\pm 2} = \frac{1}{2} [R_{xx} - R_{yy} \pm i(R_{xy} + R_{yx})]. \quad (S.6)$$

Calculated in terms of E,  $A_{ik}$ , and  $S_{ik}$  the irreducible spherical tensor components are given by

$$R_{0,0} = -\sqrt{3} E, (S.7)$$

$$R_{1,0} = -i\sqrt{2} A_{xy}, \quad R_{1,\pm 1} = -(A_{zx} \mp iA_{yz}),$$
 (S.8)

$$R_{2,0} = \sqrt{\frac{3}{2}} S_{zz}, \quad R_{2,\pm 1} = \mp (S_{zx} \pm iS_{zy}), \quad R_{2,\pm 2} = \frac{1}{2} (S_{xx} - S_{yy} \pm i2S_{xy}).$$
 (S.9)

The inverse relation between spherical tensor and second-rank symmetric Cartesian tensor elements are

$$E = -\frac{1}{\sqrt{3}}R_{0,0} \tag{S.10}$$

$$A_{xy} = \frac{i}{\sqrt{2}}R_{1,0}, \quad A_{zx} = -\frac{1}{2}(R_{1,1} + R_{1,-1}), \quad A_{yz} = -\frac{i}{2}(R_{1,1} - R_{1,-1}),$$
 (S.11)

<sup>&</sup>lt;sup>1</sup>For third rank decomposition, see https://physics.stackexchange.com/questions/635248/rank-3-tensor-decomposition

and

$$S_{xx} = \frac{1}{2}(R_{2,2} + R_{2,-2}) - \frac{1}{\sqrt{6}}R_{2,0}, \quad S_{xy} = S_{yx} = \frac{i}{2}(R_{2,-2} - R_{2,2}), \quad S_{yy} = -\frac{1}{2}(R_{2,2} + R_{2,-2}) - \frac{1}{\sqrt{6}}R_{2,0},$$

$$S_{xz} = S_{zx} = \frac{1}{2}(R_{2,-1} - R_{2,1}), \quad S_{zz} = \sqrt{\frac{2}{3}}R_{2,0}, \quad S_{yz} = S_{zy} = \frac{i}{2}(R_{2,-1} + R_{2,1}).$$
(S.12)

The  $\mathbf{R}_L$  are called irreducible because of the invariance of the rank, L, during rotations about the x, y, or z axis. When expressed in terms of spherical tensor elements, rotations of the coordinate frame, i.e., passive rotations, can be carried out according to

$$R'_{L,m} = \sum_{m'=-L}^{L} \mathcal{D}_{m,m'}^{(L)}(\alpha, \beta, \gamma) R_{L,m'}, \tag{S.13}$$

where  $\mathcal{D}_{m,m'}^{(L)}(\alpha,\beta,\gamma)$  are Wigner rotation matrix elements, given by

$$\mathcal{D}_{m,m'}^{(L)}(\alpha,\beta,\gamma) = e^{-im\alpha} d_{m,m'}^{(L)}(\beta) e^{-im'\gamma}, \tag{S.14}$$

and  $d_{m,m'}^{(L)}(\beta)$  are the reduced Wigner rotation matrix elements. For example, spherical tensor elements in an arbitrary coordinate system can be related to  $\rho_{L,m'}$ , the elements in the PAS, according to

$$R_{L,m} = \sum_{m'=-L}^{L} \mathcal{D}_{m,m'}^{(L)}(\alpha, \beta, \gamma) \, \rho_{L,m'}, \tag{S.15}$$

A useful relationship between reduced Wigner rotation matrix elements is

$$d_{m,m'}^{(L)}(\beta) = (-1)^{m-m'} d_{-m,-m'}^{(L)}(\beta) = (-1)^{m-m'} d_{m',m}^{(L)}(\beta) = d_{-m',-m}^{(L)}(\beta).$$
(S.16)

### S1.2 Principal Axis System Conventions For Cartesian Tensors

While a Cartesian second-rank tensor that is not symmetric cannot be diagonalized, we can still speak of principal axis systems for the anti-symmetric and symmetric parts of the tensor separately.

A Cartesian pseudo-tensor of rank one, i.e., a vector with even parity, has a length of

$$\zeta^{(a)} = \sqrt{A_{yz}^2 + A_{zx}^2 + A_{xy}^2}. ag{S.17}$$

With a rotation of the coordinate system, the Cartesian vector is described in its principal axis system and becomes

$$\mathbf{L}^{T}(\phi, \theta)\mathbf{A} = \zeta^{(a)}\vec{\mathbf{e}}_{z}.$$
 (S.18)

Here  $\phi$  and  $\theta$  are the angles of the rotation matrix  $\mathbf{L}(\phi, \theta)$ , and  $\vec{\mathbf{e}}_z$  is the unit vector along the z-axis. In NMR,  $\zeta^{(a)}$  is the antisymmetric first-rank tensor anisotropy. In the principal axis system of  $\mathbf{A}$ , the spherical tensor elements are given by

$$\rho_{1,0} = -i\sqrt{2} \zeta^{(a)}, \quad \rho_{1,\pm 1} = 0.$$
(S.19)

Keep in mind, however, that an anti-symmetric tensor in its principal axis system remains as an off-diagonal element of the Cartesian tensor, as indicated by Eq. (S.8).

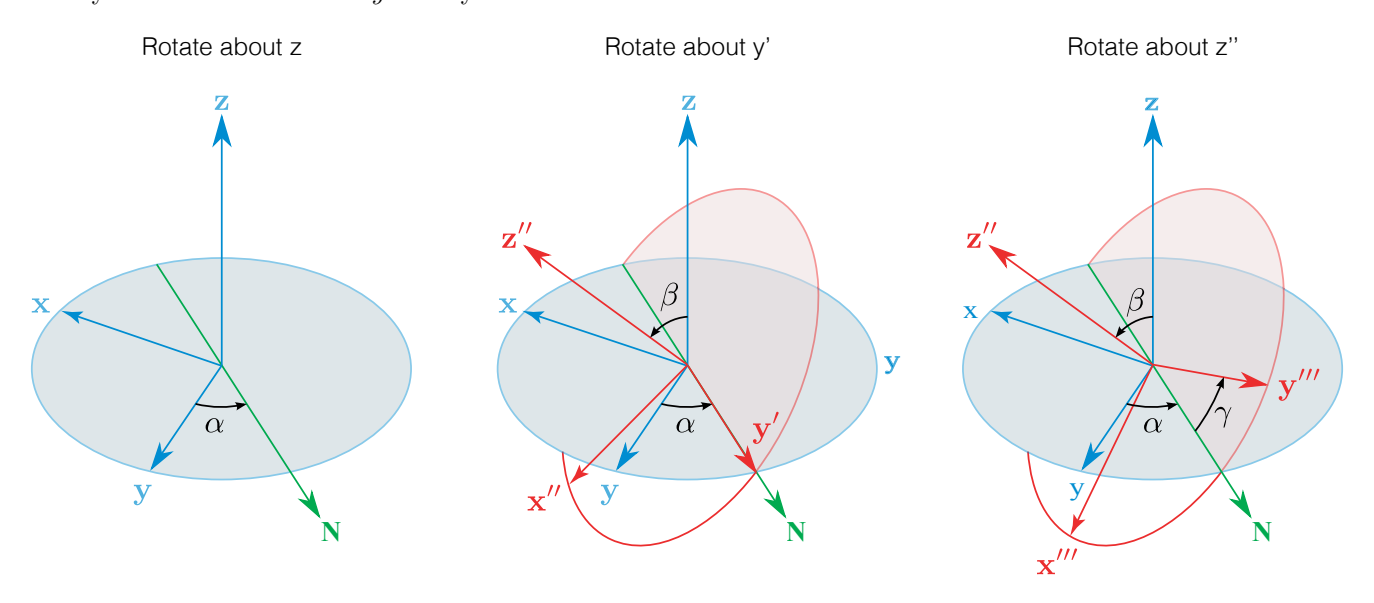
Through a rotation of the coordinate system, a Cartesian traceless symmetric tensor of rank two in its principal axis system becomes

$$\mathbf{L}^{T}(\alpha, \beta, \gamma) \{ \mathbf{ES} \} \mathbf{L}(\alpha, \beta, \gamma) = \mathbf{\Lambda}_{ES}, \quad \text{or} \quad \mathbf{L}^{T}(\alpha, \beta, \gamma) \mathbf{S} \mathbf{L}(\alpha, \beta, \gamma) = \mathbf{\Lambda}_{S},$$
 (S.20)

where  $\Lambda_{ES}$  and  $\Lambda_S$  are the diagonalized symmetric and traceless symmetric tensors, respectively, and  $\mathbf{L}(\alpha, \beta, \gamma)$  is a rotation matrix which holds the eigenvectors of  $\{\mathbf{ES}\}$  or  $\mathbf{S}$ . Here,  $\mathbf{L}^T(\alpha, \beta, \gamma)$  is the transpose of  $\mathbf{L}(\alpha, \beta, \gamma)$ . Both the *i*th column in  $\mathbf{L}$  and the *i*th row in  $\mathbf{L}^T$  are the eigenvector associated with its eigenvalue  $\lambda_i$ . The convention in spectroscopy and quantum mechanics is to use a proper Euler angle with the composite rotation z-y-z. When using Euler angles to describe a coordinate system rotation, i.e., a passive rotation, the fixed coordinate system, x,y,z, is rotated through three positive angles, the Euler angles,  $\alpha$ ,  $\beta$ , and  $\gamma$ . Each rotation produces a new set of axes, which we label with a successively more unwieldy number of primes. The three stages of a passive Euler angle rotation are

1. Rotate the (unprimed) fixed axes through an angle  $\alpha$  ( $0 \le \alpha \le 2\pi$ ) about  $\vec{e}_z$ , taking the x-y-z coordinate system into the x'-y'-z system.

- 2. Rotate the primed axes from step 1 through  $\beta$  ( $0 \le \beta \le \pi$ ) about  $\vec{e}_{y'}$ , taking the x'-y'-z system into the x''-y'-z'' system.
- 3. Rotate the double primed axes from step 2 through  $\gamma$  ( $0 \le \gamma \le 2\pi$ ) about  $\vec{e}_{z''}$ , taking the x''-y'-z'' coordinate system into the final x'''-y'''-z'' system.



In the example above, the three rotations are applied about axes of the rotated coordinate systems. This is called an *intrinsic rotation*. Alternatively, the three rotations can be applied about the three original axes of an x-y-z frame fixed in space. This is called an *extrinsic rotation*. Any intrinsic rotation can be converted to its extrinsic equivalent and vice-versa by reversing the order of elemental rotations.

Therefore, the rotation  $\mathbf{L}(\alpha, \beta, \gamma)$  can be constructed from the product of three extrinsic rotation matrices,

$$\mathbf{L}(\alpha, \beta, \gamma) = \underbrace{\begin{bmatrix} \cos \alpha & -\sin \alpha & 0 \\ \sin \alpha & \cos \alpha & 0 \\ 0 & 0 & 1 \end{bmatrix}}_{\mathbf{L}_{z}(\alpha)} \underbrace{\begin{bmatrix} \cos \beta & 0 & \sin \beta \\ 0 & 1 & 0 \\ -\sin \beta & 0 & \cos \beta \end{bmatrix}}_{\mathbf{L}_{y}(\beta)} \underbrace{\begin{bmatrix} \cos \gamma & -\sin \gamma & 0 \\ \sin \gamma & \cos \gamma & 0 \\ 0 & 0 & 1 \end{bmatrix}}_{\mathbf{L}_{z}(\gamma)}$$
$$= \begin{bmatrix} \cos \alpha \cos \beta \cos \gamma - \sin \alpha \sin \gamma & -\cos \alpha \sin \gamma - \sin \alpha \cos \beta \cos \gamma & \cos \alpha \sin \beta \\ \sin \alpha \cos \beta \cos \gamma + \cos \alpha \sin \gamma & -\sin \alpha \sin \gamma + \cos \alpha \cos \beta \cos \gamma & \sin \alpha \sin \beta \\ -\sin \beta \cos \gamma & \sin \beta \sin \gamma & \cos \beta \end{bmatrix}}_{\mathbf{S}(\alpha, \beta, \gamma)}. \quad (S.21)$$

After a numerical diagonalization of the symmetric Cartesian tensor, the Euler angles  $(\alpha, \beta, \gamma)$  can be extracted from the eigenvector matrix **L**, according to

$$\beta = \arccos(l_{33}), \qquad \beta \in [0, \pi], \qquad (S.22)$$

$$\alpha = \arctan(l_{23}, l_{13}), \qquad \qquad \alpha \in [-\pi, \pi], \tag{S.23}$$

$$\gamma = \arctan(l_{32}, -l_{31}), \qquad \gamma \in [-\pi, \pi]. \tag{S.24}$$

Using the  $\arctan 2(y,x)$  function is essential to ensure that the resulting angles correctly represent the orientation and direction of the rotations. When performing a numerical diagonalization of a tensor, the eigenvectors returned by the routine are normalized to 1, but the sign of the eigenvectors is not fixed. This means that if  $\mathbf{l}_i$  is an eigenvector,  $-\mathbf{l}_i$  is also an eigenvector with the same eigenvalue. This can lead to a discrepancy when converting the eigenvectors to Euler angles and back to a rotation matrix because the Euler angles can represent a rotation equivalent to the original rotation but with the eigenvectors flipped in sign. To resolve this issue, flip the sign of the eigenvectors if the determinant of the rotation matrix is negative. This ensures that the rotation matrix is a proper rotation (i.e., a rotation without reflection). This allows the Euler angles to be correctly extracted from the eigenvector matrix. It is also essential to be aware of the gimbal lock issue when  $\beta$  is 0 or  $\pi$ . In such cases,  $\alpha$  and  $\gamma$  become dependent on each other, and it's impossible to determine them uniquely. In this case, we can arbitrarily set  $\alpha = 0$  and calculate  $\gamma$  from Eq. (S.24).

There are six different orientations in which a symmetric Cartesian tensor will be diagonal. Thus, if  $(\alpha, \beta, \gamma)$  diagonalizes a symmetric Cartesian tensor, then so will  $(\alpha + \pi, \beta, \gamma + \pi)$ ,  $(\alpha + \pi, -\beta, \gamma)$ ,  $(\alpha, -\beta, \gamma + \pi)$ ,  $(\alpha + \pi, \pi - \beta, \gamma + \pi)$ , and  $(\alpha, \pi - \beta, \gamma)$ . Which Euler angles in this set are chosen to define  $\Lambda_S^{PAS}$  depends on the convention used to order the principal components of the tensor. In NMR, there are two common conventions, Haeberlen and Mehring. For the reasons given below, the Haeberlen convention is preferred.

### S1.2.1 Haeberlen Convention

Through a rotation of a coordinate system, a traceless symmetric Cartesian tensor of rank two in its principal axis system becomes

$$\mathbf{L}^{T}(\alpha_{h}, \beta_{h}, \gamma_{h}) \mathbf{S} \mathbf{L}(\alpha_{h}, \beta_{h}, \gamma_{h}) = \mathbf{\Lambda}_{S}^{PAS}, \tag{S.25}$$

where  $\mathbf{\Lambda}_{S}^{\mathrm{PAS}}$  is a diagonal matrix with the principal components,  $\lambda_{a}^{(s)}$ ,  $\lambda_{b}^{(s)}$ , and  $\lambda_{c}^{(s)}$ , and corresponding eigenvectors are ordered according to the Haeberlen convention[19] such that

$$\left|\lambda_c^{(s)}\right| \ge \left|\lambda_a^{(s)}\right| \ge \left|\lambda_b^{(s)}\right|. \tag{S.26}$$

Since S is traceless, we have

$$\lambda_a^{(s)} + \lambda_b^{(s)} + \lambda_c^{(s)} = 0. {(S.27)}$$

In the Haeberlen principal axis system of S, the spherical tensor elements are given by

$$\rho_{2,0} = \sqrt{\frac{3}{2}} \lambda_c^{(s)}, \quad \rho_{2,\pm 1} = 0, \quad \rho_{2,\pm 2} = \frac{1}{2} (\lambda_a^{(s)} - \lambda_b^{(s)}). \tag{S.28}$$

Additionally, we define the second-rank symmetric tensor anisotropy,  $\zeta$ , and asymmetry,  $\eta$ , parameters according to

$$\zeta = \lambda_c^{(s)}, \text{ and } \eta = \frac{\lambda_b^{(s)} - \lambda_a^{(s)}}{\zeta}, \text{ with } \rho_{2,0} = \sqrt{\frac{3}{2}} \zeta, \quad \rho_{2,\pm 1} = 0, \quad \rho_{2,\pm 2} = -\frac{1}{2}\zeta\eta.$$
 (S.29)

Conversely, we have

$$\lambda_c^{(s)} = \sqrt{\frac{2}{3}} \ \rho_{2,0} = \zeta, \quad \lambda_a^{(s)} = \rho_{2,\pm 2} - \frac{1}{\sqrt{6}} \ \rho_{2,0} = -\frac{\zeta}{2} (1+\eta), \quad \lambda_b^{(s)} = -\rho_{2,\pm 2} - \frac{1}{\sqrt{6}} \ \rho_{2,0} = -\frac{\zeta}{2} (1-\eta). \tag{S.30}$$

While a common choice for representing a distribution of  $\zeta$  and  $\eta$  parameters is a 2D Cartesian grid where the coordinates  $\zeta$  and  $\eta$  span the orthogonal dimensions, this coordinate system is numerically unstable since  $\eta$  becomes undefined as  $\zeta \to 0$ ; this is indicated as black-filled circles in Fig. S1A. Additionally, anisotropic NMR line shapes are invariant of the sign of  $\zeta$  when  $\eta = 1$ , forming a degenerate system of line shapes; this is depicted with colored circles in Fig. S1A. To overcome these issues, Srivastava et al.[34] propose an approach, similar to Czjzek[9], that re-expresses the coordinates  $\zeta$  and  $\eta$  in the first quadrant of a polar coordinate system,  $(r_{\zeta}, \theta)$ , where

$$r = |\zeta| \quad \text{and} \quad \theta = \begin{cases} \frac{\pi}{4}\eta & : \zeta \le 0, \\ \frac{\pi}{2}\left(1 - \frac{\eta}{2}\right) & : \zeta > 0. \end{cases}$$
(S.31)

They choose an x-y Cartesian grid over the r- $\theta$  polar grid because Cartesian grids are more manageable for numerical implementations. It is given by

$$x = r \cos \theta$$
 and  $y = r \sin \theta$  :  $0 \ge \theta \ge \pi/2$ . (S.32)

As shown in Fig. S1B, the magnitude of  $\zeta$  forms the radial dimension while  $\eta$  forms the angular dimension. The line |x|=|y| corresponds to  $\eta=1$ . When progressing towards the x or y-axis from this line,  $\eta$  uniformly decreases from 1 to 0, where  $\eta=0$  is along the x or y-axis, depending on the sign of  $\zeta$ . The undefined condition for  $\eta$  when  $\zeta\to 0$  is true irrespective of the choice of the coordinate system; however, this representation confines  $\zeta=0$  to a single point located at the origin. Additionally, since positive and negative values of  $\zeta$  correspond to the same  $(r,\theta)$  coordinate when  $\eta=1$ , the x-y representation also removes the anisotropic line shape degeneracy associated with the  $\zeta$ - $\eta$  grid.

For the nuclear shielding anisotropy, an  $x_{\sigma}$ - $y_{\sigma}$  Cartesian grid is used and is given by

$$x_{\sigma} = r_{\sigma} \cos \theta \text{ and } y_{\sigma} = r_{\sigma} \sin \theta : 0 \ge \theta \ge \pi/2,$$
 (S.33)

where  $r_{\sigma} = |\zeta_{\sigma}|$ . For the quadrupolar coupling anisotropy, it is more convenient to use an  $x_q$ - $y_q$  Cartesian grid is given by

$$x_q = r_q \cos \theta \text{ and } y_q = r_q \sin \theta : 0 \ge \theta \ge \pi/2,$$
 (S.34)

where  $r_q = |C_q|$ .

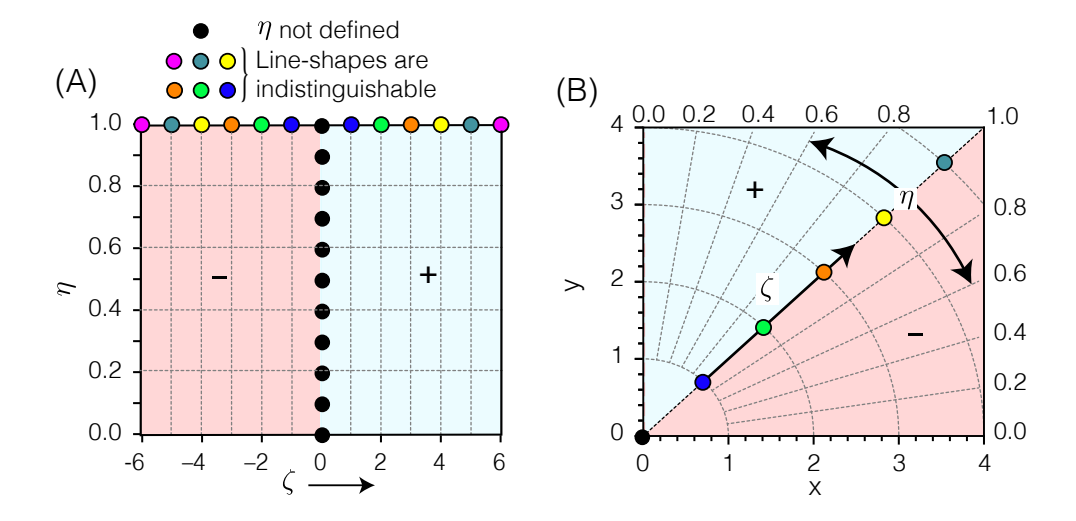


Figure S1: (A) A schematic representation of the  $\zeta$ - $\eta$  Cartesian grid system depicting the undefined regions, shown in black circles, and redundant indistinguishable regions, shown in colored circles, of the coordinate system. (B) The positive quadrant of the x-y grid. Here, the magnitude of  $\zeta$  is the radial dimension, while  $\eta$  is the angular dimension. The blue and red shading indicate regions of positive and negative  $\zeta$ , respectively.

### S1.2.2 Mehring Convention

The Mehring tensor parameters use the principal components of the chemical shift tensor, which are related to the nuclear magnetic shielding tensor by

$$\delta_i = \frac{\sigma_{\rm iso}^{\rm ref} - \sigma_i}{(1 - \sigma_{\rm iso}^{\rm ref})},\tag{S.35}$$

where  $\sigma_{\rm iso}^{\rm ref}$  is the isotropic nuclear magnetic shielding of a reference resonance. Since  $\sigma_{\rm iso}^{\rm ref} \ll 1$ , we can write

$$\delta_i \approx \sigma_{\rm iso}^{\rm ref} - \sigma_i = -\sigma_i', \text{ where } \sigma_i' = \sigma_i - \sigma_{\rm iso}^{\rm ref}.$$
 (S.36)

In the case of a single resonance in a spectrum of a static polycrystalline sample with only isotropic and anisotropic contributions from the nuclear magnetic shielding interaction, the principal components of the chemical shift tensor can be read off the spectrum as the frequency position in chemical shift of the three singularities ordered according to

$$\delta_3 \le \delta_2 \le \delta_1. \tag{S.37}$$

This results in the opposite ordering of the nuclear magnetic shielding tensor principal components, i.e.,

$$\sigma_3' \ge \sigma_2' \ge \sigma_1'. \tag{S.38}$$

In an unfortunate choice of notation, Mehring[24] represents the principal components of the chemical shift tensor with the same Greek letter as the principal components of the nuclear magnetic shielding tensor, i.e.,  $\sigma_{ii}$ . To compound this confusion, he tabulates the principal components of the chemical shift tensor in his text and refers to them as "shieldings." What Mehring refers to as  $\sigma_{11}$ ,  $\sigma_{22}$ , and  $\sigma_{33}$  are actually the principal components of the chemical shift tensor, which we indicate as  $\delta_1$ ,  $\delta_2$ , and  $\delta_3$ , respectively.

In the Mehring convention[19], after a rotation of the coordinate system, a second-rank symmetric Cartesian tensor in its principal axis system becomes

$$\mathbf{L}^{T}(\alpha_{m}, \beta_{m}, \gamma_{m}) \left\{ \mathbf{ES} \right\} \mathbf{L}(\alpha_{m}, \beta_{m}, \gamma_{m}) = \mathbf{\Lambda}_{ES}^{\mathrm{PAS}}, \tag{S.39}$$

where  $\sigma' = \{ \mathbf{ES} \}$  and  $\Lambda_{ES}^{\mathrm{PAS}}$  is a diagonal matrix with the principal components,  $\lambda_1^{(es)}$ ,  $\lambda_2^{(es)}$ , and  $\lambda_3^{(es)}$ , ordered, such that

$$\lambda_3^{(es)} \ge \lambda_2^{(es)} \ge \lambda_1^{(es)}. \tag{S.40}$$

Since  $\{ES\}$  is not traceless we have

$$\lambda_{\rm iso}^{(es)} = \frac{1}{3} \left( \lambda_1^{(es)} + \lambda_2^{(es)} + \lambda_3^{(es)} \right).$$

The Mehring ordering of the principal components of the symmetric tensor,  $\{ES\}$  is *not* consistent with the Haeberlen ordering of the principal components of the traceless symmetric tensor, S. That is, subtracting the isotropic component from the eigenvalues of  $\{ES\}$  does not follow the same ordering of the eigenvalues of S in the Haeberlen convention, i.e.,

$$\left| \lambda_3^{(es)} - \lambda_{\text{iso}}^{(es)} \right| \succeq \left| \lambda_1^{(es)} - \lambda_{\text{iso}}^{(es)} \right| \succeq \left| \lambda_2^{(es)} - \lambda_{\text{iso}}^{(es)} \right|. \tag{S.41}$$

For this reason, the Euler angles that give the Mehring ordering of the principal components will not be the same as those that give the Haeberlen ordering.

To convert between the two conventions, the isotropic component of the symmetric tensor is subtracted from the Mehring principal components of the symmetric tensor, i.e.,  $\lambda_i - \lambda_{\rm iso}$ , and assigned to  $\lambda_a$ ,  $\lambda_b$ , and  $\lambda_c$  according to the Haeberlen convention in Eq. (S.26). Converting from the Euler angles  $(\alpha_m, \beta_m, \gamma_m)$  that give the Mehring ordering of the principal components to the Euler angles  $(\alpha_h, \beta_h, \gamma_h)$  that give the Haeberlen ordering of the principal components is not as straightforward. One could reorder the column eigenvectors in  $\mathbf{L}(\alpha_m, \beta_m, \gamma_m)$  to match the reordering as the eigenvalues, and then apply Eqs. (S.22)-(S.24) used to extract  $(\alpha_h, \beta_h, \gamma_h)$ . Alternatively, one could rotate the Mehring PAS tensor back to the fixed coordinate system, diagonalize the tensor into the Haeberlen PAS system, and then extract the Euler angles from the eigenvector matrix.

### S1.3 Spherical tensor products

Products of irreducible spherical tensors can be reduced with the aid of the Clebsch-Gordon coefficients[14, 32, 33] according to

$$U_{\ell_1,m_1}V_{\ell_2,m_2} = \sum_{L=|\ell_1-\ell_2|}^{|\ell_1+\ell_2|} \langle L \ m_1+m_2|\ell_1 \ \ell_2 \ m_1 \ m_2 \rangle \mathfrak{X}_{L,m_1+m_2}, \tag{S.42}$$

where

$$\mathfrak{X}_{L,M} = \{\hat{\vec{U}}^{(\ell_1)} \otimes \hat{\vec{V}}^{(\ell_2)}\}_{L,M} = \sum_{m} \langle L M | \ell_1 \, \ell_2 \, m \, M - m \rangle U_{\ell_1,m} V_{\ell_2,M-m}.$$
 (S.43)

A few helpful symmetry properties of the Clebsch-Gordon coefficients are

$$\langle L M | \ell_1 \, \ell_2 \, m_1 \, m_2 \rangle = (-1)^{\ell_1 + \ell_2 - L} \langle L M | l_2 \, \ell_1 \, m_2 \, m_1 \rangle,$$
 (S.44)

$$\langle L M | \ell_1 \ell_2 m_1 m_2 \rangle = (-1)^{\ell_1 + \ell_2 - L} \langle L - M | \ell_1 \ell_2 - m_1 - m_2 \rangle, \tag{S.45}$$

$$\langle L M | l_1 \ell_2 m_1 m_2 \rangle = \langle L - M | \ell_2 \ell_1 - m_2 - m_1 \rangle.$$
 (S.46)

Since second-order energy corrections are needed for terms involving the quadrupolar coupling, we can narrow our focus to spatial tensor products of the form  $R_{\ell_1,-m}^{\{\lambda\}}R_{2,m}^{\{q\}}$ , which can be expanded as

$$R_{\ell_1,-m}^{\{\lambda\}} R_{2,m}^{\{q\}} = \frac{1}{2} \sum_{L=|\ell_1-2|}^{|\ell_1+2|} \left(1 + (-1)^{\ell_1-L}\right) \langle L \, 0 | \ell_1 \, 2 - m \, m \rangle \mathcal{R}_{L,0}^{\{\lambda q\}}. \tag{S.47}$$

For even values of  $\ell_1$ , only terms in the sum with even values of L survive, and vice versa. Thus, we consider the two cases separately. For the odd value of  $\ell_1 = 1$ , we have

$$R_{1,-m}^{\{\lambda\}} R_{2,m}^{\{q\}} = \langle 1 \, 0 | 1 \, 2 \, -m \, m \rangle \mathcal{A}_{1,0}^{\{\lambda q\}} + \langle 3 \, 0 | 1 \, 2 \, -m \, m \rangle \mathcal{A}_{3,0}^{\{\lambda q\}}, \tag{S.48}$$

and for the even value of  $\ell_1 = 2$ , we have

$$R_{2,-m}^{\{\lambda\}} R_{2,m}^{\{q\}} = \langle 0 \, 0 | 2 \, 2 \, -m \, m \rangle \mathcal{R}_{0,0}^{\{\lambda q\}} + \langle 2 \, 0 | 2 \, 2 \, -m \, m \rangle \mathcal{R}_{2,0}^{\{\lambda q\}} + \langle 4 \, 0 | 2 \, 2 \, -m \, m \rangle \mathcal{R}_{4,0}^{\{\lambda q\}}. \tag{S.49}$$

In either case, the tensor is related to the tensor elements in the sample holder frame using Eq. (S.13), e.g.,

$$\mathcal{A}_{L,0}^{\{\lambda q\}} = \sum_{m=-L}^{L} \mathcal{D}_{0,m}^{(L)}(\phi, \theta_R, 0) \, \mathcal{A}_{L,m}^{\prime \{\lambda q\}} \quad \text{and} \quad \mathcal{R}_{L,0}^{\{\lambda q\}} = \sum_{m=-L}^{L} \mathcal{D}_{0,m}^{(L)}(\phi, \theta_R, 0) \, \mathcal{R}_{L,m}^{\prime \{\lambda q\}}. \tag{S.50}$$

The tensor elements are further related to the elements in the principal axis of the  $\{q\}$  tensor according to

$$\mathcal{A}'^{\{\lambda q\}}_{L,m} = \sum_{m'=-L}^{L} \mathcal{D}^{(L)}_{m',m}(\Theta_q) \mathcal{A}''^{\{\lambda q\}}_{L,m'} \quad \text{and} \quad \mathcal{R}'^{\{\lambda q\}}_{L,m} = \sum_{m'=-L}^{L} \mathcal{D}^{(L)}_{m',m}(\Theta_q) \mathcal{R}''^{\{\lambda q\}}_{L,m'}, \tag{S.51}$$

λ	q	σ	$d_{II}$	$d_{IS}$	$d_{IS}$ $J_{II}$ $J_{IS}$		
$\mathbb{S}^{\{\lambda\}}/R_{0,0}^{\{\lambda\}}$	-	$-\frac{1}{\sigma_{\rm iso}}\sqrt{\frac{1}{3}}$	-	-	-	$-\frac{1}{J_{iso}}\sqrt{\frac{1}{3}}$	
$\mathbb{P}^{\{\lambda\}}/R_{1,0}^{\{\lambda\}}$	-	-	-	-	$-rac{1}{\zeta_J^{(a)}}$	-	
$\mathbb{D}^{\{\lambda\}}/R_{2,0}^{\{\lambda\}}$	$\frac{1}{3\zeta_q}$	$\frac{1}{\zeta_{\sigma}}\sqrt{\frac{2}{3}}$	$\frac{2}{\zeta_d}$	$\frac{2}{\zeta_d}\sqrt{\frac{2}{3}}$	$\frac{1}{\zeta_J}$	$\frac{1}{\zeta_J}\sqrt{\frac{2}{3}}$	
$\mathbb{S}^{\{\lambda q_I\}}/R_{0,0}^{\{\lambda q_I\}}$	$\frac{1}{9\zeta_q^2}$	$\frac{1}{\zeta_{\sigma}} \frac{1}{3\zeta_{q}} \sqrt{\frac{6}{5}}$	-	$\frac{2}{\zeta_d} \frac{1}{3\zeta_q^{\{I\}}} \sqrt{\frac{6}{5}}$	-	$\frac{1}{\zeta_J} \frac{1}{3\zeta_q^{\{I\}}} \sqrt{\frac{6}{5}}$	
$\mathbb{D}^{\{\lambda q_I\}}/R_{2,0}^{\{\lambda q_I\}}$	$\frac{1}{9\zeta_q^2}$	$-\frac{1}{\zeta_{\sigma}}\frac{1}{3\zeta_{q}}\sqrt{\frac{3}{7}}$	-	$-\frac{2}{\zeta_d} \frac{1}{3\zeta_q^{\{I\}}} \sqrt{\frac{3}{7}}$	-	$-\frac{1}{\zeta_J}\frac{1}{3\zeta_q^{\{I\}}}\sqrt{\frac{3}{7}}$	
$\mathbb{G}^{\{\lambda q_I\}}/R_{4,0}^{\{\lambda q_I\}}$	$\frac{1}{9\zeta_q^2}$	$\frac{1}{\zeta_{\sigma}} \frac{1}{3\zeta_{q}} \sqrt{\frac{48}{35}}$	-	$-\frac{2}{\zeta_d} \frac{1}{3\zeta_q^{\{I\}}} \sqrt{\frac{48}{35}}$	-	$-\frac{1}{\zeta_J} \frac{1}{3\zeta_q^{\{I\}}} \sqrt{\frac{48}{35}}$	

Table S1: Proportionality constants between  $\Xi^{\{\lambda\}}(\Theta)$  and the irreducible tensor element  $R_{L,0}^{\{\lambda\}}(\Theta)$  for various nuclear spin interactions. Here  $q \equiv$  electric quadrupole coupling,  $\sigma \equiv$  nuclear shielding,  $d_{II} \equiv$  strong dipolar coupling,  $d_{IS} \equiv$ weak dipolar coupling,  $J_{II} \equiv \text{strong } J$  coupling, and  $J_{IS} \equiv \text{weak } J$  coupling.

where  $\Theta_q = (\alpha_q, \beta_q, \gamma_q)$  are the Euler angles relating the principal axis system of the  $\{q\}$  tensor to the sample holder frame. Here, we can use Eq. (S.42) to obtain

$$\mathcal{A}''^{\{\lambda q\}}_{L,M} = \sum_{m} \langle L\,M|1\,2\,m\,M - m\rangle R^{\{\lambda\}}_{1,m}[q] \; \rho^{\{q\}}_{2,M-m} \quad \text{ and } \quad \mathcal{R}''^{\{\lambda q\}}_{L,M} = \sum_{m} \langle L\,M|2\,2\,m\,M - m\rangle R^{\{\lambda\}}_{2,m}[q] \; \rho^{\{q\}}_{2,M-m}, \quad (\text{S.52})$$

where  $R_{1,m}^{\{\lambda\}}[q]$  and  $R_{2,m}^{\{\lambda\}}[q]$  are the spherical tensor elements of the  $\{\lambda\}$  tensor in the PAS of the  $\{q\}$  tensor.

Conversely, the tensor elements,  $\mathcal{R}'^{\{\lambda q\}}_{L,m}$ , can be related to the elements in the principal axis of the  $\{\lambda\}$  tensor according to

$$\mathcal{A}'^{\{\lambda q\}}_{L,m} = \sum_{m'=-L}^{L} \mathcal{D}^{(L)}_{m',m}(\Theta_{\lambda}) \mathcal{A}'''^{\{\lambda q\}}_{L,m'} \quad \text{and} \quad \mathcal{R}'^{\{\lambda q\}}_{L,m} = \sum_{m'=-L}^{L} \mathcal{D}^{(L)}_{m',m}(\Theta_{\lambda}) \mathcal{R}'''^{\{\lambda q\}}_{L,m'}, \tag{S.53}$$

where  $\Theta_{\lambda} = (\alpha_{\lambda}, \beta_{\lambda}, \gamma_{\lambda})$  are the Euler angles relating the principal axis system of the  $\{\lambda\}$  tensor to the sample holder frame. Here, we can use Eq. (S.42) to obtain

$$\mathcal{A}_{L,M}^{\prime\prime\prime\{\lambda q\}} = \sum_{m} \langle L\,M|1\,2\,m\,m^{\prime} - m\rangle \rho_{1,m}^{\{\lambda\}} R_{2,M-m}^{\{q\}} \quad \text{ and } \quad \mathcal{R}_{L,M}^{\prime\prime\prime\{\lambda q\}} = \sum_{m} \langle L\,M|2\,2\,m\,M - m\rangle \rho_{2,m}^{\{\lambda\}} R_{2,M-m}^{\{q\}}, \quad (S.54)$$

where  $R_{1,m}^{\{q\}}[\lambda]$  and  $R_{2,m}^{\{q\}}[\lambda]$  are the spherical tensor elements of the  $\{q\}$  tensor in the PAS of the  $\{\lambda\}$  tensor. To emphasize spatial symmetries we classify the spatial functions using the upper-case symbols  $\mathbb{S}$ ,  $\mathbb{P}(\Theta)$ ,  $\mathbb{D}(\Theta)$ ,  $\mathbb{F}(\Theta)$ , and  $\mathbb{G}(\Theta)$  according to:

$$\mathbb{S}^{\{\lambda\}} \propto R_{0,0}^{\{\lambda\}}, \ \mathbb{P}^{\{\lambda\}}(\Theta) \propto R_{1,0}^{\{\lambda\}}(\Theta), \ \mathbb{D}^{\{\lambda\}}(\Theta) \propto R_{2,0}^{\{\lambda\}}(\Theta), \ \mathbb{F}^{\{\lambda\}}(\Theta) \propto R_{3,0}^{\{\lambda\}}(\Theta), \ \mathbb{G}^{\{\lambda\}}(\Theta) \propto R_{4,0}^{\{\lambda\}}(\Theta),$$
 (S.55)

where the  $R_{L,0}^{\{\lambda\}}(\Theta)$  are elements of irreducible tensors of rank L in the laboratory frame describing the spatial part of a frequency component arising from a given nuclear spin interaction, here generically labeled as  $\lambda$ . The proportionality constants are interaction specific, derived in section S5, and are given in Table S1.

### S2 Spherical tensor operators, products, and commutators

### S2.1 Irreducible spherical tensor operators

In 1942, Racah[31] introduced the concept of irreducible spherical tensor operators,  $\hat{T}_{\ell,m}(\vec{I})$ , of rank (or degree)  $\ell$  and order m for angular momentum operators  $\vec{I}$ . These operators are defined by the property that they satisfy the same commutation rules with respect to  $\vec{I}$  as the spherical harmonic operators, i.e.,

$$[\hat{I}_z, \hat{T}_{\ell,m}(\vec{I})] = m\hat{T}_{\ell,m}(\vec{I}) \text{ and } [\hat{I}_\pm, \hat{T}_{\ell,m}(\vec{I})] = \sqrt{\ell(\ell+1) - m(m\pm 1)}\hat{T}_{\ell,m\pm 1}(\vec{I}).$$
 (S.56)

$$T_{J,M}(\vec{I}) = \sum_{m} \langle J M | \ell_1 \, \ell_2 \, m \, M - m \rangle \hat{T}_{\ell_1,m}(\vec{I}) \hat{T}_{\ell_2,M-m}(\vec{I}). \tag{S.57}$$

Under an SO(3) rotation of the coordinate system, i.e., a passive rotation, the irreducible spherical tensor operators transform according to

$$\hat{\mathbf{T}}^{'(\ell)}(\vec{I}) = \hat{\mathbf{D}}(\alpha, \beta, \gamma)\hat{\mathbf{T}}^{(\ell)}(\vec{I})\hat{\mathbf{D}}^{-1}(\alpha, \beta, \gamma). \quad \text{or} \quad \hat{T}_{L,m} = \sum_{m'=-L}^{L} \mathcal{D}_{m,m'}^{(L)}(\alpha, \beta, \gamma) \hat{T}_{L,m'}^{\prime}, \tag{S.58}$$

where

$$\hat{\mathbf{D}}(\alpha, \beta, \gamma) = e^{-i\alpha \hat{I}_z} e^{-i\beta \hat{I}_y} e^{-i\gamma \hat{I}_z} \quad \text{and} \quad \hat{\mathbf{D}}^{-1}(\alpha, \beta, \gamma) = e^{i\gamma \hat{I}_z} e^{i\beta \hat{I}_y} e^{i\alpha \hat{I}_z}. \tag{S.59}$$

Note, that  $\hat{\mathbf{D}}^{-1}(\alpha, \beta, \gamma)$  is the conjugate transpose of  $\hat{\mathbf{D}}(\alpha, \beta, \gamma)$ —see chapter 4 of Varshalovich et al.[38]. In contrast, an active SO(3) rotation of the irreducible spherical tensor operators is given by

$$\hat{\mathbf{T}}^{(\ell)}(\vec{I}) = \hat{\mathbf{D}}^{-1}(\alpha, \beta, \gamma)\hat{\mathbf{T}}^{'(\ell)}(\vec{I})\hat{\mathbf{D}}(\alpha, \beta, \gamma) \quad \text{or} \quad \hat{T}_{L,m} = \sum_{m'=-L}^{L} \mathcal{D}_{m',m}^{*(L)}(\alpha, \beta, \gamma)\hat{T}_{L,m'}^{'}. \tag{S.60}$$

### S2.2 Irreducible spherical tensor operator products

The product of irreducible spherical tensor operators, which are consistently normalized, can be generally expanded[7, 23, 5, 6] as

$$\hat{T}_{\ell_1, m_1}(\vec{I}) \hat{T}_{\ell_2, m_2}(\vec{I}) = \sum_{J=|\ell_1 - \ell_2|}^{|\ell_1 + \ell_2|} \sum_{M=-J}^{J} B(\ell_1, \ell_2, J, I) \langle J M | \ell_1 \ell_2 m_1 m_2 \rangle \hat{T}_{J, M}(\vec{I}), \tag{S.61}$$

where the  $\hat{T}_{J,M}(\vec{I})$  for J=0 to J=3 are given in Table S3, and

$$B(\ell_1, \ell_2, J, I) = (2J + 1)^{1/2} \begin{pmatrix} -1 \end{pmatrix}^{J+2I} \begin{cases} \ell_1 & \ell_2 & J \\ I & I & I \end{cases} \frac{\langle I || \hat{\mathbf{T}}^{(\ell_1)}(\vec{I}) || I \rangle \langle I || \hat{\mathbf{T}}^{(\ell_2)}(\vec{I}) || I \rangle}{\langle I || \hat{\mathbf{T}}^{(J)}(\vec{I}) || I \rangle}.$$
 (S.62)

Here, the term in curly brackets is a 6-j symbol, and the reduced matrix elements are given by

$$\langle I||\hat{\mathbf{T}}^{(\ell)}(\vec{I})||I\rangle = \left[\frac{\ell!\ell!(2I+\ell+1)!}{2^{\ell}(2\ell)!(2I-\ell)!}\right]^{1/2}.$$
(S.63)

$\overline{M}$	$T_{0,M}(\vec{U},\vec{V})$	$T_{1,M}(ec{U},ec{V})$	$T_{2,M}(ec{U},ec{V})$
0	$-\frac{1}{\sqrt{3}}\vec{U}\cdot\vec{V}$	$-\frac{1}{2\sqrt{2}}[U_+V UV_+]$	$\frac{1}{\sqrt{6}} \left[ 3U_z V_z - \vec{U} \cdot \vec{V} \right]$
$\pm 1$	-	$\frac{1}{2}[U_zV_{\pm}-U_{\pm}V_z]$	$\mp \frac{1}{2} \left[ U_z V_{\pm} + U_{\pm} V_z \right]$
$\pm 2$	-	-	$\frac{1}{2}U_{\pm}V_{\pm}$

Table S2: Irreducible spherical tensors,  $T_{J,M}(\vec{U},\vec{V})$ , formed from the tensor product of two vectors  $\vec{U}$  and  $\vec{V}$ , and expressed in terms of their Cartesian components for  $J \leq 2$ .

$\overline{k}$	$\hat{T}_{0,k}(\vec{I})$	$\hat{T}_{1,M}(\vec{I})$	$\hat{T}_{2,M}(ec{I})$	$\hat{T}_{3,M}(ec{I})$
0	î	$\hat{I}_z$	$\left(\frac{1}{6}\right)^{1/2} \left[3\hat{I}_{z}^{2} - I(I+1)\right]$	$\left(\frac{1}{10}\right)^{1/2} \left[5\hat{I}_z^2 - (3I(I+1)-1)\right]\hat{I}_z$
$\pm 1$	-	$\mp \left(\frac{1}{2}\right)^{\tilde{1}/2} \hat{I}_{\pm}$	$\mp rac{1}{2} \left\{ \hat{I}_z, \hat{I}_\pm  ight\}$	$ \left( \frac{\left(\frac{1}{10}\right)^{1/2} \left[5\hat{I}_z^2 - \left(3I(I+1) - 1\right)\right]\hat{I}_z}{\mp \left(\frac{3}{10}\right)^{1/2} \frac{1}{4} \left\{ \left(5\hat{I}_z^2 - I(I+1) - \frac{1}{2}\right), \hat{I}_{\pm} \right\} } \right) $
$\pm 2$	-	-	$rac{1}{2}\hat{I}_{\pm}^2$	$\left(rac{3}{4} ight)^{1/2}rac{1}{2}\left\{\hat{I}_z,\hat{I}_\pm^2 ight\}$
<u>±3</u>	-	-	-	$\mp \frac{1}{2} \left(\frac{1}{2}\right)^{1/2} \hat{I}_{\pm}^{3}$

Table S3: Irreducible spherical tensor operators,  $\hat{T}_{J,M}(\vec{I})$  formed from the tensor product with the same vector and expressed in terms of Cartesian operators for  $J \leq 3$  after Buckmaster et al.[7, 5]. Here  $\{\hat{A}, \hat{B}\}$  represents the anticommutator of operators  $\hat{A}$  and  $\hat{B}$ .

### S2.3 Irreducible spherical tensor operator commutators

The commutator,  $[\hat{T}_{l_1,m_1}(\vec{I}),\hat{T}_{l_2,m_2}(\vec{I})]$ , can be written as

$$[\hat{T}_{l_1,m_1}(\vec{I}),\hat{T}_{l_2,m_2}(\vec{I})] = \sum_{J=|\ell_1-\ell_2|}^{|\ell_1+\ell_2|} \sum_{M=-J}^{J} B(\ell_1,\ell_2,J,I) \left[ \langle J M | \ell_1 \ell_2 m_1 m_2 \rangle - \langle J M | \ell_2 \ell_1 m_2 m_1 \rangle \right] \hat{T}_{J,M}(\vec{I}). \quad (S.64)$$

From Eq. (S.44) this simplifies to

$$[\hat{T}_{l_1,m_1}(\vec{I}),\hat{T}_{l_2,m_2}(\vec{I})] = \sum_{J=|\ell_1-\ell_2|}^{|\ell_1+\ell_2|} \sum_{M=-J}^{J} B(\ell_1,\ell_2,J,I) \left[ 1 - (-1)^{\ell_1+\ell_2-J} \right] \langle J \ M | \ell_1 \ \ell_2 \ m_1 \ m_2 \rangle \hat{T}_{J,M}(\vec{I}). \tag{S.65}$$

We narrow our focus to the specific commutator for non-zero values of m,

$$[\hat{T}_{l_1,m}(\vec{I}), \hat{T}_{2,-m}(\vec{I})] = \sum_{J=|\ell_1-2|}^{|\ell_1+2|} B(\ell_1, 2, J, I) \left[ 1 - (-1)^{\ell_1-J} \right] \langle J \ 0 | \ell_1 \ 2 \ m \ -m \rangle \hat{T}_{J,0}(\vec{I}). \tag{S.66}$$

Equation (S.66) shows that the coefficient vanishes when  $l_1 + J$  is an even value. Thus, for even values of  $l_1$ , only terms in the sum with odd values of J survive, and vice versa. Thus, we consider the two cases separately. For the odd value of  $l_1 = 1$ , we have

$$[\hat{T}_{1,m}(\vec{I}), \hat{T}_{2,-m}(\vec{I})] = 2B(1,2,2,I)\langle 2 \ 0|1 \ 2 \ m \ -m \rangle \, \hat{T}_{2,0}(\vec{I}), \tag{S.67}$$

and

$$[\hat{T}_{2,m}(\vec{I}), \hat{T}_{2,-m}(\vec{I})] = 2B(2,2,1,I) \langle 1 \ 0 | 2 \ 2 \ m \ -m \rangle \hat{T}_{1,0}(\vec{I}) + 2B(2,2,3,I) \langle 3 \ 0 | 2 \ 2 \ m \ -m \rangle \hat{T}_{3,0}(\vec{I}). \tag{S.68}$$

Focusing on B(1,2,2,I) we have

$$B(1,2,2,I) = [I(I+1)(2I+1)]^{1/2}(-1)^{2I}\sqrt{5} \left\{ \begin{array}{ccc} 1 & 2 & 2\\ I & I & I \end{array} \right\}.$$
 (S.69)

Using a symmetry property of the 6-j symbols, we can write

$$\left\{\begin{array}{ccc} 1 & 2 & 2\\ I & I & I \end{array}\right\} = \left\{\begin{array}{ccc} I & I & 2\\ 2 & 1 & I \end{array}\right\},\tag{S.70}$$

and use the general relationship

$$\left\{ \begin{array}{ccc} a & b & c \\ 2 & c-1 & b \end{array} \right\} = (-1)^{s+1} 2(X-c-1) \left[ \frac{6(s+1)(s-2c+1)(s-2b)(s-2a)(2b-2)!(2c-3)!}{(2b+3)!(2c+2)!} \right]^{1/2},$$
(S.71)

where s = a + b + c and X = -a(a + 1) + b(b + 1) + c(c + 1), to obtain

$$\left\{ \begin{array}{cc} I & I & 2\\ 2 & 1 & I \end{array} \right\} = -\sqrt{\frac{3}{10}} (-1)^{2I} \left[ \frac{1}{I(I+1)(2I+1)} \right]^{1/2}, \tag{S.72}$$

with s = 2(I+1) and X = 6. Thus, we obtain

$$B(1,2,2,I) = -\sqrt{\frac{3}{2}},\tag{S.73}$$

and

$$[\hat{T}_{1,m}(\vec{I}), \hat{T}_{2,-m}(\vec{I})] = -\sqrt{6} \langle 2 \ 0 | 1 \ 2 \ m \ -m \rangle \, \hat{T}_{2,0}(\vec{I}). \tag{S.74}$$

Similarly, one can show that

$$B(2,2,1,I) = \sqrt{\frac{2}{5}}[I(I+1) - 3/4], \quad \text{and} \quad B(2,2,3,I) = -2,$$
 (S.75)

and

$$[\hat{T}_{2,m}(\vec{I}), \hat{T}_{2,-m}(\vec{I})] = 2\sqrt{\frac{2}{5}}[I(I+1) - 3/4] \langle 1 \ 0|2 \ 2 \ m \ -m \rangle \hat{T}_{1,0}(\vec{I}) - 4\langle 3 \ 0|2 \ 2 \ m \ -m \rangle \hat{T}_{3,0}(\vec{I}). \tag{S.76}$$

### S3 Transition Symmetry Functions

In the symmetry pathway approach,[17], the concept of coherence order is extended to form a set of spin transition symmetry functions. A complete set of spin transition symmetry functions arising from the irreducible spherical tensor operators,  $\hat{T}_{\ell,0}$ , are given by

$$\xi_{\ell}(i,j) = \langle j|\hat{T}_{\ell,0}|j\rangle - \langle i|\hat{T}_{\ell,0}|i\rangle, \tag{S.77}$$

where the  $\hat{T}_{\ell,0}$  are irreducible tensor operators. The function symbol  $\xi_{\ell}(i,j)$  is replaced with the lower-case symbols  $\mathbb{P}(i,j)$ ,  $\mathbb{P}(i,j)$ ,  $\mathbb{P}(i,j)$ , ..., i.e., we follow the spectroscopic sub-shell letter designations:

To simplify usage in figures and discussions (but not in frequency expressions!), we scale the transition symmetry functions to integer values according to

$$p(i,j) = p(i,j), \quad d(i,j) = \sqrt{\frac{2}{3}} d(i,j), \quad f(i,j) = \sqrt{\frac{10}{9}} f(i,j), \quad \cdots$$
 (S.79)

The  $\ell = 0$  function is dropped as it evaluates to zero.

### S3.1 Single-spin transition symmetry functions

For a single spin, I, a complete set of functions is defined up to  $\ell = 2I$ . In the case of a single spin system,  $\{I\}$ , the integer-scaled transition symmetry functions evaluate to

$$p_{I}(m_{i}, m_{j}) = m_{j} - m_{i}, \quad d_{I}(m_{i}, m_{j}) = m_{j}^{2} - m_{i}^{2},$$

$$f_{I}(m_{i}, m_{j}) = \frac{1}{3} \left[ 5(m_{j}^{3} - m_{i}^{3}) + (1 - 3I(I + 1))(m_{j} - m_{i}) \right]. \quad (S.80)$$

Transition symmetry functions can be used to identify transitions in a spin-system agnostic manner. For example, by selecting only single-spin transitions with  $p_I = -1$ , you get all the "observed" transitions from the set of all possible transitions. Similarly, you can use  $p_I$  to select any subset of single-spin transitions, such as double-quantum ( $p_I = \pm 2$ ) transitions, triple-quantum ( $p_I = \pm 3$ ) transitions, etc. While specifying  $p_I$  alone is not enough to select an individual transition, any individual single-spin transition can be identified by a combination of the integer-scaled transition symmetry functions  $p_I$  and  $d_I$ . This is illustrated in Fig. S2A and S2B in the case of an integer spin nucleus. For single quantum  $p_I = -1$  transitions in an integer spin, we find  $d_I = \pm 1, \pm 3, \dots, \pm (2I - 1)$  with increasing spin I. While  $d_I = 0$  for symmetric  $m \to -m$  transitions, they remain distinguished by the opposite signs of  $p_I = \pm 2$ . Note that  $d_I$  values always evaluate to zero for symmetric  $m \to -m$  transitions. Similarly, in the case of the half-integer spins, we find that all transitions can be uniquely identified by their integer-scaled transition symmetry function values  $p_I$  and  $d_I$ , as illustrated in Figs. S2C and S2D, respectively. Here, we find that single quantum transitions with  $p_I = -1$  are distinguished by the opposite signs of  $d_I$ , which take on values of  $d_I = \pm 2$ ,  $\pm 4, \dots, \pm (2I - 1)$  with increasing spin I. When modeling an NMR method, single-spin transitions can be selected in a spin-system agnostic fashion by specifying the desired  $p_I$  and  $d_I$  values. One caveat, however, is that the  $(p_I, d_I)$  combination specified for a given  $m_I \to m_I$  transition depends on whether the spin is integer or half-integer.

For 2nd-order quadrupolar coupling frequency contributions, it is convenient to define "hybrid" spin transition functions as linear combinations of the spin transition functions

$$c_0 = \frac{4}{\sqrt{125}} \left[ I(I+1) - 3/4 \right] p_I + \sqrt{\frac{18}{25}} f_I,$$

$$c_2 = \frac{2}{\sqrt{175}} \left[ I(I+1) - 3/4 \right] p_I - \frac{6}{\sqrt{35}} f_I,$$

$$c_4 = -\frac{184}{\sqrt{875}} \left[ I(I+1) - 3/4 \right] p_I - \frac{17}{\sqrt{175}} f_I.$$
(S.81)

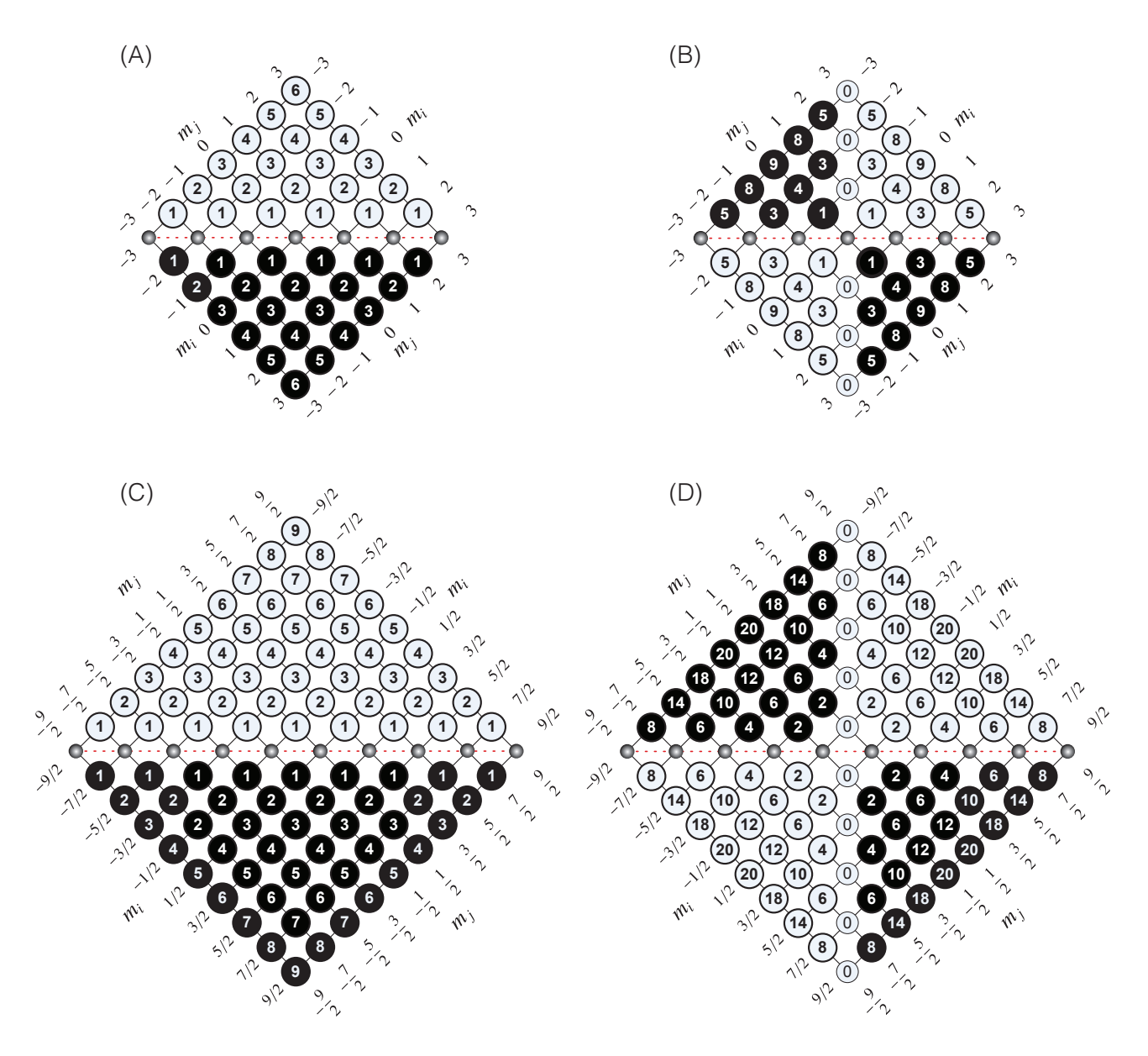


Figure S2: Values of the integer-scaled spin transition symmetry function for (A)  $p_I(m_i, m_j)$  and (B)  $d_I(m_i, m_j)$  for integer spin values, and (C)  $p_I(m_i, m_j)$  and (D)  $d_I(m_i, m_j)$  for half-integer spin values. Values inside black circles are negative.

$\boxed{m_{A,i}, m_{M,i}, m_{X,i} \rightarrow m_{A,j}, m_{M,j}, m_{X,j}}$	Label	$p_A$	$p_M$	$p_X$	$(pp)_{AM}$	$(pp)_{AX}$	$(pp)_{MX}$
$+\frac{1}{2}, +\frac{1}{2}, +\frac{1}{2} \rightarrow -\frac{1}{2}, +\frac{1}{2}, +\frac{1}{2}$	$\hat{A}_1$	-1	0	0	-1	-1	0
$+\frac{1}{2}, -\frac{1}{2}, +\frac{1}{2} \rightarrow -\frac{1}{2}, -\frac{1}{2}, +\frac{1}{2}$	$\hat{A}_2$	-1	0	0	+1	-1	0
$+\frac{1}{2}, +\frac{1}{2}, -\frac{1}{2} \rightarrow -\frac{1}{2}, +\frac{1}{2}, -\frac{1}{2}$	$\hat{A}_3$	-1	0	0	-1	+1	0
$+\frac{1}{2}, -\frac{1}{2}, -\frac{1}{2} \rightarrow -\frac{1}{2}, -\frac{1}{2}, -\frac{1}{2}$	$\hat{A}_4$	-1	0	0	+1	+1	0
$+\frac{1}{2}, +\frac{1}{2}, -\frac{1}{2} \to +\frac{1}{2}, -\frac{1}{2}, -\frac{1}{2}$	$\hat{M}_1$	0	-1	0	-1	0	+1
$+\frac{1}{2}, +\frac{1}{2}, +\frac{1}{2} \rightarrow +\frac{1}{2}, -\frac{1}{2}, +\frac{1}{2}$	$\hat{M}_2$	0	-1	0	-1	0	-1
$-\frac{1}{2}, +\frac{1}{2}, -\frac{1}{2} \rightarrow -\frac{1}{2}, -\frac{1}{2}, -\frac{1}{2}$	$\hat{M}_3$	0	-1	0	+1	0	+1
$-\frac{1}{2}, +\frac{1}{2}, +\frac{1}{2} \rightarrow -\frac{1}{2}, -\frac{1}{2}, +\frac{1}{2}$	$\hat{M}_4$	0	-1	0	+1	0	-1
$-\frac{1}{2}, -\frac{1}{2}, +\frac{1}{2} \to -\frac{1}{2}, -\frac{1}{2}, -\frac{1}{2}$	$\hat{X}_1$	0	0	-1	0	+1	+1
$-\frac{1}{2}, +\frac{1}{2}, +\frac{1}{2} \rightarrow -\frac{1}{2}, +\frac{1}{2}, -\frac{1}{2}$	$\hat{X}_2$	0	0	-1	0	+1	-1
$+\frac{1}{2}, -\frac{1}{2}, +\frac{1}{2} \to +\frac{1}{2}, -\frac{1}{2}, -\frac{1}{2}$	$\hat{X}_3$	0	0	-1	0	-1	+1
$+\frac{1}{2}, +\frac{1}{2}, +\frac{1}{2} \to +\frac{1}{2}, +\frac{1}{2}, -\frac{1}{2}$	$\hat{X}_4$	0	0	-1	0	-1	-1
$+\frac{1}{2}, +\frac{1}{2}, -\frac{1}{2} \rightarrow -\frac{1}{2}, -\frac{1}{2}, +\frac{1}{2}$	$\hat{S}_1$	-1	-1	+1	0	0	0
$+\frac{1}{2}, -\frac{1}{2}, +\frac{1}{2} \rightarrow -\frac{1}{2}, +\frac{1}{2}, -\frac{1}{2}$	$\hat{S}_2$	-1	+1	-1	0	0	0
$-\frac{1}{2}, +\frac{1}{2}, +\frac{1}{2} \to +\frac{1}{2}, -\frac{1}{2}, -\frac{1}{2}$	$\hat{S}_3$	+1	-1	-1	0	0	0

Table S4: Values of  $\mathbb{p}_A$ ,  $\mathbb{p}_M$ ,  $\mathbb{p}_X$ ,  $(\mathbb{pp})_{AM}$ ,  $(\mathbb{pp})_{AX}$ , and  $(\mathbb{pp})_{MX}$  for the  $\mathbb{p}_{AMX} = -1$  single quantum transitions of three weakly coupled spin 1/2 nuclei illustrated in Figs. S4 and S5.

### S3.2 Multi-spin transition symmetry functions

For  $n_I$  weakly coupled nuclei, we define the multi-spin transition symmetry functions

$$\xi_{\ell_1,\ell_2,\dots,\ell_{n_I}}(i,j) = \langle j | \hat{T}_{\ell_1,0}(\vec{I}_1) \hat{T}_{\ell_2,0}(\vec{I}_2) \dots \hat{T}_{\ell_{n_I},0}(\vec{I}_{n_I}) | j \rangle - \langle i | \hat{T}_{\ell_1,0}(\vec{I}_1) \hat{T}_{\ell_2,0}(\vec{I}_2) \dots \hat{T}_{\ell_{n_I},0}(\vec{I}_{n_I}) | i \rangle. \tag{S.82}$$

### S3.2.1 Single-spin transition functions

Replacing the symmetry function symbol using sub-shell letter designations becomes more cumbersome in this case. When the  $\ell$  values are zero on all nuclei except one, we identify these single-spin functions as

$$\mathbb{P}_{1} = \xi_{1,0,\dots,0}(i,j), \quad \mathbb{P}_{2} = \xi_{0,1,\dots,0}(i,j), \quad \dots, \quad \mathbb{P}_{n_{I}} = \xi_{0,0,\dots,1}(i,j), 
d_{1} = \xi_{2,0,\dots,0}(i,j), \quad d_{2} = \xi_{0,2,\dots,0}(i,j), \quad \dots, \quad d_{n_{I}} = \xi_{0,0,\dots,2}(i,j), 
f_{1} = \xi_{3,0,\dots,0}(i,j), \quad f_{2} = \xi_{0,3,\dots,0}(i,j), \quad \dots, \quad f_{n_{I}} = \xi_{0,0,\dots,3}(i,j), 
\vdots \qquad \vdots \qquad \vdots$$
(S.83)

The set of nuclei,  $\mathfrak{I}$ , in a spin system can be partitioned into  $n_{\mathfrak{I}}$  disjoint subsets of  $\{\mathfrak{I}_{1},\mathfrak{I}_{2},\ldots,\mathfrak{I}_{n_{\mathfrak{I}}}\}$ , called *channels*, where  $\mathfrak{I}_{c}$  is the set of nuclei in the  $c^{\text{th}}$  subset, i.e., the  $c^{\text{th}}$  channel. This partitioning is useful for separating nuclei into subsets of nuclei of the same isotope, although it could also be used to separate nuclei into subsets for other purposes, such as selective excitation of a subset of nuclei within a specific excitation bandwidth. When working with such subsets, i.e., channels, it is useful to define the functions

$$p_c(i,j) = \sum_{u \in \mathfrak{I}_c} p_u(i,j), \quad d_c(i,j) = \sum_{u \in \mathfrak{I}_c} d_u(i,j), \quad \mathbb{f}_c(i,j) = \sum_{u \in \mathfrak{I}_c} \mathbb{f}_u(i,j), \quad \cdots$$
 (S.84)

While these functions are not used in evaluating frequency contributions, they can be utilized to select sets of transitions.

These are illustrated in Fig. S3 in the case of two coupled spin I = 1/2 nuclei. For three coupled spin I = 1/2 nuclei, the transition symmetry functions are illustrated in Figs. S4, S5, and S6 and in Tables S4, S5 and S6.

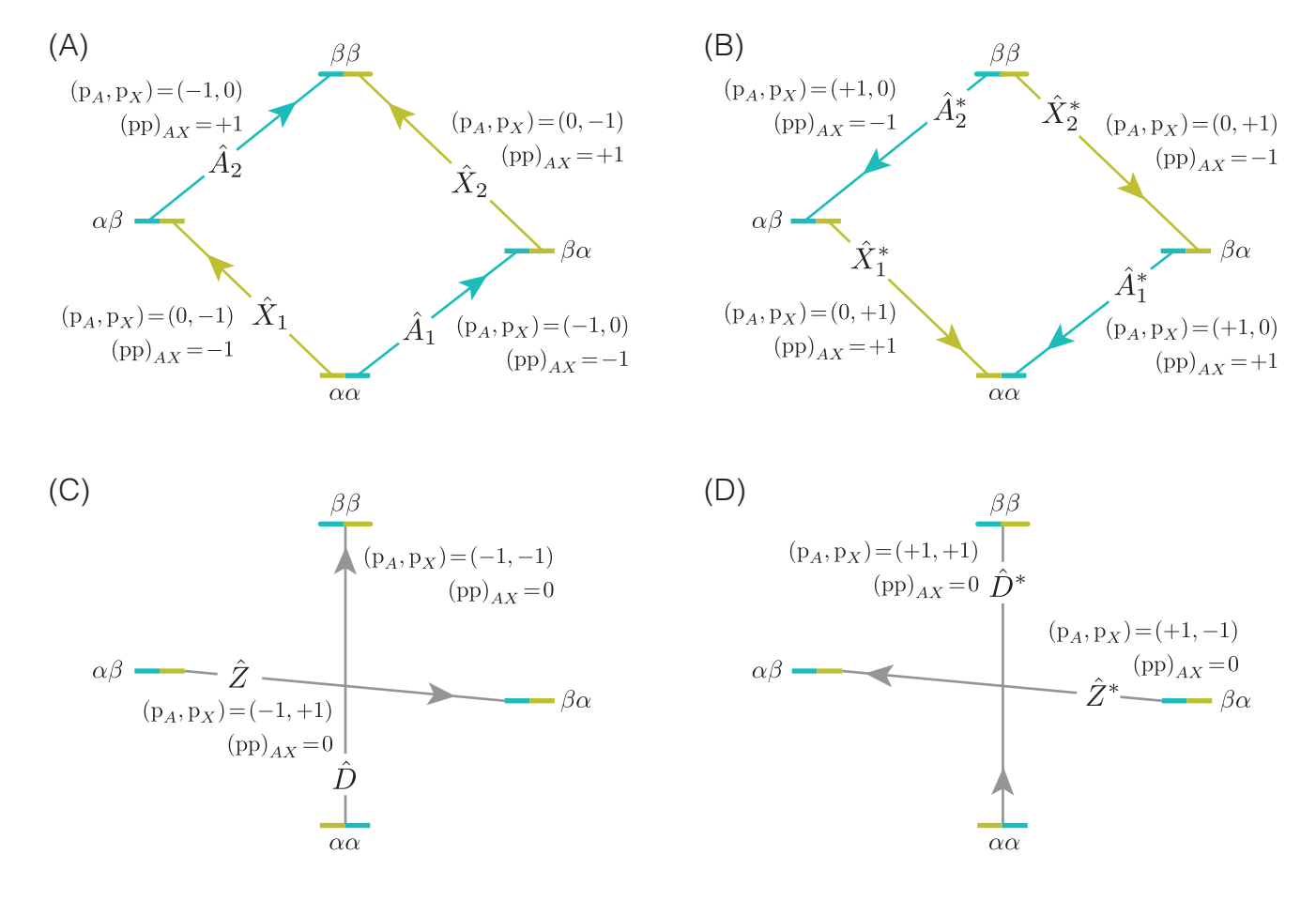


Figure S3: Energy level diagram of two coupled spin I=1/2 nuclei, where  $\alpha=m=+1/2$  and  $\beta=m=-1/2$ , with transition labeled according to their transition symmetry function values for (A)  $p_{AX}=-1$  transitions, i.e.,  $\hat{A}_1$ ,  $\hat{A}_2$ ,  $\hat{X}_1$ , and  $\hat{X}_2$ , (B)  $p_{AX}=-1$  transitions, i.e.,  $\hat{A}_1^*$ ,  $\hat{A}_2^*$ ,  $\hat{X}_1^*$ , and  $\hat{X}_2^*$ , (C)  $p_{AX}=-2$  transitions, i.e.,  $\hat{D}$  and  $\hat{Z}$ , and (D)  $p_{AX}=+2$  transitions, i.e.,  $\hat{D}^*$  and  $\hat{Z}^*$ . Note that each transition has a unique set of transition symmetry function values,  $p_A$ ,  $p_X$ , and  $(pp)_{AX}$ .

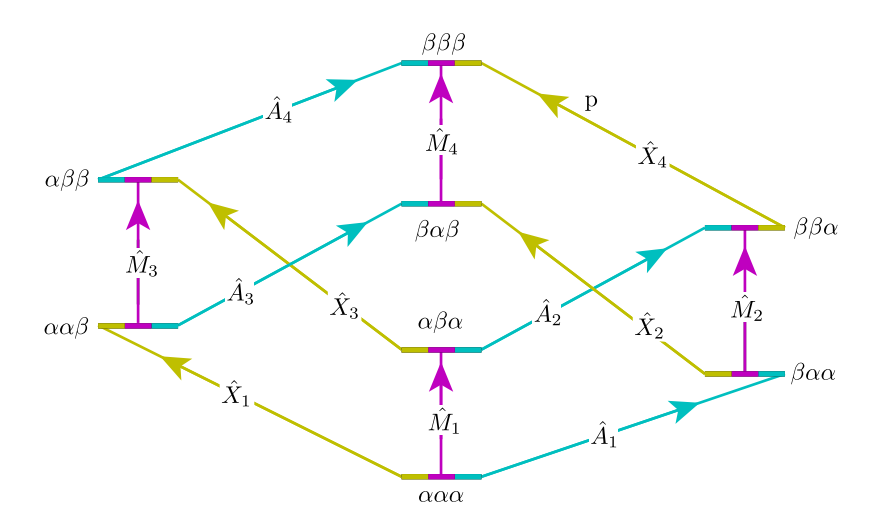


Figure S4: Energy level diagram for three coupled spin I=1/2 nuclei and the corresponding single-spin single-quantum transitions. Arrows beginning at the initial state and ending at the final state represent the single-spin single-quantum transitions. Transitions are labeled with their corresponding single-spin  $p_i$  transition symmetry function values.

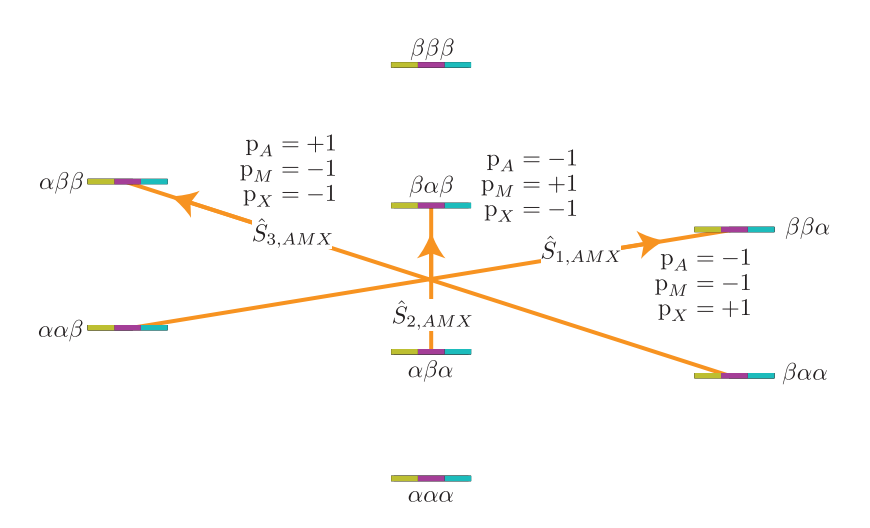


Figure S5: Energy level diagram for three coupled spin I=1/2 nuclei and the corresponding three-site single-quantum transitions. Arrows beginning at the initial state and ending at the final state represent the single-spin single-quantum transitions. Transitions are labeled with their corresponding single-spin  $p_i$  transition symmetry function values.

$\boxed{m_{A,i}, m_{M,i}, m_{X,i} \rightarrow m_{A,j}, m_{M,j}, m_{X,j}}$	Label	$p_A$	$p_M$	$p_X$	$(pp)_{AM}$	$(pp)_{AX}$	$(pp)_{MX}$
$-\frac{1}{2}, +\frac{1}{2}, +\frac{1}{2} \to +\frac{1}{2}, +\frac{1}{2}, +\frac{1}{2}$	$\hat{A}_1^*$	+1	0	0	+1	+1	0
$-\frac{1}{2}, -\frac{1}{2}, +\frac{1}{2} \to +\frac{1}{2}, -\frac{1}{2}, +\frac{1}{2}$	$\hat{A}_2^*$	+1	0	0	-1	+1	0
$-\frac{1}{2}, +\frac{1}{2}, -\frac{1}{2} \to +\frac{1}{2}, +\frac{1}{2}, -\frac{1}{2}$	$\hat{A}_3^*$	+1	0	0	+1	-1	0
$-\frac{1}{2}, -\frac{1}{2}, -\frac{1}{2} \to +\frac{1}{2}, -\frac{1}{2}, -\frac{1}{2}$	$\hat{A}_4^*$	+1	0	0	-1	-1	0
$+\frac{1}{2}, -\frac{1}{2}, -\frac{1}{2} \to +\frac{1}{2}, +\frac{1}{2}, -\frac{1}{2}$	$\hat{M}_1^*$	0	+1	0	+1	0	-1
$+\frac{1}{2}, -\frac{1}{2}, +\frac{1}{2} \to +\frac{1}{2}, +\frac{1}{2}, +\frac{1}{2}$	$\hat{M}_2^*$	0	+1	0	+1	0	+1
$-\frac{1}{2}, -\frac{1}{2}, -\frac{1}{2} \to -\frac{1}{2}, +\frac{1}{2}, -\frac{1}{2}$	$\hat{M}_3^*$	0	+1	0	-1	0	-1
$-\frac{1}{2}, -\frac{1}{2}, +\frac{1}{2} \to -\frac{1}{2}, +\frac{1}{2}, +\frac{1}{2}$	$\hat{M}_4^*$	0	+1	0	-1	0	+1
$-\frac{1}{2}, -\frac{1}{2}, -\frac{1}{2} \to -\frac{1}{2}, -\frac{1}{2}, +\frac{1}{2}$	$\hat{X}_1^*$	0	0	+1	0	-1	-1
$-\frac{1}{2}, +\frac{1}{2}, -\frac{1}{2} \rightarrow -\frac{1}{2}, +\frac{1}{2}, +\frac{1}{2}$	$\hat{X}_2^*$	0	0	+1	0	-1	+1
$+\frac{1}{2}, -\frac{1}{2}, -\frac{1}{2} \to +\frac{1}{2}, -\frac{1}{2}, +\frac{1}{2}$	$\hat{X}_3^*$	0	0	+1	0	+1	-1
$+\frac{1}{2}, +\frac{1}{2}, -\frac{1}{2} \to +\frac{1}{2}, +\frac{1}{2}, +\frac{1}{2}$	$\hat{X}_4^*$	0	0	+1	0	+1	+1
$-\frac{1}{2}, -\frac{1}{2}, +\frac{1}{2} \to +\frac{1}{2}, +\frac{1}{2}, -\frac{1}{2}$	$\hat{S}_1^*$	+1	+1	-1	0	0	0
$-\frac{1}{2}, +\frac{1}{2}, -\frac{1}{2} \to +\frac{1}{2}, -\frac{1}{2}, +\frac{1}{2}$	$\hat{S}_2^*$	+1	-1	+1	0	0	0
$+\frac{1}{2}, -\frac{1}{2}, -\frac{1}{2} \rightarrow -\frac{1}{2}, +\frac{1}{2}, +\frac{1}{2}$	$\hat{S}_3^*$	-1	+1	+1	0	0	0

Table S5: Values of  $\mathbb{p}_A$ ,  $\mathbb{p}_M$ ,  $\mathbb{p}_X$ ,  $(\mathbb{pp})_{AM}$ ,  $(\mathbb{pp})_{AX}$ , and  $(\mathbb{pp})_{MX}$  for the  $\mathbb{p}_{AMX} = +1$  single quantum transitions of three weakly coupled spin 1/2 nuclei.

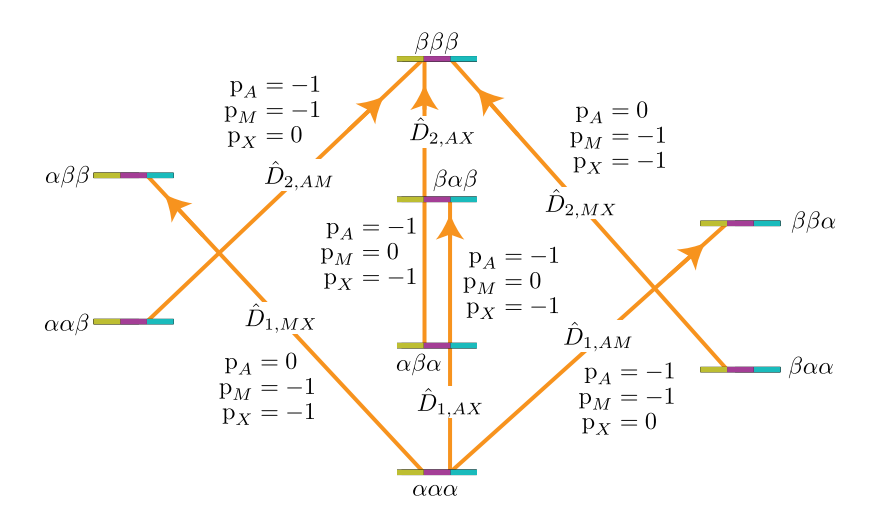


Figure S6: Energy level diagram for three coupled spin I=1/2 nuclei and the corresponding three-spin  $\mathbb{P}_{AMX}=-2$  transitions. Arrows beginning at the initial state and ending at the final state represent the three-spin double-quantum transitions. Transitions are labeled with their corresponding single-spin  $\mathbf{p}_i$  transition symmetry function values.

$m_{A,i}, m_{M,i}, m_{X,i} \rightarrow m_{A,j}, m_{M,j}, m_{X,j}$	Label	$p_A$	$p_M$	$p_X$	$(pp)_{AM}$	$(pp)_{AX}$	$(pp)_{MX}$	$p_{AMX}$
$+\frac{1}{2}, +\frac{1}{2}, +\frac{1}{2} \rightarrow -\frac{1}{2}, +\frac{1}{2}, -\frac{1}{2}$	$\hat{D}_{1,AX}$	-1	0	-1	-1	0	-1	-2
$+\frac{1}{2}, +\frac{1}{2}, +\frac{1}{2} \rightarrow -\frac{1}{2}, -\frac{1}{2}, +\frac{1}{2}$	$\hat{D}_{1,AM}$	-1	-1	0	0	-1	-1	-2
$+\frac{1}{2}, +\frac{1}{2}, +\frac{1}{2} \to +\frac{1}{2}, -\frac{1}{2}, -\frac{1}{2}$	$\hat{D}_{1,MX}$	0	-1	-1	-1	-1	0	-2
$+\frac{1}{2}, -\frac{1}{2}, +\frac{1}{2} \rightarrow -\frac{1}{2}, -\frac{1}{2}, -\frac{1}{2}$	$\hat{D}_{2,AX}$	-1	0	-1	+1	0	+1	-2
$+\frac{1}{2}, +\frac{1}{2}, -\frac{1}{2} \rightarrow -\frac{1}{2}, -\frac{1}{2}, -\frac{1}{2}$	$\hat{D}_{2,AM}$	-1	-1	0	0	+1	+1	-2
$-\frac{1}{2}, +\frac{1}{2}, +\frac{1}{2} \rightarrow -\frac{1}{2}, -\frac{1}{2}, -\frac{1}{2}$	$\hat{D}_{2,MX}$	0	-1	-1	+1	+1	0	-2
$-\frac{1}{2}, +\frac{1}{2}, -\frac{1}{2} \to +\frac{1}{2}, +\frac{1}{2}, +\frac{1}{2}$	$\hat{D}_{1,AX}^*$	+1	0	+1	+1	0	+1	+2
$-\frac{1}{2}, -\frac{1}{2}, +\frac{1}{2} \to +\frac{1}{2}, +\frac{1}{2}, +\frac{1}{2}$	$\hat{D}_{1,AM}^*$	+1	+1	0	0	+1	+1	+2
$+\frac{1}{2}, -\frac{1}{2}, -\frac{1}{2} \to +\frac{1}{2}, +\frac{1}{2}, +\frac{1}{2}$	$\hat{D}_{1,MX}^*$	0	+1	+1	+1	+1	0	+2
$-\frac{1}{2}, -\frac{1}{2}, -\frac{1}{2} \to +\frac{1}{2}, -\frac{1}{2}, +\frac{1}{2}$	$\hat{D}_{2,AX}^*$	+1	0	+1	-1	0	-1	+2
$-\frac{1}{2}, -\frac{1}{2}, -\frac{1}{2} \to +\frac{1}{2}, +\frac{1}{2}, -\frac{1}{2}$	$\hat{D}_{2,AM}^*$	+1	+1	0	0	-1	-1	+2
$-\frac{1}{2}, -\frac{1}{2}, -\frac{1}{2} \to -\frac{1}{2}, +\frac{1}{2}, +\frac{1}{2}$	$\hat{D}_{2,MX}^*$	0	+1	+1	-1	-1	0	+2
$+\frac{1}{2}, +\frac{1}{2}, +\frac{1}{2} \rightarrow -\frac{1}{2}, -\frac{1}{2}, -\frac{1}{2}$	$\hat{T}_{1,AMX}$	-1	-1	-1	0	0	0	-3
$-\frac{1}{2}, -\frac{1}{2}, -\frac{1}{2} \to +\frac{1}{2}, +\frac{1}{2}, +\frac{1}{2}$	$\hat{T}_{1,AMX}^*$	+1	+1	+1	0	0	0	+3

Table S6: Values of  $p_A$ ,  $p_M$ ,  $p_M$ ,  $(pp)_{AM}$ ,  $(pp)_{AX}$ , and  $(pp)_{MX}$  for the  $p_{AMX} = \pm 2$  and  $\pm 3$  transitions of three weakly coupled spin 1/2 nuclei illustrated in Fig. S6.

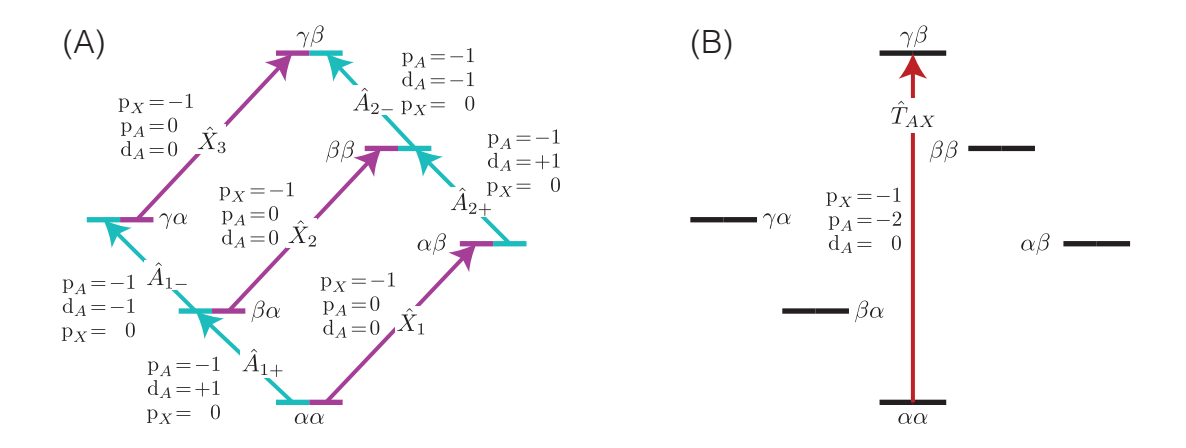


Figure S7: Energy level diagram for two coupled nuclei with spins I = 1 and I = 1/2. Arrows beginning at the initial state and ending at the final state represent the single-spin single-quantum transitions (left) and the two-spin triple-quantum transition. Transitions are labeled with their corresponding  $p_i$  and  $d_i$  single-spin transition symmetry function values.

#### S3.2.2 Two-spin transition functions

When the  $\ell$  values are zero on all nuclei except two, then we identify these two-spin functions using a concatenation of sub-shell letter designations, e.g.,

$$(\mathbb{pp})_{1,2} = \xi_{1,1,0,\dots,0}(i,j), \quad (\mathbb{pp})_{1,3} = \xi_{1,0,1,\dots,0}(i,j), \quad \dots, \quad (\mathbb{pp})_{1,n_I} = \xi_{1,0,0,\dots,1}(i,j),$$

$$(\mathbb{pd})_{1,2} = \xi_{1,2,0,\dots,0}(i,j), \quad (\mathbb{pd})_{1,3} = \xi_{1,0,2,\dots,0}(i,j), \quad \dots, \quad (\mathbb{pd})_{1,n_I} = \xi_{1,0,\dots,2}(i,j),$$

$$(\mathbb{dp})_{1,2} = \xi_{2,1,0,\dots,0}(i,j), \quad (\mathbb{dp})_{1,3} = \xi_{2,0,1,\dots,0}(i,j), \quad \dots, \quad (\mathbb{dp})_{1,n_I} = \xi_{2,0,\dots,1}(i,j),$$

$$\vdots \qquad \qquad \vdots \qquad \qquad \vdots$$

$$(S.85)$$

As before, to simplify usage in figures and discussions, we further define integer-scaled transition symmetry functions, e.g.,

$$(pp)_{IS}(m_{I,i}, m_{S,i}, m_{I,j}, m_{S,j}) = 2(pp)_{IS}(m_{I,i}, m_{S,i}, m_{I,j}, m_{S,j}),$$
(S.86)

$$(dp)_{IS}(m_{I,i}, m_{S,i}, m_{I,j}, m_{S,j}) = 2\sqrt{6} (dp)_{IS}(m_{I,i}, m_{S,i}, m_{I,j}, m_{S,j}), \tag{S.87}$$

$$(pd)_{IS}(m_{I,i}, m_{S,i}, m_{I,j}, m_{S,j}) = 2\sqrt{6} (pd)_{IS}(m_{I,i}, m_{S,i}, m_{I,j}, m_{S,j}),$$
(S.88)

which evaluate to

$$(pp)_{IS}(m_{I,i}, m_{S,i}, m_{I,j}, m_{S,j}) = 2m_{I,j}m_{S,j} - 2m_{I,i}m_{S,i}$$
 for  $I \ge \frac{1}{2}$ ,  $S \ge \frac{1}{2}$ , (S.89)

$$(\mathrm{dp})_{IS}(m_{I,i}, m_{S,i}, m_{I,j}, m_{S,j}) = 6\left(m_{I,j}^2 m_{S,j} - m_{I,i}^2 m_{S,i}\right) - 2I(I+1)(m_{S,j} - m_{S,i}), \quad \text{for } I \ge 1, S \ge \frac{1}{2}, \quad (S.90)$$

$$(\mathrm{pd})_{IS}(m_{I,i}, m_{S,i}, m_{I,j}, m_{S,j}) = 6\left(m_{S,j}^2 m_{I,j} - m_{S,i}^2 m_{I,i}\right) - 2S(S+1)(m_{I,j} - m_{I,i}). \quad \text{for } I \ge \frac{1}{2}, S \ge 1. \quad (S.91)$$

The two-spin functions are needed for frequency contributions arising from first-order dipolar and J couplings and cross-terms involving dipolar couplings in a second-order perturbation theory treatment of a sizeable quadrupolar coupling. Values of  $(pp)_{IS}$  are illustrated in Fig. S3 for two coupled spin 1/2 nuclei, and in Tables S4, S5 and S6. Again, we see in coupled spin systems that transition symmetry functions can be used to identify transitions in a spin-system agnostic manner.

Three- or higher-spin functions occur in higher-order perturbation theory cross-terms, which are not considered here.

# S4 Perturbation theory

In the absence of excitation, the spins evolve under the stationary state Hamiltonian,  $\hat{\mathcal{H}}_S$ , whose representation in its diagonal frame,  $\hat{D}_S$ , is related to the laboratory frame representation by

$$\hat{D}_S = \hat{V}^{\dagger} \hat{\mathcal{H}}_S \hat{V}, \tag{S.92}$$

where  $\hat{V}$  is a unitary transformation between the diagonal and laboratory frames. Here, we consider a Hamiltonian whose diagonalization transformation, *i.e.*,  $\hat{V}$ , is time-independent. See reference [36] for the case of a time-dependent diagonalization in the context of rotating samples treated using the adiabatic approximation.

We assume that the Zeeman interaction is the dominant interaction in  $\hat{\mathcal{H}}_S$ ,

$$\hat{\mathcal{H}}_S = \hbar \omega_0 \hat{I}_Z + \hat{\mathcal{H}}_S^{(1)},\tag{S.93}$$

where  $\omega_0 = -\gamma B_0$  and

$$\hat{\mathcal{H}}_S^{(1)} = \sum_{\lambda \in \Gamma} \hat{\mathcal{H}}_\lambda^{(1)} \tag{S.94}$$

is the part of the stationary state Hamiltonian arising from a set  $\Gamma = \{q, \sigma, J, d\}$  of spin couplings internal to the sample. Using the static perturbation approach, as outlined by Goldman et al.[16], and limited here to non-degenerate systems,  $\hat{D}_S$  and  $\hat{V}$  can be obtained through the perturbation expansion,

$$\hat{D}_S = \hat{\mathcal{H}}^{(0)} + \hat{D}^{(1)} + \hat{D}^{(2)} + \cdots, \tag{S.95}$$

$$\hat{V} = \hat{1} + \hat{V}^{(1)} + \hat{V}^{(2)} + \cdots, \tag{S.96}$$

with each correction given by

$$\hat{D}^{(n)} = \sum_{i=1}^{\Upsilon} E_i^{(n)} |i\rangle\langle i|, \tag{S.97}$$

$$\hat{V}^{(n)} = \sum_{i=1}^{\Upsilon} \left| v_i^{(n)} \right\rangle \langle i|, \tag{S.98}$$

where  $\Upsilon$  is the number of states and the eigenvalues,  $E_i^{(n)}$ , and eigenvectors  $\left|v_i^{(n)}\right\rangle$ , can be obtained with conventional static perturbation theory[25]:

$$E_i^{(0)} = \langle i | \hat{\mathcal{H}}^{(0)} | i \rangle. \tag{S.99}$$

$$E_i^{(1)} = \sum_{\lambda \in \Gamma} \langle i | \hat{\mathcal{H}}_{\lambda}^{(1)} | i \rangle, \tag{S.100}$$

$$E_{i}^{(2)} = \sum_{\lambda \in \Gamma} \left[ \sum_{\substack{i=1\\j \neq i}}^{\Upsilon} \frac{\langle i | \hat{\mathcal{H}}_{\lambda}^{(1)} | j \rangle \langle j | \hat{\mathcal{H}}_{\lambda}^{(1)} | i \rangle}{E_{i}^{(0)} - E_{j}^{(0)}} \right] + \sum_{\lambda \in \Gamma} \sum_{\substack{\lambda' \in \Gamma\\\lambda' \neq \lambda}} \left[ \sum_{\substack{i=1\\j \neq i}}^{\Upsilon} \frac{\langle i | \hat{\mathcal{H}}_{\lambda}^{(1)} | j \rangle \langle j | \hat{\mathcal{H}}_{\lambda'}^{(1)} | i \rangle}{E_{i}^{(0)} - E_{j}^{(0)}} \right], \tag{S.101}$$

$$\left|v_i^{(1)}\right\rangle = \sum_{\lambda \in \Gamma} \left[ \sum_{\substack{i=1\\ i \neq j}}^{\Upsilon} \frac{\langle j | \hat{\mathcal{H}}_{\lambda}^{(1)} | i \rangle}{E_i^{(0)} - E_j^{(0)}} | j \rangle \right], \tag{S.102}$$

$$E_i^{(3)} = \sum_{k \neq i} \sum_{j \neq i} \frac{\langle i|\hat{\mathcal{H}}_{\lambda}^{(1)}|i\rangle\langle j|\hat{\mathcal{H}}_{\lambda}^{(1)}|k\rangle\langle k|\hat{\mathcal{H}}_{\lambda}^{(1)}|i\rangle}{\left(E_i^{(0)} - E_m^{(0)}\right) \left(E_i^{(0)} - E_k^{(0)}\right)} - \langle i|\hat{\mathcal{H}}_{\lambda}^{(1)}|i\rangle \sum_{j \neq i} \frac{|\langle i|\hat{\mathcal{H}}_{\lambda}^{(1)}|j\rangle|^2}{\left(E_i^{(0)} - E_j^{(0)}\right)^2}.$$
 (S.103)

The expression for the third-order correction to the eigenvalues excludes cross-terms.

In NMR, the number of states,  $\Upsilon$ , is given by

$$\Upsilon_{\{I_1, I_2, \dots, I_N\}} = \prod_{u=1}^{N} (2I_u + 1). \tag{S.104}$$

Here,  $I_u$  is the total spin angular momentum quantum number of the uth nucleus,

Operators in terms of matrix elements and outer products are obtained when Eqs (S.97) and (S.98) are combined with Eqs. (S.100)-(S.101). As we show below, these matrix elements and outer products can be readily simplified in the case of NMR using the general selection rule for irreducible tensors,

$$\langle j|\hat{T}_{\ell,m}|i\rangle = \delta_{j,i+m}\langle i+m|\hat{T}_{\ell,m}|i\rangle,$$
 (S.105)

to obtain pure irreducible tensor expansions for the  $\hat{D}_S$  and  $\hat{V}$  operators[16]. Here, we will consider only fundamental transitions, that is, Zeeman allowed ( $\Delta m = \pm 1$ ) transitions. For such situations, the transformation,  $\hat{V}$ , between the laboratory and diagonal frame[16, 36], will, to a good approximation, not need evaluation.

We will only consider the quadrupolar coupling strong enough to require a correction higher than the first order at conventional NMR magnetic field strengths. Note, however, that the second- and higher-order corrections involve the product of matrix elements and will mix matrix elements coming from different contributions to  $\hat{\mathcal{H}}_S^{(1)}$ . While the second-order terms involving the product of quadrupolar Hamiltonian matrix elements will be the largest, there will be situations where cross-terms between the quadrupolar coupling and the nuclear shielding, J, or dipolar couplings will not be negligible [37, 35, 30, 20, 26, 41, 27, 21, 29, 28]. Additionally, there will be situations where third-order corrections are not negligible, particularly for non-symmetric transitions of quadrupolar nuclei [15, 4, 36].

# S5 Hamiltonians and Transition Frequency Contributions

This section summarizes the SPT Hamiltonians and frequency expressions derived in the appendix of our symmetry pathways paper [17]—updated to include the latest definitions and conventions used here. These expressions also correct a few typographical errors in the original article[17] appendix.

Using the definitions of this section, including Tables S7 and S2, one can write the NMR Hamiltonian contributions terms of irreducible tensor elements of ranks L=0, 1, and 2 in the lab coordinate system as

$$\hat{\mathcal{H}}_{\lambda} = \Lambda^{\{\lambda\}} \sum_{L=0}^{2} \sum_{m=-L}^{L} (-1)^{m} R_{L,-m}^{\{\lambda\}} \hat{T}_{L,m}^{\{\lambda\}} (\hat{\vec{U}}, \vec{V}). \tag{S.106}$$

Here,  $R_{L,-m}^{\{\lambda\}}$  are the spherical tensor elements, and  $\hat{T}_{L,m}^{\{\lambda\}}(\vec{\hat{U}},\vec{V})$  are the irreducible spherical tensor element operators. With the definitions of the previous sections in place, we give results for various first- and second-order corrections to the NMR frequency.

#### S5.1 Zeeman

The Zeeman Hamiltonian is

$$\hat{\mathcal{H}}_z = -\vec{\hat{\mu}} \cdot \vec{B} = -\hbar \gamma_I \vec{\hat{I}} \cdot \vec{B},\tag{S.107}$$

where

$$\vec{\hat{\mu}} = \gamma_I \hbar \hat{\hat{I}}. \tag{S.108}$$

Since  $\vec{B} = (0, 0, B_0)$ , we have

$$\hat{\mathcal{H}}_z/\hbar = \omega_0 \hat{I}_z,\tag{S.109}$$

where  $\omega_0 = -\gamma_I B_0$ .

### S5.2 Electric quadrupole coupling

In the principal axis system of the EFG tensor, where the principal components of the second-rank symmetric Cartesian EFG tensor are  $\lambda_{xx}^{\{q\}}$ ,  $\lambda_{yy}^{\{q\}}$ , and  $\lambda_{zz}^{\{q\}}$ , we define

$$\rho_{2,0}^{\{q\}} = \sqrt{\frac{3}{2}} \zeta_q, \quad \rho_{2,\pm 1}^{\{q\}} = 0, \quad \rho_{2,\pm 2}^{\{q\}} = -\eta_q \zeta_q / 2, \tag{S.110}$$

where the second-rank symmetric EFG tensor anisotropy,  $\zeta_q$ , is defined as

$$\zeta_q = \lambda_{zz}^{\{q\}},\tag{S.111}$$

	quadrupolar	nuclear shielding	dipolar	J
λ	q	$\sigma$	d	J
$ec{\hat{U}}$	$ec{\hat{I}}$	$ec{\hat{I}}$	$ec{\hat{I}_1}$	$ec{\hat{I}}_1$
$ec{V}$	$ec{\hat{I}}$	$ec{B}$	$ec{\hat{I}_2}$	$ec{\hat{I}}_2$
$\Lambda^{\{\lambda\}}$	$\frac{q_e Q_I}{2I(2I-1)}$	$\gamma_I$	$-(\mu_0/4\pi)\gamma_1\gamma_2\hbar$	$2\pi$
$\rho_{0,0}^{\{\lambda\}}$	0	$-\sqrt{3} \sigma_{\rm iso}$	0	$-\sqrt{3} J_{iso}$
$\rho_{1,0}^{\{\lambda\}}$	0	$-i\sqrt{2} \zeta_{\sigma}^{(a)}$	0	$-i\sqrt{2} \zeta_J^{(a)}$
$\rho_{1,\pm 1}^{\{\lambda\}}$	0	0	0	0
$\rho_{2,0}^{\{\lambda\}}$	$\sqrt{\frac{3}{2}} \zeta_q$	$\sqrt{\frac{3}{2}} \zeta_{\sigma}$	$\sqrt{rac{3}{2}}  \zeta_d$	$\sqrt{\frac{3}{2}} \zeta_J$
$\rho_{2,\pm 1}^{\{\lambda\}}$	0	0	0	0
$\rho_{2,\pm 2}^{\{\lambda\}}$	$-\eta_q \zeta_q/2$	$-\eta_{\sigma}\zeta_{\sigma}/2$	0	$-\eta_J \zeta_J/2$

Table S7: Definitions for the irreducible spherical tensor elements for the quadrupolar, nuclear shielding, and dipolar coupling tensors in the principal axis system (PAS) for a Hamiltonian in the form of Eq. (S.106). Here, we define the first rank nuclear shielding or J antisymmetric tensor in its PAS as  $\rho_{1,0}$ , which is related to its value,  $r_{1,m}$ , in the PAS of the second rank symmetric tensor by  $r_{1,m} = \sum_{m} \mathcal{D}_{0,m}^{(2)}(0,\theta,\phi) \, \rho_{1,0}$ .

and the second-rank symmetric EFG tensor asymmetry parameter is defined as

$$\eta_q = \frac{\lambda_{yy}^{\{q\}} - \lambda_{xx}^{\{q\}}}{\zeta_q}.$$
 (S.112)

The quadrupolar coupling constant is given by

$$C_q = \frac{q_e Q_I}{h} \zeta_q,\tag{S.113}$$

and the quadrupolar splitting is given by

$$\omega_{q} \; = \; \frac{6\pi C_{q}}{2I(2I-1)} \; = \; \Lambda^{\{q\}} \cdot \frac{3\zeta_{q}}{\hbar} \; = \; \frac{q_{e}Q_{\gamma I}}{2I(2I-1)} \cdot \frac{3\zeta_{q}}{\hbar}. \tag{S.114}$$

For convenience, in the derivations to follow, we express the quadrupole Hamiltonian as

$$\hat{\mathcal{H}}_q/\hbar = \omega_q \sum_{m=-2}^2 (-1)^m \frac{R_{2,-m}^{\{q\}}}{3\zeta_q} \hat{T}_{2,m}(\vec{I}).$$
(S.115)

#### S5.2.1 First-order electric quadrupole coupling correction

Using static perturbation theory and Eq. (S.105), we obtain the first-order contribution of the quadrupolar Hamiltonian in the tilted rotating frame

$$\hat{D}_q^{(1)}/\hbar = \omega_q \frac{R_{2,0}^{\{q\}}}{3\zeta_q} \hat{T}_{2,0}(\vec{I}). \tag{S.116}$$

The first-order contribution to the transition frequency between levels j and i is given by

$$\boxed{\Omega_q^{(1)}(\Theta_q, m_i, m_j) = \omega_q \, \mathbb{D}^{\{q\}}(\Theta_q) \, \mathsf{d}_I(m_i, m_j),}$$
(S.117)

where

$$\mathbb{D}^{\{q\}}(\Theta_q) = \frac{R_{2,0}^{\{q\}}(\Theta_q)}{3\zeta_q},\tag{S.118}$$

and

$$d_{I}(m_{i}, m_{j}) = \langle I, m_{j} | \hat{T}_{2,0}(\vec{I}) | I, m_{j} \rangle - \langle I, m_{i} | \hat{T}_{2,0}(\vec{I}) | I, m_{i} \rangle = \sqrt{\frac{3}{2}} (m_{j}^{2} - m_{i}^{2}). \tag{S.119}$$

#### S5.2.2 Second-order electric quadrupole coupling correction

The second-order contribution of the quadrupolar Hamiltonian in the tilted rotating frame is given by

$$\hat{D}_{q,q}^{(2)}/\hbar = \frac{\omega_q^2}{\omega_0} \sum_{m=1}^2 \frac{R_{2,m}^{\{q\}} R_{2,-m}^{\{q\}}}{9\zeta_q^2} \frac{[\hat{T}_{2,m}(\vec{I}), \hat{T}_{2,-m}(\vec{I})]}{m}.$$
 (S.120)

Within the second-order quadrupole Hamiltonian in Eq. (S.120), we find the product of two second-rank spherical tensors, i.e.,  $R_{2,m}^{\{q\}} R_{2,-m}^{\{q\}}$  and the commutator of two second-rank spherical tensor operators, i.e.,  $[\hat{T}_{2,m}(\vec{I}), \hat{T}_{2,-m}(\vec{I})]$ . Using the results of Section S2, we can write the second-order quadrupolar Hamiltonian in the rotating tilted frame:

$$\hat{D}_{q,q}^{(2)}//\hbar = \frac{\omega_q^2}{\omega_0} \sum_{L=0,2,4} \frac{\mathcal{R}_{L,0}^{\{qq\}}}{9\zeta_q^2} \sum_{J=1,3} \pi_{L,J}^{\{2,2\}} \hat{T}_{J,0}(\vec{I}) = \frac{\omega_q^2}{\omega_0} \sum_{L=0,2,4} \frac{\mathcal{R}_{L,0}^{\{qq\}}}{9\zeta_q^2} \hat{C}_L(\vec{I}), \tag{S.121}$$

where

$$\pi_{L,J}^{\{2,2\}} = 2B(2,2,J,I) \sum_{m=1}^{2} \frac{\langle L \, 0 | 2 \, 2 \, m \, - m \rangle \, \langle J \, 0 | 2 \, 2 \, m \, - m \rangle}{m}, \tag{S.122}$$

and

$$\hat{C}_L(\vec{I}) = \sum_{J=1.3} \pi_{L,J}^{\{2,2\}} \, \hat{T}_{J,0}(\vec{I}). \tag{S.123}$$

$\pi_{L,J}^{\{2,2\}}$	J=1	J=3
L=0	$\frac{4}{\sqrt{125}} \left[ I(I+1) - 3/4 \right]$	$\sqrt{18/25}$
L=2	$\sqrt{\frac{2}{175}} \left[ I(I+1) - 3/4 \right]$	$-6/\sqrt{35}$
L=4	$-\sqrt{\frac{18}{875}}\left[I(I+1) - 3/4\right]$	$-17/\sqrt{175}$

Table S8:  $\pi_{L,J}^{\{2,2\}}$  coefficients in second-order electric quadrupole coupling Hamiltonian.

Values of the  $\pi_{L,J}^{\{2,2\}}$  are given in Table S8, and the  $\hat{C}_L$  operators are given by

$$\hat{C}_0(\vec{I}) = \frac{4}{\sqrt{125}} \left[ I(I+1) - 3/4 \right] \hat{T}_{1,0}(\vec{I}) + \sqrt{\frac{18}{25}} \, \hat{T}_{3,0}(\vec{I}), \tag{S.124}$$

$$\hat{C}_2(\vec{I}) = \sqrt{\frac{2}{175}} \left[ I(I+1) - 3/4 \right] \hat{T}_{1,0}(\vec{I}) - \frac{6}{\sqrt{35}} \hat{T}_{3,0}(\vec{I}), \tag{S.125}$$

$$\hat{C}_4(\vec{I}) = -\sqrt{\frac{18}{875}} \left[ I(I+1) - 3/4 \right] \hat{T}_{1,0}(\vec{I}) - \frac{17}{\sqrt{175}} \hat{T}_{3,0}(\vec{I}). \tag{S.126}$$

The tensor  $\mathcal{R}_{L,0}^{\{qq\}}$  is related to the tensor elements in the sample holder frame,  $\mathcal{R}_{L,M}^{\{qq\}}$ , using Eq. (S.13). The tensor  $\mathcal{R}_{L,M}^{\{qq\}}$  is related to the principal values of the  $R_{2,m}^{\{qq\}}$  tensor by

$$\mathcal{R}_{L,M}^{\prime \{qq\}} = \sum_{M'=-L}^{L} \mathcal{D}_{M',M}^{(L)}(\Theta_q) \, \sigma_{L,M'}^{\{qq\}}, \tag{S.127}$$

where

$$\sigma_{L,M}^{\{qq\}} = \sum_{m=-2}^{2} \langle L M | 2 \ 2 \ m \ M - m \rangle \, \rho_{2,m}^{\{q\}} \, \rho_{2,M-m}^{\{q\}}. \tag{S.128}$$

From Eq. (S.128) we obtain the relationships:

$$\sigma_{0,0}^{\{qq\}} = \frac{9\zeta_q^2}{6\sqrt{5}} \left(\frac{\eta_q^2}{3} + 1\right),\tag{S.129}$$

$$\sigma_{2,0}^{\{qq\}} = \frac{9\zeta_q^2}{6}\sqrt{\frac{2}{7}}\left(\frac{\eta_q^2}{3} - 1\right), \quad \sigma_{2,\pm 2}^{\{qq\}} = -\frac{9\zeta_q^2\eta_q}{3\sqrt{21}},\tag{S.130}$$

$$\sigma_{4,0}^{\{qq\}} = \frac{9\zeta_q^2}{\sqrt{70}} \left( \frac{\eta_q^2}{18} + 1 \right), \quad \sigma_{4,\pm 2}^{\{qq\}} = -\frac{9\zeta_q^2 \eta_q}{6\sqrt{7}}, \quad \sigma_{4,\pm 4}^{\{qq\}} = \frac{9\zeta_q^2 \eta_q^2}{36}. \tag{S.131}$$

The second-order contribution to the transition frequency between levels  $|j\rangle$  and  $|i\rangle$  obtained from Eq. (S.121) is

$$\overline{\Omega_{q,q}^{(2)}(\Theta_q, m_i, m_j) = \frac{\omega_q^2}{\omega_0} \mathbb{S}^{\{qq\}} \, \mathbb{c}_0(m_i, m_j) + \frac{\omega_q^2}{\omega_0} \mathbb{D}^{\{qq\}}(\Theta_q) \, \mathbb{c}_2(m_i, m_j) + \frac{\omega_q^2}{\omega_0} \mathbb{G}^{\{qq\}}(\Theta_q) \, \mathbb{c}_4(m_i, m_j),} \tag{S.132}$$

where

$$\mathbb{S}^{\{qq\}} = \frac{\mathcal{R}_{0,0}^{\{qq\}}}{9\zeta_q^2} = \frac{1}{6\sqrt{5}} \left( \frac{\eta_q^2}{3} + 1 \right), \quad \mathbb{D}^{\{qq\}}(\Theta_q) = \frac{\mathcal{R}_{2,0}^{\{qq\}}(\Theta_q)}{9\zeta_q^2}, \quad \mathbb{G}^{\{qq\}}(\Theta_q) = \frac{\mathcal{R}_{4,0}^{\{qq\}}(\Theta_q)}{9\zeta_q^2}, \quad (S.133)$$

and using  $c_L(i,j)$  values calculated from

$$\mathbb{E}_{L}(m_{i}, m_{j}) = \sum_{J=1,3} \pi_{L,J}^{\{2,2\}} \left\{ \langle I, m_{j} | \hat{T}_{J,0} | I, m_{j} \rangle - \langle I, m_{i} | \hat{T}_{J,0} | I, m_{i} \rangle \right\} = \sum_{J=1,3} \pi_{L,J}^{\{2,2\}} \xi_{J}(m_{i}, m_{j}). \tag{S.134}$$

### S5.3 Nuclear shielding

The nuclear shielding Hamiltonian is given by

$$\left| \hat{\mathcal{H}}_{\sigma}/\hbar = -\omega_0 \sum_{L=0}^{2} \sum_{m=-1}^{1} (-1)^m R_{L,-m}^{\{\sigma\}} \langle L \ m | 1 \ 1 \ m \ 0 \rangle \, \hat{T}_{1,m}(\vec{I}). \right|$$
 (S.135)

Here, we follow the IUPAC definitions for the nuclear shielding interaction[19]. The isotropic nuclear shielding,  $\sigma_{iso}$ , is derived from the trace of the shielding tensor,

$$\sigma_{\rm iso} = \frac{1}{3}(\sigma_{xx} + \sigma_{yy} + \sigma_{zz}). \tag{S.136}$$

In the principal axis system of the antisymmetric shielding tensor, we define

$$\rho_{1,0}^{\{\sigma\}} = -i\sqrt{2} \,\zeta_{\sigma}^{(a)}, \quad \rho_{1,\pm 1}^{\{\sigma\}} = 0, \tag{S.137}$$

where

$$\zeta_{\sigma}^{(a)} = \frac{1}{2} \sqrt{(\sigma_{xy} - \sigma_{yx})^2 + (\sigma_{yz} - \sigma_{zy})^2 + (\sigma_{zx} - \sigma_{xz})^2}.$$
 (S.138)

In the principal axis system of the second-rank symmetric Cartesian shielding tensor, where  $\lambda_a^{\{\sigma\}}$ ,  $\lambda_b^{\{\sigma\}}$ , and  $\lambda_c^{\{\sigma\}}$  are the principal components of the symmetric part of the shielding tensor ordered according to the Haeberlen convention, we define

$$\rho_{2,0}^{\{\sigma\}} = \sqrt{\frac{3}{2}} \zeta_{\sigma}, \quad \rho_{2,\pm 1}^{\{\sigma\}} = 0, \quad \rho_{2,\pm 2}^{\{\sigma\}} = -\eta_{\sigma} \zeta_{\sigma}/2, \tag{S.139}$$

where the second-rank symmetric nuclear shielding tensor anisotropy,  $\zeta_{\sigma}$ , is defined as

$$\zeta_{\sigma} = \lambda_c^{\{\sigma\}},\tag{S.140}$$

and the second-rank symmetric nuclear shielding tensor asymmetry parameter is defined as

$$\eta_{\sigma} = \frac{\lambda_b^{\{\sigma\}} - \lambda_a^{\{\sigma\}}}{\zeta_{\sigma}}.$$
 (S.141)

#### S5.3.1 First-order nuclear shielding correction

The nuclear shielding is generally orders of magnitude smaller in strength than the Zeeman interaction and, therefore, can be approximated to high accuracy using first-order perturbation theory as

$$\hat{D}_{\sigma}^{(1)}/\hbar = -\omega_0 \left\{ -\sqrt{\frac{1}{3}} R_{0,0}^{\{\sigma\}} + \sqrt{\frac{2}{3}} R_{2,0}^{\{\sigma\}} \right\} \hat{T}_{1,0}(\vec{I}). \tag{S.142}$$

We write the first-order nuclear shielding contribution to the  $|i\rangle \rightarrow |j\rangle$  transition frequency as

$$\Omega_{\sigma}^{(1)}(\Theta, m_i, m_j) = -\omega_0 \,\sigma_{\rm iso} \,\mathbb{S}^{\{\sigma\}} \,\mathbb{p}_I(m_i, m_j) - \omega_0 \,\zeta_\sigma \,\mathbb{D}^{\{\sigma\}}(\Theta) \,\mathbb{p}_I(m_i, m_j).$$
(S.143)

where

$$\mathbb{S}^{\{\sigma\}} = -\sqrt{\frac{1}{3}} \frac{R_{0,0}^{\{\sigma\}}}{\sigma_{\text{iso}}} = 1, \quad \mathbb{D}^{\{\sigma\}}(\Theta_{\sigma}) = \sqrt{\frac{2}{3}} \frac{R_{2,0}^{\{\sigma\}}(\Theta_{\sigma})}{\zeta_{\sigma}}, \tag{S.144}$$

and

$$\mathbb{p}_{I}(m_{i}, m_{j}) = \langle I, m_{j} | \hat{T}_{1,0}(\vec{I}) | I, m_{j} \rangle - \langle I, m_{i} | \hat{T}_{1,0}(\vec{I}) | I, m_{i} \rangle = m_{j} - m_{i}. \tag{S.145}$$

#### S5.3.2 Nuclear Shielding - Electric Quadrupole Cross Term

The second-order cross-term contribution between the nuclear shielding and the electric quadrupole coupling in the tilted rotating frame is given by

$$\hat{D}_{\sigma,q}^{(2)}/\hbar = -\omega_q \sum_{L=1}^{2} \sum_{\substack{m=-1\\m\neq 0}}^{1} \frac{\langle L \ m|1 \ 1 \ m \ 0 \rangle}{m} \frac{R_{L,-m}^{\{\sigma\}} R_{2,m}^{\{q\}}}{3\zeta_q} \left[ \hat{T}_{1,m}(\vec{I}), \hat{T}_{2,-m}(\vec{I}) \right]. \tag{S.146}$$

Using the results of Sections S1.3 and S2, this expression becomes

$$\hat{D}_{\sigma,q}^{(2)}/\hbar = -\omega_q \left[ \pi_{1,1}^{\{1,2\}} \frac{\mathcal{A}_{1,0}^{\{\sigma q\}}}{3\zeta_q} + \pi_{1,3}^{\{1,2\}} \frac{\mathcal{A}_{3,0}^{\{\sigma q\}}}{3\zeta_q} + \pi_{2,0}^{\{1,2\}} \frac{\mathcal{R}_{0,0}^{\{\sigma q\}}}{3\zeta_q} + \pi_{2,2}^{\{1,2\}} \frac{\mathcal{R}_{2,0}^{\{\sigma q\}}}{3\zeta_q} + \pi_{2,4}^{\{1,2\}} \frac{\mathcal{R}_{4,0}^{\{\sigma q\}}}{3\zeta_q} \right] \hat{T}_{2,0}(\vec{I}), \tag{S.147}$$

where

$$\mathcal{A}_{L,M}^{\{\sigma q\}} = \sum_{m=-1}^{1} \langle L \ M | 1 \ 2 \ m \ M - m \rangle R_{1,m}^{\{\sigma\}} R_{2,M-m}^{\{q\}}, \tag{S.148}$$

$$\mathcal{R}_{L,M}^{\{\sigma q\}} = \sum_{m=-2}^{2} \langle L \ M | 2 \ 2 \ m \ M - m \rangle R_{2,m}^{\{\sigma\}} R_{2,M-m}^{\{q\}}, \tag{S.149}$$

and the coefficient  $\pi_{L,K}^{\{1,2\}}$  is given by

$$\pi_{L,K}^{\{1,2\}} = -\sqrt{6} \sum_{\substack{m=-1\\m\neq 0}}^{1} \frac{\langle L \ m|1 \ 1 \ m \ 0 \rangle \langle 2 \ 0|1 \ 2 \ m \ -m \rangle \langle K \ 0|L \ 2 \ -m \ m \rangle}{m}. \tag{S.150}$$

One can show that the anti-symmetric contributions vanish, leaving the second-order correction involving the nuclear shielding tensor as

$$\hat{D}_{\sigma,q}^{(2)}/\hbar = -\omega_q \left( \sum_{K=0,2,4} \pi_{2,K}^{\{1,2\}} \frac{\mathcal{R}_{K,0}^{\{\sigma q\}}}{3\zeta_q} \right) \hat{T}_{2,0}(\vec{I}). \tag{S.151}$$

We can write the contribution to the  $i \to j$  transition frequency from the second-order cross term between the nuclear shielding and quadrupole coupling as

$$\boxed{\Omega_{\sigma,q}^{(2)}(\Theta, m_i, m_j) = -\omega_q \, \zeta_\sigma \, \mathbb{S}^{\{\sigma q\}} \, \mathbb{d}_I(m_i, m_j) - \omega_q \, \zeta_\sigma \, \mathbb{D}^{\{\sigma q\}}(\Theta) \, \mathbb{d}_I(m_i, m_j) - \omega_q \, \zeta_\sigma \, \mathbb{G}^{\{\sigma q\}}(\Theta) \, \mathbb{d}_I(m_i, m_j),}$$
(S.152)

where

$$\mathbb{S}^{\{\sigma q\}} = \sqrt{\frac{6}{5}} \frac{\mathcal{R}_{0,0}^{\{\sigma q\}}}{3\zeta_q \zeta_\sigma}, \quad \mathbb{D}^{\{\sigma q\}}(\Theta) = -\sqrt{\frac{3}{7}} \frac{\mathcal{R}_{2,0}^{\{\sigma q\}}(\Theta)}{3\zeta_q \zeta_\sigma}, \quad \mathbb{G}^{\{\sigma q\}}(\Theta) = -\sqrt{\frac{48}{35}} \frac{\mathcal{R}_{4,0}^{\{\sigma q\}}(\Theta)}{3\zeta_q \zeta_\sigma}. \quad (S.153)$$

### S5.4 J coupling

The J Coupling Hamiltonian can be written

$$\hat{\mathcal{H}}_J/\hbar = 2\pi \sum_{L=0}^2 \sum_{m=-L}^L (-1)^m R_{L,-m}^{\{J\}} \hat{T}_{L,m}(\vec{I}_1, \vec{I}_2), \tag{S.154}$$

where the  $\hat{T}_{L,m}(\vec{I}_1,\vec{I}_2)$  are formed from the spin angular momentum vectors  $\vec{I}_1$  and  $\vec{I}_2$ , given by the expansion

$$\hat{T}_{L,m}(\vec{I}_1, \vec{I}_2) = \sum_{n=-1}^{1} \langle L \ m | 1 \ 1 \ n+m \ -n \rangle \, \hat{T}_{1,n+m}(\vec{I}_1) \, \hat{T}_{1,-n}(\vec{I}_2). \tag{S.155}$$

The isotropic J coupling,  $J_{iso}$ , is derived from the trace of the J coupling tensor,

$$J_{\rm iso} = \frac{1}{3}(J_{xx} + J_{yy} + J_{zz}). \tag{S.156}$$

In the principal axis system of the first-rank antisymmetric J coupling tensor, we define

$$\rho_{1,0}^{\{J\}} = -i\sqrt{2} \,\zeta_J^{(a)}, \quad \rho_{1,\pm 1}^{\{J\}} = 0, \tag{S.157}$$

where

$$\zeta_J^{(a)} = \frac{1}{2} \sqrt{(J_{xy} - J_{yx})^2 + (J_{yz} - J_{zy})^2 + (J_{zx} - J_{xz})^2}.$$
 (S.158)

In the principal axis system of the second-rank symmetric J coupling Cartesian tensor, where  $\lambda_a^{\{J\}}$ ,  $\lambda_b^{\{J\}}$ , and  $\lambda_c^{\{J\}}$  are principal components ordered according to the Haeberlen convention, we define

$$\rho_{2,0}^{\{J\}} = \sqrt{\frac{3}{2}}\zeta_J, \quad \rho_{2,\pm 1}^{\{J\}} = 0, \quad \rho_{2,\pm 2}^{\{J\}} = -\eta_J \zeta_J / 2, \tag{S.159}$$

where the second-rank symmetric J coupling tensor anisotropy,  $\zeta_J$ , is defined as

$$\zeta_J = \lambda_c^{\{J\}},\tag{S.160}$$

the second-rank symmetric J coupling tensor asymmetry parameter is defined as

$$\eta_J = \frac{\lambda_b^{\{J\}} - \lambda_a^{\{J\}}}{\zeta_J}.$$
 (S.161)

### S5.4.1 First-Order *J*-Coupling Correction.

To obtain the first-order Hamiltonian in the weak coupling limit Eq. (S.155) is substituted into Eq. (S.154), replacing  $I_1$  with I and  $I_2$  with S, and again eliminating  $m \neq 0$  terms to obtain

$$\hat{D}_{J_{IS}}^{(1)}/\hbar = 2\pi \sum_{L=0}^{2} \langle L \ 0|1 \ 1 \ 0 \ 0 \rangle R_{L,0}^{\{J\}} \, \hat{T}_{1,0}(\vec{I}_1) \, \hat{T}_{1,0}(\vec{I}_2). \tag{S.162}$$

Since  $\langle L \ 0 | 1 \ 1 \ 0 \ 0 \rangle = 0$ , the L = 1 term disappears and the first-order energy correction is

$$\hat{D}_{J_{IS}}^{(1)}/\hbar = 2\pi \sum_{L=0,2} \langle L \ 0|1 \ 1 \ 0 \ 0 \rangle R_{L,0}^{\{J\}} \, \hat{T}_{1,0}(\vec{I}_1) \, \hat{T}_{1,0}(\vec{I}_2). \tag{S.163}$$

The first-order weak J coupling correction to the transition frequency is,

$$\boxed{\Omega_{J_{IS}}^{(1)}(\Theta, m_{I,i}, m_{S,i}, m_{I,j}, m_{S,j}) = 2\pi J_{iso} \mathbb{S}^{\{J_{IS}\}}(\mathbb{PP})_{IS}(m_{I,i}, m_{S,i}, m_{I,j}, m_{S,j}) + 2\pi \zeta_{J} \mathbb{D}^{\{J_{IS}\}}(\Theta)(\mathbb{PP})_{IS}(m_{I,i}, m_{S,i}, m_{I,j}, m_{S,j}),}$$
(S.164)

where

$$\mathbb{S}^{\{J_{IS}\}} = -\sqrt{\frac{1}{3}} \frac{R_{0,0}^{\{J\}}}{J_{iso}} = 1, \quad \mathbb{D}^{\{J_{IS}\}}(\Theta) = \sqrt{\frac{2}{3}} \frac{R_{2,0}^{\{J\}}(\Theta)}{\zeta_J}, \quad (S.165)$$

and the  $(pp)_{IS}$  are calculated in the weakly coupled basis set,  $|m_I m_S\rangle$ ,

$$(\mathbb{pp})_{IS}(m_{I,i}, m_{S,i}, m_{I,j}, m_{S,j}) = \langle m_{I,j}, m_{S,j} | \hat{T}_{1,0}(\vec{I}) \hat{T}_{1,0}(\vec{S}) | m_{I,j}, m_{S,j} \rangle - \langle m_{I,i}, m_{S,i} | \hat{T}_{1,0}(\vec{I}) \hat{T}_{1,0}(\vec{S}) | m_{I,i}, m_{S,i} \rangle = m_{I,i} m_{S,i} - m_{I,i} m_{S,i}. \quad (S.166)$$

#### S5.4.2 J-Coupling Quadrupolar Cross Term

The second-order cross-term contribution in the weak coupling limit between the J coupling and the electric quadrupole coupling in the tilted rotating frame is given by

$$\hat{D}_{J,q_{I}}^{(2)}/\hbar = 2\pi \left(\frac{\omega_{q,I}}{\omega_{0,I}}\right) \sum_{L=1}^{2} \sum_{\substack{m=-1\\m\neq 0}}^{1} \frac{\langle L \ m|1 \ 1 \ m \ 0 \rangle}{m} R_{L,-m}^{\{J\}} \frac{R_{2,m}^{\{q_{I}\}}}{3\zeta_{q_{I}}} \left[\hat{T}_{1,m}(\vec{I}), \hat{T}_{2,-m}(\vec{I})\right] \hat{T}_{1,0}(\vec{S}). \tag{S.167}$$

Using the results of Sections S1.3 and S2, this expression becomes

$$\hat{D}_{J,q_{I}}^{(2)}/\hbar = 2\pi \left(\frac{\omega_{q,I}}{\omega_{0,I}}\right) \left[\pi_{1,1}^{\{1,2\}} \frac{\mathcal{A}_{1,0}^{\{Jq_{I}\}}}{3\zeta_{q_{I}}} \hat{T}_{2,0}(\vec{I}) \hat{T}_{1,0}(\vec{S}) + \pi_{1,3}^{\{1,2\}} \frac{\mathcal{A}_{3,0}^{\{Jq_{I}\}}}{3\zeta_{q_{I}}} \hat{T}_{2,0}(\vec{I}) \hat{T}_{1,0}(\vec{S}) + \pi_{1,3}^{\{1,2\}} \frac{\mathcal{A}_{3,0}^{\{Jq_{I}\}}}{3\zeta_{q_{I}}} \hat{T}_{2,0}(\vec{I}) \hat{T}_{1,0}(\vec{S}) + \pi_{2,2}^{\{Jq_{I}\}} \frac{\mathcal{A}_{3,0}^{\{Jq_{I}\}}}{3\zeta_{q_{I}}} \hat{T}_{2,0}(\vec{I}) \hat{T}_{1,0}(\vec{S}) + \pi_{2,4}^{\{1,2\}} \frac{\mathcal{A}_{4,0}^{\{Jq_{I}\}}}{3\zeta_{q_{I}}} \hat{T}_{2,0}(\vec{I}) \hat{T}_{1,0}(\vec{S})\right], \quad (S.168)$$

where the product involving the antisymmetric part of the J tensor is given by

$$\mathcal{A}_{L,M}^{\{Jq_I\}} = \sum_{m=-1}^{1} \langle L M | 1 \, 2 \, m \, M - m \rangle R_{1,m}^{\{J\}} R_{2,M-m}^{\{q_I\}}, \tag{S.169}$$

and the product involving the symmetric part of the J tensor by

$$\mathcal{R}_{L,M}^{\{Jq_I\}} = \sum_{m=-2}^{2} \langle L M | 2 \, 2 \, m \, M - m \rangle R_{2,m}^{\{J\}} R_{2,M-m}^{\{q_I\}}. \tag{S.170}$$

As noted earlier, the  $\pi_{L,K}^{\{1,2\}}$  coefficients vanish for odd values of K, leaving only the symmetric tensor contributions

$$\hat{D}_{J,q_{I}}^{(2)}/\hbar = 2\pi \left(\frac{\omega_{q,I}}{\omega_{0,I}}\right) \left(\sum_{K=0,2,4} \pi_{2,K}^{\{1,2\}} \frac{\mathcal{R}_{K,0}^{\{Jq_{I}\}}}{3\zeta_{q_{I}}}\right) \hat{T}_{2,0}(\vec{I}) \hat{T}_{1,0}(\vec{S}). \tag{S.171}$$

Using Eq. (S.121), the second-order contribution to the transition frequency between levels  $|m_I m_S\rangle$  and  $|m_I' m_S'\rangle$  is obtained

$$\Omega_{J,q_{I}}^{(2)}(\Theta, m_{I,i}, m_{S,i}, m_{I,j}, m_{S,j}) = 2\pi\zeta_{J} \left(\frac{\omega_{q,I}}{\omega_{0,I}}\right) \mathbb{S}^{\{Jq_{I}\}} (\mathbb{dp})_{IS}(m_{I,i}, m_{S,i}, m_{I,j}, m_{S,j}) \\
+2\pi\zeta_{J} \left(\frac{\omega_{q,I}}{\omega_{0,I}}\right) \mathbb{D}^{\{Jq_{I}\}}(\Theta) (\mathbb{dp})_{IS}(m_{I,i}, m_{S,i}, m_{I,j}, m_{S,j}) \\
+2\pi\zeta_{J} \left(\frac{\omega_{q,I}}{\omega_{0,I}}\right) \mathbb{G}^{\{Jq_{I}\}}(\Theta) (\mathbb{dp})_{IS}(m_{I,i}, m_{S,i}, m_{I,j}, m_{S,j}), \tag{S.172}$$

where

$$\mathbb{S}^{\{Jq_I\}} = \sqrt{\frac{6}{5}} \frac{\mathcal{R}_{0,0}^{\{Jq_I\}}}{3\zeta_{q_I}\zeta_J}, \quad \mathbb{D}^{\{Jq_I\}}(\Theta) = -\sqrt{\frac{3}{7}} \frac{\mathcal{R}_{2,0}^{\{Jq_I\}}(\Theta)}{3\zeta_{q_I}\zeta_J}, \quad \mathbb{G}^{\{Jq_I\}}(\Theta) = -\sqrt{\frac{48}{35}} \frac{\mathcal{R}_{4,0}^{\{Jq_I\}}(\Theta)}{3\zeta_{q_I}\zeta_J}, \quad (S.173)$$

and the  $(dp)_{IS}(m_{I,i}, m_{S,i}, m_{I,j}, m_{S,j})$  are calculated in the weakly coupled basis set,  $|m_I m_S\rangle$ 

$$(\text{dp})_{IS}(m_{I,i}, m_{S,i}, m_{I,j}, m_{S,j}) = \langle m_{I,j}, m_{S,j} | \hat{T}_{2,0}(\vec{I}) \hat{T}_{1,0}(\vec{S}) | m_{I,j}, m_{S,j} \rangle - \langle m_{I,i}, m_{S,i} | \hat{T}_{2,0}(\vec{I}) \hat{T}_{1,0}(\vec{S}) | m_{I,i}, m_{S,i} \rangle$$

$$= \sqrt{\frac{3}{2}} \left( m_{I,j}^2 m_{S,j} - m_{I,i}^2 m_{S,i} \right) - \frac{1}{\sqrt{6}} I(I+1) (m_{S,j} - m_{S,i}). \quad (S.174)$$

Similarly, one obtains

$$\Omega_{J,q_{S}}^{(2)}(\Theta, m_{I,i}, m_{S,i}, m_{I,j}, m_{S,j}) = 2\pi \zeta_{J} \left(\frac{\omega_{q,S}}{\omega_{0,S}}\right) \mathbb{S}^{\{Jq_{S}\}} \left(\mathbb{pd}\right)_{IS}(m_{I,i}, m_{S,i}, m_{I,j}, m_{S,j}) \\
+2\pi \zeta_{J} \left(\frac{\omega_{q,S}}{\omega_{0,S}}\right) \mathbb{D}^{\{Jq_{S}\}}(\Theta) \left(\mathbb{pd}\right)_{IS}(m_{I,i}, m_{S,i}, m_{I,j}, m_{S,j}) \\
+2\pi \zeta_{J} \left(\frac{\omega_{q,S}}{\omega_{0,S}}\right) \mathbb{G}^{\{Jq_{S}\}}(\Theta) \left(\mathbb{pd}\right)_{IS}(m_{I,i}, m_{S,i}, m_{I,j}, m_{S,j}), \tag{S.175}$$

where

$$\mathbb{S}^{\{Jq_S\}} = \sqrt{\frac{6}{5}} \frac{\mathcal{R}_{0,0}^{\{Jq_S\}}}{3\zeta_{q_S}\zeta_J}, \quad \mathbb{D}^{\{Jq_S\}}(\Theta) = -\sqrt{\frac{3}{7}} \frac{\mathcal{R}_{2,0}^{\{Jq_S\}}(\Theta)}{3\zeta_{q_S}\zeta_J}, \quad \mathbb{G}^{\{Jq_S\}}(\Theta) = -\sqrt{\frac{48}{35}} \frac{\mathcal{R}_{4,0}^{\{Jq_S\}}(\Theta)}{3\zeta_{q_S}\zeta_J}, \quad (S.176)$$

and the  $(pd)_{IS}$  are calculated in the weakly coupled basis set,  $|m_I m_S\rangle$ ,

$$(\text{pd})_{IS}(m_{I,i}, m_{S,i}, m_{I,j}, m_{S,j}) = \langle m_{I,j}, m_{S,j} | \hat{T}_{1,0}(\vec{I}) \hat{T}_{2,0}(\vec{S}) | m_{I,j}, m_{S,j} \rangle - \langle m_{I,i}, m_{S,i} | \hat{T}_{1,0}(\vec{I}) \hat{T}_{2,0}(\vec{S}) | m_{I,i}, m_{S,i} \rangle$$

$$= \sqrt{\frac{3}{2}} \left( m_{S,j}^2 m_{I,j} - m_{S,i}^2 m_{I,i} \right) - \frac{1}{\sqrt{6}} S(S+1) (m_{I,j} - m_{I,i}). \quad (S.177)$$

### S5.5 Magnetic dipole coupling

The through-space magnetic dipole coupling Hamiltonian can be written

$$\hat{\mathcal{H}}_d/\hbar = -\frac{\mu_0}{4\pi} \, \hbar \gamma_1 \gamma_2 \sum_{m=-2}^2 (-1)^m R_{2,-m}^{\{d\}} \, \hat{T}_{2,m}(\vec{I}_1, \vec{I}_2). \tag{S.178}$$

In the principal axis system of the dipolar coupling tensor, we define

$$\rho_{2,0}^{\{d\}} = \sqrt{\frac{3}{2}} \zeta_d, \quad \rho_{2,\pm 1}^{\{d\}} = 0, \quad \rho_{2,\pm 2}^{\{d\}} = 0, \tag{S.179}$$

where the second-rank symmetric dipolar coupling tensor anisotropy,  $\zeta_d$ , is defined as

$$\zeta_d = \lambda_c^{\{d\}} = \frac{2}{r^3}.$$
 (S.180)

The dipolar splitting is given by

$$\omega_d = -\frac{\mu_0}{4\pi} \frac{\gamma_1 \gamma_2 \hbar}{r^3} = -\frac{\mu_0}{8\pi} \zeta_d \gamma_1 \gamma_2 \hbar. \tag{S.181}$$

For convenience, in the derivations to follow, we express the dipole coupling Hamiltonian as

$$\hat{\mathcal{H}}_d/\hbar = \omega_d \sum_{m=-2}^2 (-1)^m \frac{R_{2,-m}^{\{d\}}}{\zeta_d/2} \hat{T}_{2,m}(\vec{I}_1, \vec{I}_2). \tag{S.182}$$

#### S5.5.1 First-Order Magnetic Dipole Coupling Correction

Like nuclear shielding, the dipolar coupling is generally orders of magnitude smaller in strength than the Zeeman interaction. Thus, following our earlier approach, the first-order Hamiltonian in the strong coupling limit is obtained by eliminating  $m \neq 0$  terms to obtain

$$\hat{D}_{d_{II}}^{(1)}/\hbar = \omega_d \frac{R_{2,0}^{\{d\}}}{\zeta_d/2} \hat{T}_{2,0}^{\circ}(\vec{I}_1, \vec{I}_2). \tag{S.183}$$

The first-order strong dipolar coupling correction to the transition frequency is,

$$\Omega_{d_{II}}^{(1)}(\Theta, M_i, M_j) = \omega_d \, \mathbb{D}^{\{d_{II}\}}(\Theta) \, d_{II}(M_i, M_j), \tag{S.184}$$

where

$$\mathbb{D}^{\{d_{II}\}}(\Theta) = \frac{R_{2,0}^{\{d\}}(\Theta)}{\zeta_d/2},\tag{S.185}$$

and the  $d_{II}$  are calculated in the strongly coupled basis set.

To obtain the first-order Hamiltonian in the weak coupling limit, Eq. (S.155) is substituted into Eq. (S.178), replacing  $I_1$  with I and  $I_2$  with S, and again eliminating  $m \neq 0$  terms to obtain

$$\hat{D}_{d_{IS}}^{(1)}/\hbar = \omega_d \sqrt{\frac{2}{3}} \frac{A_{2,0}^{\{d\}}}{\zeta_d/2} \hat{T}_{1,0}^{\circ}(\vec{I}) \hat{T}_{1,0}^{\circ}(\vec{S}). \tag{S.186}$$

The first-order weak dipolar coupling correction to the transition frequency is,

$$\Omega_{d_{IS}}^{(1)}(\Theta, m_{I,i}, m_{S,i}, m_{I,j}, m_{S,j}) = \omega_d \, \mathbb{D}^{\{d_{IS}\}}(\Theta) \, (pp)_{IS}(m_{I,i}, m_{S,i}, m_{I,j}, m_{S,j}), \tag{S.187}$$

where

$$\mathbb{D}^{\{d_{IS}\}}(\Theta) = \sqrt{\frac{2}{3}} \, \frac{R_{2,0}^{\{d\}}(\Theta)}{\zeta_d/2},\tag{S.188}$$

and the  $(pp)_{IS}(m_{I,i}, m_{S,i}, m_{I,j}, m_{S,j})$  are calculated in the weakly coupled basis set,  $|m_I m_S\rangle$ .

### S5.5.2 Magnetic Dipole-Electric Quadrupole Coupling Cross Term in Weak Dipole Coupling Limit

The second-order cross-term contribution in the weak coupling limit between the dipolar coupling and the electric quadrupole coupling in the tilted rotating frame is given by

$$\hat{D}_{d,q_{I}}^{(2)}/\hbar = \omega_{d} \left(\frac{\omega_{q,I}}{\omega_{0,I}}\right) \sum_{\substack{m=-1\\m\neq 0}}^{1} \frac{\langle 2 \ m|1 \ 1 \ m \ 0 \rangle}{m} \frac{R_{2,-m}^{\{d\}}}{\zeta_{d}/2} \frac{R_{2,m}^{\{q_{I}\}}}{3\zeta_{q_{I}}} \left[\hat{T}_{1,m}(\vec{I}), \hat{T}_{2,-m}(\vec{I})\right] \hat{T}_{1,0}(\vec{S}). \tag{S.189}$$

Using the results of Sections S1.3 and S2, this expression becomes

$$\hat{D}_{d,q_{I}}^{(2)}/\hbar = \omega_{d} \left(\frac{\omega_{q,I}}{\omega_{0,I}}\right) \left(\sum_{J=0,2,4} \pi_{2,J}^{\{1,2\}} \frac{\mathcal{R}_{J,0}^{\{dq_{I}\}}}{3\zeta_{q_{I}}\zeta_{d}/2}\right) \hat{T}_{2,0}(\vec{I}) \,\hat{T}_{1,0}(\vec{S}),\tag{S.190}$$

where

$$\pi_{2,0}^{\{1,2\}} = \sqrt{\frac{6}{5}}, \quad \pi_{2,2}^{\{1,2\}} = -\sqrt{\frac{3}{7}}, \quad \pi_{2,4}^{\{1,2\}} = \sqrt{\frac{48}{35}},$$
(S.191)

to obtain

$$\hat{D}_{d,q_{I}}^{(2)}/\hbar = \omega_{d} \left(\frac{\omega_{q,I}}{\omega_{0,I}}\right) \left(\sqrt{\frac{6}{5}} \frac{\mathcal{R}_{0,0}^{\{dq_{I}\}}}{3\zeta_{q_{I}}\zeta_{d}/2} - \sqrt{\frac{3}{7}} \frac{\mathcal{R}_{2,0}^{\{dq_{I}\}}}{3\zeta_{q_{I}}\zeta_{d}/2} - \sqrt{\frac{48}{35}} \frac{\mathcal{R}_{4,0}^{\{dq_{I}\}}}{3\zeta_{q_{I}}\zeta_{d}/2}\right) \hat{T}_{2,0}(\vec{I}) \,\hat{T}_{1,0}(\vec{S}).$$

Using Eq. (S.121) the second-order contribution to the transition frequency between levels  $|m_I m_S\rangle$  and  $|m'_I m'_S\rangle$  is obtained

$$\Omega_{d,q_{I}}^{(2)}(\Theta, m_{I,i}, m_{S,i}, m_{I,j}, m_{S,j}) = \omega_{d} \left(\frac{\omega_{q,I}}{\omega_{0,I}}\right) \mathbb{S}^{\{dq_{I}\}} (\mathbb{dp})_{IS}(m_{I,i}, m_{S,i}, m_{I,j}, m_{S,j}) 
+ \omega_{d} \left(\frac{\omega_{q,I}}{\omega_{0,I}}\right) \mathbb{D}^{\{dq_{I}\}}(\Theta) (\mathbb{dp})_{IS}(m_{I,i}, m_{S,i}, m_{I,j}, m_{S,j}) 
+ \omega_{d} \left(\frac{\omega_{q,I}}{\omega_{0,I}}\right) \mathbb{G}^{\{dq_{I}\}}(\Theta) (\mathbb{dp})_{IS}(m_{I,i}, m_{S,i}, m_{I,j}, m_{S,j}),$$
(S.192)

where

$$\mathbb{S}^{\{dq_I\}} = \sqrt{\frac{6}{5}} \frac{\mathcal{R}_{0,0}^{\{dq_I\}}}{3\zeta_{q_I}\zeta_d/2}, \qquad \mathbb{D}^{\{dq_I\}}(\Theta) = -\sqrt{\frac{3}{7}} \frac{\mathcal{R}_{2,0}^{\{dq_I\}}(\Theta)}{3\zeta_{q_I}\zeta_d/2}, \qquad \mathbb{G}^{\{dq_I\}}(\Theta) = -\sqrt{\frac{48}{35}} \frac{\mathcal{R}_{4,0}^{\{dq_I\}}(\Theta)}{3\zeta_{q_I}\zeta_d/2}. \tag{S.193}$$

Similarly, one obtains

$$\Omega_{d,q_{S}}^{(2)}(\Theta, m_{I,i}, m_{S,i}, m_{I,j}, m_{S,j}) = \omega_{d} \left(\frac{\omega_{q,S}}{\omega_{0,S}}\right) \mathbb{S}^{\{dq_{S}\}} (\mathbb{pd})_{IS}(m_{I,i}, m_{S,i}, m_{I,j}, m_{S,j}) 
+ \omega_{d} \left(\frac{\omega_{q,S}}{\omega_{0,S}}\right) \mathbb{D}^{\{dq_{S}\}}(\Theta) (\mathbb{pd})_{IS}(m_{I,i}, m_{S,i}, m_{I,j}, m_{S,j}) 
+ \omega_{d} \left(\frac{\omega_{q,S}}{\omega_{0,S}}\right) \mathbb{G}^{\{dq_{S}\}}(\Theta) (\mathbb{pd})_{IS}(m_{I,i}, m_{S,i}, m_{I,j}, m_{S,j}),$$
(S.194)

where

$$\mathbb{S}^{\{dq_S\}} = \sqrt{\frac{6}{5}} \frac{\mathcal{R}_{0,0}^{\{dq_S\}}}{3\zeta_{q_S}\zeta_d/2}, \qquad \mathbb{D}^{\{dq_S\}}(\Theta) = -\sqrt{\frac{3}{7}} \frac{\mathcal{R}_{2,0}^{\{dq_S\}}(\Theta)}{3\zeta_{q_S}\zeta_d/2}, \qquad \mathbb{G}^{\{dq_S\}}(\Theta) = -\sqrt{\frac{48}{35}} \frac{\mathcal{R}_{4,0}^{\{dq_S\}}(\Theta)}{3\zeta_{q_S}\zeta_d/2}. \tag{S.195}$$

# S6 Transition Frequency Tensor Contributions

Here, we consider frequency contributions arising from the first- and second-order perturbation terms, which are summed to give the total transition frequency,  $\Omega(\Theta, i, j)$ , for the  $i \to j$  transition as[17]

$$\Omega(\Theta, i, j) = \sum_{k} \omega_k \,\Xi_L^{(k)}(\Theta) \,\xi^{(k)}(i, j), \tag{S.196}$$

where  $\omega_k$  is the size,  $\Xi_L^{(k)}(\Theta)$  is the sample's spatial orientation function corresponding to the  $L^{\text{th}}$  rank spatial irreducible spherical tensor, and  $\xi^{(k)}(i,j)$  is the spin transition symmetry function of the  $k^{\text{th}}$  frequency contribution. The spatial orientation functions,  $\Xi_L^{(k)}(\Theta)$ , in Eq. (S.196), are defined in the laboratory frame, where the z-axis is the direction of the external magnetic field. Here,  $\Theta(t)$  are the Euler angles that determine the sample's lattice spatial orientation, which can carry a time dependence due to sample rotation.

We can expand the orientation dependence of a given transition frequency using a series of rotations from the common frame<sup>2</sup> of each frequency contribution to the laboratory frame and re-express Eq. (S.196) as

$$\Omega(t,i,j) = \sum_{k \in \mathcal{S}} \underbrace{\left[ \sum_{m_0 = -L_k}^{L_k} \mathcal{D}_{m_0,0}^{(L_k)}(\omega_R t + \phi_0, \theta_R, 0) \sum_{m_1 = -L_k}^{L_k} \mathcal{D}_{m_1,m_0}^{(L_k)}(\alpha, \beta, \gamma) \Delta_{L_k,m_1}^{\{\delta_k\}} \right]}_{\omega_k} \xi^{(k)}(i,j), \tag{S.197}$$

where  $\Delta_L^{\{\delta_k\}}$  is the frequency-scaled spatial spherical (fsSST) tensor part of the  $k^{\text{th}}$  frequency contribution of rank  $L_k$  arising from the perturbation term  $\delta_k$  in the common frame.

### S6.1 Single interaction frequency scaled spatial tensor parts

For frequency contributions from first-order perturbation theory, i.e., involving a single interaction, the components of  $\Delta_{L}^{\{\lambda\}}$  are given by

$$\Delta_{L,m}^{\{\lambda\}} = \sum_{m'=-L}^{L} \mathcal{D}_{m,m'}^{(L)}(\Theta_{PAS}^{\{\lambda\}}) \, \varsigma_{L,m'}^{\{\lambda\}}, \tag{S.198}$$

where  $\varsigma_L^{\{\lambda\}}$  is an fsSST part of rank L in the PAS of the single interaction spatial tensor, and  $\Theta_{\rm PAS}^{\{\lambda\}}$  is the orientation of the PAS relative to the common frame. From Eqs. (S.117) and (S.118), we obtain the fsSSTs for the first-order and second-order quadrupolar contributions as

$$\varsigma_{2,m}^{\{q\}} = \omega_q \frac{\rho_{2,m}^{\{q\}}}{3\zeta_q}, \quad \text{and} \quad \varsigma_{L,m}^{\{qq\}} = \frac{\omega_q^2}{\omega_0} \frac{\sigma_{L,m}^{\{qq\}}}{9\zeta_q^2}. \tag{S.199}$$

The transition frequency contributions are obtained from the products  $\varsigma_{2,m}^{\{q\}} d_I(m_i,m_f)$  and  $\varsigma_{L,m}^{\{qq\}} c_L(m_i,m_f)$  transformed into the laboratory frame. We can also rewrite the first and second-order quadrupolar interaction contributions to the Hamiltonian in terms of the fsSSTs as

$$\hat{D}_{q}^{(1)}/\hbar = \omega_{q} \frac{R_{2,0}^{\{q\}}}{3\zeta_{q}} \hat{T}_{2,0}(\vec{I}) = \mathfrak{R}_{2,0}^{\{q\}} \hat{T}_{2,0}(\vec{I}), \tag{S.200}$$

and

$$\hat{D}_{q,q}^{(2)}/\hbar = \sum_{L=0,2,4} \frac{\omega_q^2}{\omega_0} \frac{\Re_{L,0}^{\{qq\}}}{9\zeta_q^2} \hat{C}_L(\vec{I}), = \sum_{L=0,2,4} \Re_{L,0}^{\{qq\}} \hat{C}_L(\vec{I}), \tag{S.201}$$

where

$$\mathfrak{R}_{L,0}^{\{\lambda\}} = \sum_{n=-L}^{L} \mathcal{D}_{n,0}^{(L)}(\omega_R t + \phi_0, \theta_R, 0) \, \Delta_{L,n}^{\{\lambda\}}. \tag{S.202}$$

From Eqs. (S.117) and (S.118) we obtain the sSST for the first-order shielding contribution as

$$\varsigma_{0,0}^{\{\sigma\}} = -\omega_0 \,\sigma_{\text{iso}}, \quad \text{and} \quad \varsigma_{2,m}^{\{\sigma\}} = -\omega_0 \,\sqrt{\frac{2}{3}} \rho_{2,m}^{\{\sigma\}}.$$
(S.203)

<sup>&</sup>lt;sup>2</sup>For crystalline samples, the crystal frame is typically used as the common frame.

The transition frequency contributions are obtained from the products  $\zeta_{0,0}^{\{\sigma\}} \mathbb{p}_I(m_i, m_f)$  and  $\zeta_{2,m}^{\{\sigma\}} \mathbb{p}(m_i, m_f)$  transformed into the laboratory frame. The first-order shielding interaction contributions to the Hamiltonian in terms of the fsSSTs is given by

$$\hat{D}_{\sigma}^{(1)}/\hbar = -\omega_0 \left\{ -\sqrt{\frac{1}{3}} R_{0,0}^{\{\sigma\}} + \sqrt{\frac{2}{3}} R_{2,0}^{\{\sigma\}} \right\} \hat{T}_{1,0}(\vec{I}) = \mathfrak{R}_{0,0}^{\{\sigma\}} \hat{T}_{1,0}(\vec{I}) + \mathfrak{R}_{2,0}^{\{\sigma\}} \hat{T}_{1,0}(\vec{I}), \tag{S.204}$$

From Eqs. (S.164) and (S.165) we obtain the sSST for the first-order weak J-coupling contribution as

$$\varsigma_{0,0}^{\{J\}} = 2\pi J_{iso}, \quad \text{and} \quad \varsigma_{2,m}^{\{J\}} = 2\pi \sqrt{\frac{2}{3}} \rho_{2,m}^{\{J\}}.$$
(S.205)

The transition frequency contributions are obtained from the products  $\zeta_{0,0}^{\{J\}}(\mathbb{PP})_{IS}(m_{I,i},m_{S,i},m_{I,j},m_{S,j})$  and  $\zeta_{2,m}^{\{J\}}(\mathbb{PP})_{IS}(m_{I,i},m_{S,i},m_{I,j},m_{S,j})$  transformed into the laboratory frame. The first-order weak J interaction contributions to the Hamiltonian in terms of the fsSSTs is given by

$$\hat{D}_{J_{LS}}^{(1)}/\hbar = \Re_{0,0}^{\{J\}} \hat{T}_{1,0}(\vec{I}) \hat{T}_{1,0}(\vec{S}) + \Re_{2,0}^{\{J\}} \hat{T}_{1,0}(\vec{I}) \hat{T}_{1,0}(\vec{S})$$
(S.206)

From Eqs. (S.187) and (S.188), we obtain the sSST for the first-order weak dipolar-coupling contribution as

$$\varsigma_{2,m}^{\{d\}} = \omega_d \sqrt{\frac{2}{3}} \frac{\rho_{2,m}^{\{d\}}}{\zeta_d/2}.$$
(S.207)

The transition frequency contributions are obtained from the product  $\varsigma_{2,m}^{\{d\}}(\mathbb{Pp})_{IS}(m_{I,i},m_{S,i},m_{I,j},m_{S,j})$  transformed into the laboratory frame. The first-order weak dipolar interaction contributions to the Hamiltonian in terms of the fsSSTs is given by

$$\hat{D}_{d_{1S}}^{(1)}/\hbar = \mathfrak{R}_{0,0}^{\{d\}} \,\hat{T}_{1,0}(\vec{I}) \,\hat{T}_{1,0}(\vec{S}) + \mathfrak{R}_{2,0}^{\{d\}} \,\hat{T}_{1,0}(\vec{I}) \,\hat{T}_{1,0}(\vec{S}) \tag{S.208}$$

The components of  $\varsigma_L^{(k)}$  for each contribution are expanded and given in Table S9.

#### S6.2 Cross-term interaction frequency scaled spatial tensor parts

The general expression for the spatial tensor products arising in the cross-term between two interactions is given by

$$\mathcal{R}_{L,M}^{\{\lambda q\}} = \sum_{m=-2}^{2} \langle L \ M | 2 \ 2 \ m \ M - m \rangle R_{2,m}^{\{\lambda\}} \ R_{2,M-m}^{\{q\}}. \tag{S.209}$$

#### S6.2.1 Quadrupolar-Quadrupolar 2nd-order Contributions

From Eqs. (S.132) and (S.133), we obtain the sSST for the quadrupolar-quadrupolar frequency contribution as

$$\Delta_{0,0}^{\{qq\}} = \frac{\omega_q^2}{\omega_0} \frac{\mathcal{R}_{0,0}^{\{qq\}}}{9\zeta_q^2} = \frac{\omega_q^2}{\omega_0 9\zeta_q^2} \sum_m \langle 0 \ 0 | 2 \ 2 \ m \ -m \rangle R_{2,m}^{\{q\}} R_{2,-m}^{\{q\}}, \tag{S.210}$$

$$\Delta_{2,M}^{\{qq\}} = \frac{\omega_q^2}{\omega_0} \frac{\mathcal{R}_{2,M}^{\{qq\}}}{9\zeta_q^2} = \frac{\omega_q^2}{\omega_0 9\zeta_q^2} \sum_m \langle 2\ M|2\ 2\ m\ M - m \rangle R_{2,m}^{\{q\}}\ R_{2,M-m}^{\{q\}}, \tag{S.211}$$

$$\Delta_{4,M}^{\{qq\}} = \frac{\omega_q^2}{\omega_0} \frac{\mathcal{R}_{4,M}^{\{qq\}}}{9\zeta_q^2} = \frac{\omega_q^2}{\omega_0 9\zeta_q^2} \sum_m \langle 4 \ M|2 \ 2 \ m \ M - m \rangle R_{2,m}^{\{q\}} \ R_{2,M-m}^{\{q\}}. \tag{S.212}$$

(S.213)

The scaling factors from the previous page,

$$R_{2,m}^{(q)} = \frac{3\zeta_q}{\omega_q} \Delta_{2,m}^{\{q\}},\tag{S.214}$$

=					
contribution			$arsigma_{L,n}^{(\lambda)}$		
quadrupolar	$\varsigma_{2,0}^{(q)} = \omega_q \frac{1}{\sqrt{6}}$	$\varsigma_{2,\pm 1}^{(q)} = 0$	$\varsigma_{2,\pm 2}^{(q)} = -\omega_q \frac{\eta_q}{6}$		
	$\varsigma_{0,0}^{(qq)} = \frac{\omega_q^2}{\omega_0} \frac{1}{6\sqrt{5}} \left( \frac{\eta_q^2}{3} + 1 \right)$				
	$\varsigma_{2,0}^{(qq)} = \frac{\omega_q^2}{\omega_0} \frac{\sqrt{2}}{6\sqrt{7}} \left( \frac{\eta_q^2}{3} - 1 \right)$	$\varsigma_{2,\pm 1}^{(qq)} = 0$	$ \varsigma_{2,\pm 2}^{(qq)} = -\frac{\omega_q^2}{\omega_0} \frac{1}{3\sqrt{21}} \eta_q $		
	$\varsigma_{4,0}^{(qq)} = \frac{\omega_q^2}{\omega_0} \frac{1}{\sqrt{70}} \left( \frac{\eta_q^2}{18} + 1 \right)$	$\varsigma_{4,\pm 1}^{(qq)} = 0$	$\varsigma_{4,\pm 2}^{(qq)} = -\frac{\omega_q^2}{\omega_0} \frac{\eta_q}{6\sqrt{7}}$	$\varsigma_{4,\pm 3}^{(qq)} = 0$	$\varsigma_{4,\pm 4}^{(qq)} = \frac{\omega_q^2}{\omega_0} \frac{\eta_q^2}{36}$
shielding	$ \varsigma_{0,0}^{(\sigma)} = -\omega_0 \sigma_{\rm iso} $				
	$\varsigma_{2,0}^{(\sigma)} = -\omega_0 \zeta_{\sigma}$	$\varsigma_{2,\pm 1}^{(\sigma)} = 0$	$\varsigma_{2,\pm 2}^{(\sigma)} = \omega_0 \zeta_\sigma \frac{\eta_\sigma}{\sqrt{6}}$		
dipolar	$\varsigma_{2,0}^{(d)} = 2\omega_d$	$\varsigma_{2,\pm 1}^{(d)} = 0$	$\varsigma_{2,\pm 2}^{(d)} = 0$		
J	$\varsigma_{0,0}^{(J)} = 2\pi J_{\rm iso}$				
	$\varsigma_{2,0}^{(J)} = 2\pi\zeta_J$	$\varsigma_{2,\pm 1}^{(J)} = 0$	$\varsigma_{2,\pm 2}^{(J)} = -2\pi\zeta_J \frac{\eta_J}{\sqrt{6}}$		

Table S9: Frequency-scaled spatial spherical tensor elements in the principal axis system for the various NMR interactions.

can be substituted into the above equations to give

$$\Delta_{0,0}^{\{qq\}} = \frac{1}{\omega_0} \sum_{m} \langle 0 \ 0 | 2 \ 2 \ m \ -m \rangle \Delta_{2,m}^{\{q\}} \ \Delta_{2,-m}^{\{q\}}, \tag{S.215}$$

$$\Delta_{2,M}^{\{qq\}} = \frac{1}{\omega_0} \sum_{m} \langle 2 \ M | 2 \ 2 \ m \ M - m \rangle \Delta_{2,m}^{\{q\}} \ \Delta_{2,M-m}^{\{q\}}, \tag{S.216}$$

$$\Delta_{4,M}^{\{qq\}} = \frac{1}{\omega_0} \sum_{m} \langle 4 \ M | 2 \ 2 \ m \ M - m \rangle \Delta_{2,m}^{\{q\}} \ \Delta_{2,M-m}^{\{q\}}. \tag{S.217}$$

The transition frequency contributions are obtained from the products  $\Delta_{L,M}^{\{qq\}} c_L(m_i, m_j)$  transformed into the laboratory frame.

#### S6.2.2 Quadrupolar-Shielding 2nd-order Contributions

From Eqs. (S.152) and (S.153), we obtain the sSST for the quadrupolar-Shielding Cross Term frequency contribution as

$$\Delta_{0,0}^{\{\sigma q\}} = -\omega_q \, \zeta_\sigma \sqrt{\frac{6}{5}} \frac{\mathcal{R}_{0,0}^{\{\sigma q\}}}{3\zeta_q \zeta_\sigma} = -\sqrt{\frac{6}{5}} \frac{\omega_q}{3\zeta_q} \sum_m \langle 0 \ 0 | 2 \ 2 \ m \ -m \rangle R_{2,m}^{\{\sigma\}} R_{2,-m}^{\{q\}}, \tag{S.218}$$

$$\Delta_{2,M}^{\{\sigma q\}} = \omega_q \, \zeta_\sigma \sqrt{\frac{3}{7}} \frac{\mathcal{R}_{2,M}^{\{\sigma q\}}}{3\zeta_q \zeta_\sigma} = \sqrt{\frac{3}{7}} \frac{\omega_q}{3\zeta_q} \sum_m \langle 2 \ M | 2 \ 2 \ m \ M - m \rangle R_{2,m}^{\{\sigma\}} R_{2,M-m}^{\{q\}}$$
 (S.219)

$$\Delta_{4,M}^{\{\sigma q\}} = \omega_q \, \zeta_\sigma \sqrt{\frac{48}{35}} \frac{\mathcal{R}_{4,M}^{\{\sigma q\}}}{3\zeta_q \zeta_\sigma} = \sqrt{\frac{48}{35}} \frac{\omega_q}{3\zeta_q} \sum_m \langle 4 \ M | 2 \ 2 \ m \ M - m \rangle R_{2,m}^{\{\sigma\}} \ R_{2,M-m}^{\{q\}}. \tag{S.220}$$

(S.221)

The scaling factors from the previous page,

$$R_{2,m}^{(q)} = \frac{3\zeta_q}{\omega_q} \Delta_{2,m}^{\{q\}} \quad \text{and} \quad R_{2,m}^{\{\sigma\}} = -\frac{1}{\omega_0} \sqrt{\frac{3}{2}} \Delta_{2,m}^{\{\sigma\}}, \tag{S.222}$$

can be substituted into the above equations to give

$$\Delta_{0,0}^{\{\sigma q\}} = \frac{1}{\omega_0} \sqrt{\frac{9}{5}} \sum_{m} \langle 0 \ 0 | 2 \ 2 \ m \ -m \rangle \Delta_{2,m}^{\{\sigma\}} \ \Delta_{2,-m}^{\{q\}}, \tag{S.223}$$

$$\Delta_{2,M}^{\{\sigma q\}} = -\frac{1}{\omega_0} \sqrt{\frac{9}{14}} \sum_{m} \langle 2 \ M | 2 \ 2 \ m \ M - m \rangle \Delta_{2,m}^{\{\sigma\}} \ \Delta_{2,M-m}^{\{q\}}, \tag{S.224}$$

$$\Delta_{4,M}^{\{\sigma q\}} = -\frac{1}{\omega_0} \sqrt{\frac{72}{35}} \sum_{m} \langle 4 \ M | 2 \ 2 \ m \ M - m \rangle \Delta_{2,m}^{\{\sigma\}} \ \Delta_{2,M-m}^{\{q\}}. \tag{S.225}$$

The transition frequency contributions are obtained from the products  $\Delta_{L,M}^{\{\sigma q\}} \mathbf{d}_I(m_i,m_j)$  transformed into the laboratory frame. The second-order quadrupolar-shielding cross-term contributions to the Hamiltonian in terms of the fsSSTs is given by

$$\hat{D}_{\sigma,q}^{(2)}/\hbar = \left(-\sqrt{\frac{6}{5}} \frac{\omega_q}{3\zeta_q} \mathcal{R}_{0,0}^{\{\sigma q\}} + \sqrt{\frac{3}{7}} \frac{\omega_q}{3\zeta_q} \mathcal{R}_{2,0}^{\{\sigma q\}} + \sqrt{\frac{48}{35}} \frac{\omega_q}{3\zeta_q} \mathcal{R}_{4,0}^{\{\sigma q\}}\right) \hat{T}_{2,0}(\vec{I})$$

$$= \left[\sum_{L=0,2,4} \sum_{M=-L}^{L} \mathcal{D}_{M,0}^{(L)}(\omega_R t + \phi_0, \theta_R, 0) \Delta_{L,M}^{\{\sigma q\}}\right] \hat{T}_{2,0}(\vec{I}). \quad (S.226)$$

#### S6.2.3 Quadrupolar-weak J 2nd-order Contributions

From Eqs. (S.172) and (S.173) we obtain the sSST for the quadrupolar-weak J cross term frequency contribution as

$$\Delta_{0,0}^{\{Jq_I\}} = 2\pi\zeta_J \left(\frac{\omega_{q,I}}{\omega_{0,I}}\right) \sqrt{\frac{6}{5}} \frac{\mathcal{R}_{0,0}^{\{Jq_I\}}}{3\zeta_{q_I}\zeta_J} = \left(\frac{\omega_{q,I}}{\omega_{0,I}}\right) \sqrt{\frac{6}{5}} \frac{2\pi}{3\zeta_{q_I}} \sum_m \langle 0 \ 0|2 \ 2 \ m \ -m \rangle R_{2,m}^{\{J\}} \ R_{2,-m}^{\{q_I\}}, \tag{S.227}$$

$$\Delta_{2,m}^{\{Jq_I\}} = -2\pi\zeta_J \left(\frac{\omega_{q,I}}{\omega_{0,I}}\right) \sqrt{\frac{3}{7}} \frac{\Re_{2,0}^{\{Jq_I\}}}{3\zeta_{q_I}\zeta_J} = -\left(\frac{\omega_{q,I}}{\omega_{0,I}}\right) \sqrt{\frac{3}{7}} \frac{2\pi}{3\zeta_{q_I}} \sum_m \langle 2\ M|2\ 2\ m\ M-m \rangle R_{2,m}^{\{J\}}\ R_{2,M-m}^{\{q_I\}}, \tag{S.228}$$

$$\Delta_{4,M}^{\{Jq_I\}} = -2\pi\zeta_J \left(\frac{\omega_{q,I}}{\omega_{0,I}}\right) \sqrt{\frac{48}{35}} \frac{\mathcal{R}_{4,0}^{\{Jq_I\}}}{3\zeta_{q_I}\zeta_J} = -\left(\frac{\omega_{q,I}}{\omega_{0,I}}\right) \sqrt{\frac{48}{35}} \frac{2\pi}{3\zeta_{q_I}} \sum_m \langle 4 \ M|2 \ 2 \ m \ M-m \rangle R_{2,m}^{\{J\}} \ R_{2,M-m}^{\{q_I\}}. \tag{S.229}$$

The scaling factors from the previous page,

$$R_{2,M}^{(q_I)} = \frac{3\zeta_{q_I}}{\omega_{q,I}} \Delta_{2,M}^{\{q_I\}} \quad \text{and} \quad R_{2,M}^{\{J\}} = \frac{1}{2\pi} \sqrt{\frac{3}{2}} \Delta_{2,M}^{\{J\}}, \tag{S.230}$$

can be substituted into the above equations to give

$$\Delta_{0,0}^{\{Jq_I\}} = \frac{1}{\omega_{0,I}} \sqrt{\frac{9}{5}} \sum_{m} \langle 0 \ 0 | 2 \ 2 \ m \ -m \rangle \Delta_{2,m}^{\{J\}} \Delta_{2,-m}^{\{q_I\}}, \tag{S.231}$$

$$\Delta_{2,M}^{\{Jq_I\}} = -\frac{1}{\omega_{0,I}} \sqrt{\frac{9}{14}} \sum_{m} \langle 2 \ M | 2 \ 2 \ m \ M - m \rangle \Delta_{2,m}^{\{J\}} \Delta_{2,M-m}^{\{q_I\}}, \tag{S.232}$$

$$\Delta_{4,M}^{\{Jq_I\}} = -\frac{1}{\omega_{0,I}} \sqrt{\frac{72}{35}} \sum_{m} \langle 4 \ M | 2 \ 2 \ m \ M - m \rangle \Delta_{2,m}^{\{J\}} \Delta_{2,M-m}^{\{q_I\}}. \tag{S.233}$$

The transition frequency contributions are obtained from the products  $\Delta_{L,M}^{\{Jq_I\}}(d\mathbb{p})_{IS}(m_{I,i},m_{S,i},m_{I,j},m_{S,j})$  transformed into the laboratory frame. The second-order quadrupolar-J cross-term contributions to the Hamiltonian in terms of the fsSSTs is given by

$$\hat{D}_{J,q_I}^{(2)}/\hbar = \left[\sum_{L=0,2,4} \sum_{M=-L}^{L} \mathcal{D}_{M,0}^{(L)}(\omega_R t + \phi_0, \theta_R, 0) \Delta_{L,M}^{\{Jq_I\}}\right] \hat{T}_{2,0}(\vec{I}) \hat{T}_{1,0}(\vec{S}). \tag{S.234}$$

Similarly, one obtains

$$\Delta_{0,0}^{\{Jq_S\}} = \frac{1}{\omega_{0,S}} \sqrt{\frac{9}{5}} \sum_{m} \langle 0 \ 0 | 2 \ 2 \ m \ -m' \rangle \Delta_{2,m}^{\{J\}} \Delta_{2,-m}^{\{q_S\}}, \tag{S.235}$$

$$\Delta_{2,M}^{\{Jq_S\}} = -\frac{1}{\omega_{0,S}} \sqrt{\frac{9}{14}} \sum_{m} \langle 2 \ M|2 \ 2 \ m \ M - m \rangle \Delta_{2,m}^{\{J\}} \Delta_{2,M-m}^{\{q_S\}}, \tag{S.236}$$

$$\Delta_{4,M}^{\{Jq_S\}} = -\frac{1}{\omega_{0,S}} \sqrt{\frac{72}{35}} \sum_{m} \langle 4 \ M | 2 \ 2 \ m \ M - m \rangle \Delta_{2,m}^{\{J\}} \Delta_{2,M-m'}^{\{q_S\}}. \tag{S.237}$$

The transition frequency contributions are obtained from the products  $\Delta_{L,M}^{\{Jq_S\}}(\mathbb{pd})_{IS}(m_{I,i},m_{S,i},m_{I,j},m_{S,j})$  transformed into the laboratory frame. The second-order quadrupolar-J cross-term contributions to the Hamiltonian in terms of the fsSSTs is given by

$$\hat{D}_{J,q_S}^{(2)}/\hbar = \left[\sum_{L=0,2,4} \sum_{M=-L}^{L} \mathcal{D}_{M,0}^{(L)}(\omega_R t + \phi_0, \theta_R, 0) \Delta_{L,M}^{\{Jq_S\}}\right] \hat{T}_{1,0}(\vec{I}) \hat{T}_{2,0}(\vec{S}). \tag{S.238}$$

#### S6.2.4 Quadrupolar-Dipolar 2nd-order Contributions

From Eqs. (S.192) and (S.193), we obtain the sSST for the quadrupolar-weak dipolar cross-term frequency contribution as

$$\Delta_{0,0}^{\{dq_I\}} = \frac{1}{\omega_{0,I}} \sqrt{\frac{9}{5}} \sum_{m} \langle 0 \ 0 | 2 \ 2 \ m \ -m \rangle \Delta_{2,m}^{\{d\}} \Delta_{2,-m}^{\{q_I\}}, \tag{S.239}$$

$$\Delta_{2,M}^{\{dq_I\}} = -\frac{1}{\omega_{0,I}} \sqrt{\frac{9}{14}} \sum_{m} \langle 2 \ M | 2 \ 2 \ m \ M - m \rangle \Delta_{2,m}^{\{d\}} \Delta_{2,M-m}^{\{q_I\}}, \tag{S.240}$$

$$\Delta_{4,M}^{\{dq_I\}} = -\frac{1}{\omega_{0,I}} \sqrt{\frac{72}{35}} \sum_{m} \langle 4 \ M | 2 \ 2 \ m \ M - m \rangle \Delta_{2,m}^{\{d\}} \Delta_{2,M-m}^{\{q_I\}}. \tag{S.241}$$

The transition frequency contributions are obtained from the products  $\Delta_{L,M}^{\{dq_I\}}(d\mathbb{p})_{IS}(m_{I,i},m_{S,i},m_{I,j},m_{S,j})$  transformed into the laboratory frame. The second-order quadrupolar-dipolar cross-term contributions to the Hamiltonian in terms of the fsSSTs is given by

$$\hat{D}_{d,q_I}^{(2)}/\hbar = \left[\sum_{L=0,2,4} \sum_{M=-L}^{L} \mathcal{D}_{M,0}^{(L)}(\omega_R t + \phi_0, \theta_R, 0) \Delta_{L,M}^{\{dq_I\}}\right] \hat{T}_{2,0}(\vec{I}) \hat{T}_{1,0}(\vec{S}). \tag{S.242}$$

Similarly, from Eqs. (S.194) and (S.195), we obtain the sSST for the quadrupolar-weak dipolar cross-term frequency contribution as

$$\Delta_{0,0}^{\{dq_S\}} = \frac{1}{\omega_{0,S}} \sqrt{\frac{9}{5}} \sum_{m} \langle 0 \ 0 | 2 \ 2 \ m \ -m \rangle \Delta_{2,m}^{\{d\}} \Delta_{2,-m}^{\{q_S\}}, \tag{S.243}$$

$$\Delta_{2,M}^{\{dq_S\}} = -\frac{1}{\omega_{0,S}} \sqrt{\frac{9}{14}} \sum_{m} \langle 2 \ M | 2 \ 2 \ m \ M - m \rangle \Delta_{2,m}^{\{d\}} \Delta_{2,M-m}^{\{q_S\}}, \tag{S.244}$$

$$\Delta_{4,M}^{\{dq_S\}} = -\frac{1}{\omega_{0,S}} \sqrt{\frac{72}{35}} \sum_{m} \langle 4 \ M | 2 \ 2 \ m \ M - m \rangle \Delta_{2,m}^{\{d\}} \Delta_{2,M-m}^{\{q_S\}}. \tag{S.245}$$

The transition frequency contributions are obtained from the products  $\Delta_{L,M}^{\{dq_S\}}(\mathbb{pd})_{IS}(m_{I,i},m_{S,i},m_{I,j},m_{S,j})$  transformed into the laboratory frame. The second-order quadrupolar-dipolar cross-term contributions to the Hamiltonian in terms of the fsSSTs is given by

$$\hat{D}_{d,q_S}^{(2)}/\hbar = \left[\sum_{L=0,2,4} \sum_{M=-L}^{L} \mathcal{D}_{M,0}^{(L)}(\omega_R t + \phi_0, \theta_R, 0) \Delta_{L,M}^{\{dq_S\}}\right] \hat{T}_{1,0}(\vec{I}) \hat{T}_{2,0}(\vec{S}). \tag{S.246}$$

### S6.3 Total Transition Frequency Tensor in the Common Frame

The product of each  $\Delta_L$  with its corresponding spin transition function for each perturbation term creates a frequency tensor contribution. The transition frequency tensor contributions currently available in mrsimulator are in Tables 2 of the main article. We can sum all the frequency tensor contributions of similar ranks together into total transition frequency tensors of rank L, as illustrated below:

$$\mathbf{F}_{0} = \mathbf{\Delta}_{0}^{\{\sigma\}} \mathbb{p}_{I} + \mathbf{\Delta}_{0}^{\{J\}} (\mathbb{pp})_{IS} + \mathbf{\Delta}_{0}^{\{qq\}} \mathbb{c}_{0} + \mathbf{\Delta}_{0}^{\{\sigma q\}} \mathbb{d}_{I} + \mathbf{\Delta}_{0}^{\{dq\}} (\mathbb{dp})_{IS} + \mathbf{\Delta}_{0}^{\{Jq\}} (\mathbb{dp})_{IS}, \tag{S.247}$$

$$\mathbf{F}_{2} = \mathbf{\Delta}_{2}^{\{\sigma\}} \mathbb{p}_{I} + \mathbf{\Delta}_{2}^{\{J\}} (\mathbb{pp})_{IS} + \mathbf{\Delta}_{2}^{\{d_{IS}\}} (\mathbb{pp})_{IS} + \mathbf{\Delta}_{2}^{\{q\}} \mathbb{d}_{I} + \mathbf{\Delta}_{2}^{\{qq\}} \mathbb{c}_{2} + \mathbf{\Delta}_{2}^{\{\sigma q\}} \mathbb{d}_{I} + \mathbf{\Delta}_{2}^{\{dq\}} (\mathbb{dp})_{IS} + \mathbf{\Delta}_{2}^{\{Jq\}} (\mathbb{dp})_{IS}, \quad (S.248)$$

$$\mathbf{F}_4 = \mathbf{\Delta}_4^{\{qq\}} \mathbf{c}_4 + \mathbf{\Delta}_4^{\{\sigma q\}} \mathbf{d}_I + \mathbf{\Delta}_4^{\{dq\}} (\mathbf{dp})_{IS} + \mathbf{\Delta}_4^{\{Jq\}} (\mathbf{dp})_{IS}. \tag{S.249}$$

From the total transition frequency tensor in the common frame, we obtain the total transition frequency in the lab frame from the total transition frequency tensor in the common frame,  $\mathbf{F}_L$ , as

$$\Omega(t,i,j) = \sum_{L=0,2,4} \sum_{m=-L}^{L} e^{-im(\omega_R t + \phi)} d_{m,0}^{(L)}(\theta_R) \sum_{m'=-L}^{L} e^{-im_1 \alpha} d_{m',m}^{(L)}(\beta) e^{-im\gamma} F_{L,m'}(i,j).$$
 (S.250)

# S7 Single Transition Coherence Transfer in High $\omega_1$ Limit

The RF Hamiltonian after transforming into the multiply rotating interaction frame of the nuclei in each channel, can be written

$$\hat{\mathcal{H}}_{RF}/\hbar = \sum_{c=1}^{n_c} \sum_{u \in \mathcal{I}_c} \omega_{1,c} \left[ \hat{I}_{x,u} \cos \psi_c + \hat{I}_{y,u} \sin \psi_c \right], \tag{S.251}$$

where  $\omega_{1,c}$  and  $\psi_c$  are the RF amplitude and phase for the nuclei in the  $c^{\text{th}}$  channel, respectively, and  $\hat{I}_{x,u}$  and  $\hat{I}_{y,u}$  are the x and y components of the spin operator for the  $u^{\text{th}}$  nucleus.  $n_{\mathcal{I}} = \sum_{c} n_{c}$ 

Describing the state space by a direct product space,

$$|I_1, \dots, I_{n_{\mathcal{I}}}, m_{1,i}, \dots, m_{n_{\mathcal{I}},i}\rangle = |I_1, m_1\rangle \otimes |I_2, m_2\rangle \otimes \dots \otimes |I_n, m_n\rangle = \bigotimes_{c=1}^{n_c} \bigotimes_{u \in \mathcal{I}_c} |I_u, m_u\rangle, \tag{S.252}$$

a single transition operator is written as

$$\hat{\chi}_A = |I_1, \dots, I_{n_{\mathcal{I}}}, m_{1,j}, \dots, m_{n_{\mathcal{I}},j}\rangle \langle I_1, \dots, I_{n_{\mathcal{I}}}, m_{1,i}, \dots, m_{n_{\mathcal{I}},i}| = \left[\bigotimes_{c=1}^{n_c} \bigotimes_{u \in \mathcal{I}_c} |I_u, m_{u,j}\rangle \langle I_u, m_{u,i}|\right]. \tag{S.253}$$

The propagator for an ideal pulse in NMR is given by

$$\hat{U}_{RF} = e^{-\frac{i}{\hbar}\mathcal{H}_{RF}t} = \bigotimes_{c=1}^{n_c} \bigotimes_{u \in \mathfrak{I}_c} e^{-i\theta_c \left(\hat{I}_{u,x} \cos \phi_c + \hat{I}_{u,y} \sin \phi_c\right)} = \bigotimes_{c=1}^{n_c} \bigotimes_{u \in \mathfrak{I}_c} \hat{\mathbf{D}}_u^{(I_u)}(\alpha_c, \beta_c, \gamma_c), \tag{S.254}$$

where we define  $\theta_c = \omega_{1,c}t$  is the angle of rotation, and

$$\alpha_c = \psi_c - \frac{\pi}{2}, \quad \beta_c = \theta_c, \quad \gamma_c = \frac{\pi}{2} - \psi_c,$$
 (S.255)

with

$$\hat{\mathbf{D}}^{(I)}(\alpha,\beta,\gamma) = e^{-i\alpha\hat{I}_z} e^{-i\beta\hat{I}_y} e^{-i\gamma\hat{I}_z}.$$
(S.256)

Thus, we write the propagator as a rotation of the operator,  $\hat{\chi}_A$ , in the Zeeman basis as,

$$\hat{U}_{RF}\hat{\chi}_{A}\hat{U}_{RF}^{\dagger} = \bigotimes_{c=1}^{n_{c}} \bigotimes_{u \in \mathcal{I}_{c}} \hat{\mathbf{D}}_{u}^{(I_{u})}(\alpha_{c}, \beta_{c}, \gamma_{c}) |I_{u^{*}}, m_{u^{*}, j}\rangle \langle I_{u^{*}}, m_{u^{*}, i} | \left[ \hat{\mathbf{D}}_{u}^{(I_{u'})}(\alpha_{c'}, \beta_{c'}, \gamma_{c'}) \right]^{-1}$$
(S.257)

where

$$\left[\hat{\mathbf{D}}^{(I)}(\alpha,\beta,\gamma)\right]^{-1} = e^{i\gamma\hat{I}_z}e^{i\beta\hat{I}_y}e^{i\alpha\hat{I}_z}.$$
 (S.258)

We can insert the identity operator in the form of

$$\hat{1}_{u} = \sum_{m'_{u,j}} |I_{u}, m'_{u,j}\rangle \langle I_{u}, m'_{u,j}| = \sum_{m'_{u,i}} |I_{u}, m'_{u,i}\rangle \langle I_{u}, m'_{u,i}|$$
(S.259)

into Eq.(S.257) and obtain,

$$\hat{U}_{RF}\hat{\chi}_{A}\hat{U}_{RF}^{\dagger} = \bigotimes_{c=1}^{n_{c}} \bigotimes_{u \in \mathfrak{I}_{c}} \sum_{m'_{u,j}} \sum_{m'_{u,i}} \left| I_{u}, m'_{u,j} \right\rangle \left\langle I_{u}, m'_{u,j} \middle| \hat{\mathbf{D}}_{u}^{(I_{u})}(\alpha_{c}, \beta_{c}, \gamma_{c}) \middle| I_{u}, m_{u,j} \right\rangle \\
\left\langle I_{u}, m_{u,i} \middle| \hat{\mathbf{D}}_{u}^{-1}(\alpha_{c}, \beta_{c}, \gamma_{c}) \middle| I_{u}, m'_{u,i} \middle\rangle \left\langle I_{u}, m'_{u,i} \middle| . \quad (S.260) \right\rangle$$

Since

$$\langle I, m_i | \hat{\mathbf{D}}^{-1}(\alpha, \beta, \gamma) | I, m_i' \rangle = \mathcal{D}_{m_i', m_i}^{*(I)}(\alpha, \beta, \gamma), \quad \text{and} \quad \langle I, m_j | \hat{\mathbf{D}}(\alpha, \beta, \gamma) | I, m_j' \rangle = \mathcal{D}_{m_j, m_i'}^{(I)}(\alpha, \beta, \gamma),$$
 (S.261)

we write Eq.(S.260) as,

$$\hat{U}_{RF}\hat{\chi}_{A}\hat{U}_{RF}^{\dagger} = \bigotimes_{c=1}^{n_{c}} \bigotimes_{u \in \mathfrak{I}_{c}} \sum_{m'_{u,j}} \mathcal{D}_{m'_{u,i}}^{(I)} \mathcal{D}_{m'_{u,j},m_{u,j}}^{(I)} (\alpha_{c},\beta_{c},\gamma) \mathcal{D}_{m'_{u,i},m_{u,i}}^{*(I)} (\alpha_{c},\beta_{c},\gamma_{c}) |I_{u},m'_{u,j}\rangle \langle I_{u},m'_{u,i}|.$$
 (S.262)

The Wigner  $\mathcal{D}$ -functions can be written in terms of the reduced Wigner d-functions and exponentials allowing for us to write Eq.(S.262) as,

$$\hat{U}_{RF}\hat{\chi}_{A}\hat{U}_{RF}^{\dagger} = \bigotimes_{c=1}^{n_{c}} \bigotimes_{u \in \mathfrak{I}_{c}} \sum_{m'_{u,i}} \sum_{m'_{u,i}} d_{m'_{u,j},m_{u,j}}^{(I)}(\beta_{c}) d_{m'_{u,i},m_{u,i}}^{(I)}(\beta_{c}) e^{-ip'_{u}\alpha_{c}} e^{-ip_{u}\gamma_{c}} |I_{u}, m'_{u,j}\rangle \langle I_{u}, m'_{u,i}|,$$
(S.263)

combining terms, defining  $p'_u = m'_{u,j} - m'_{u,i}$ ,  $p_u = m_{u,j} - m_{u,i}$ . Using the definitions in Eq.(S.255) we write Eq.(S.263) as,

$$\hat{U}_{RF}\hat{\chi}_{A}\hat{U}_{RF}^{\dagger} = \bigotimes_{c=1}^{n_{c}} \bigotimes_{u \in \mathfrak{I}_{c}} \sum_{m'_{u,i}} \sum_{m'_{u,i}} d_{m'_{u,i},m_{u,j}}^{(I)}(\theta_{c}) d_{m'_{u,i},m_{u,i}}^{(I)}(\theta_{c}) e^{-i(p'_{u}-p_{u})\psi_{c}} e^{i(p'_{u}-p_{u})\frac{\pi}{2}} |I_{u}, m'_{u,j}\rangle \langle I_{u}, m'_{u,i}|.$$
 (S.264)

Further defining  $\Delta p_u = p'_u - p_u$ , Eq.(S.264) becomes,

$$\hat{U}_{RF}\hat{\chi}_{A}\hat{U}_{RF}^{\dagger} = \bigotimes_{c=1}^{n_{c}} \bigotimes_{u \in \mathfrak{I}_{c}} \sum_{m'_{u,i}} \sum_{m'_{u,i}} d_{m'_{u,j},m_{u,j}}^{(I)}(\theta_{c}) d_{m'_{u,i},m_{u,i}}^{(I)}(\theta_{c}) e^{-i\Delta p_{u}\psi_{c}}(i)^{\Delta p_{u}} |I_{u}, m'_{u,j}\rangle \langle I_{u}, m'_{u,i}|.$$
 (S.265)

From Eq.(S.265) we find that the efficiency associated with the transition  $\bigotimes_{c=1}^{n_c} \bigotimes_{u \in \mathfrak{I}_c} |I_u, m_{u,j}\rangle \langle I_u, m_{u,i}| \to \bigotimes_{c=1}^{n_c} \bigotimes_{u \in \mathfrak{I}_c} |I_u, m'_{u,j}\rangle \langle I_u, m'_{u,i}|$  is

$$\prod_{c=1}^{n_c} \prod_{u \in \mathfrak{I}_c} d_{m'_{u,j},m_{u,j}}^{(I_u)}(\theta_c) d_{m'_{u,i},m_{u,i}}^{(I_u)}(\theta_c) e^{-i\Delta p_u \psi_c} (i)^{\Delta p_u}.$$
(S.266)

# S8 Transition Pathway Signal in a Rotating Sample

The free evolution of a transition  $\hat{\chi} = |j\rangle \langle i|$  under the quantum mechanical propagator, arising from a Hamiltonian that is diagonal in the Zeeman basis, is given by

$$\hat{U}(t_1, t_0 | \alpha, \beta, \gamma) \hat{\chi} \hat{U}^{\dagger}(t_1, t_0 | \alpha, \beta, \gamma) = \exp \left\{ -\frac{i}{\hbar} \int_{t_0}^{t_1} \hat{\mathcal{H}}(s) ds \right\} |j\rangle \langle i| \exp \left\{ \frac{i}{\hbar} \int_{t_0}^{t_1} \hat{\mathcal{H}}(s) ds \right\} \\
= u_{\chi}(t_1, t_0 | \alpha, \beta, \gamma) |j\rangle \langle i|, \quad (S.267)$$

where

$$u_{\chi}(t_1, t_0 | \alpha, \beta, \gamma) = \exp\left\{-i \int_{t_0}^{t_1} \Omega_{\chi}(s) ds\right\}.$$
 (S.268)

Here,  $\Omega_{\chi}(t) = E_j(t) - E_i(t)$  is the time-dependent frequency for the  $i \to j$  transition, which we write by recasting Eq. (S.250) into the form

$$\Omega_{\chi}(t) = \sum_{L=0,2,4} \left[ \varpi_{L,0}(\theta_R, \alpha, \beta) + \sum_{\substack{m=-L\\m\neq 0}}^{L} \varpi_{L,m}(\theta_R, \alpha, \beta) e^{-im(\omega_R t + \phi + \gamma)} \right],$$

where  $\omega_R$  is the rotor frequency,  $\phi$  is the initial rotor phase, and

$$\varpi_{L,m}(\theta_R, \alpha, \beta)e^{-im(\omega_R t + \phi + \gamma)} = d_{m,0}^{(L)}(\theta_R)e^{-im(\omega_R t + \phi + \gamma)} \sum_{m' = -L}^{L} e^{-im'\alpha} d_{m',m}^{(L)}(\beta)F_{L,m'}(i,j). \tag{S.269}$$

Note that

$$\varpi_{L,m}^{*}\left(\theta_{R},\alpha,\beta\right) = \varpi_{L,-m}\left(\theta_{R},\alpha,\beta\right). \tag{S.270}$$

Evaluating the integral in Eq. (S.268) gives

$$\Psi(t_1, t_0) = \int_{t_0}^{t_1} \Omega_{\chi}(s) ds = W_{\chi}(\theta_R, \alpha, \beta)(t_1 - t_0) + \sum_{\substack{m = -4 \\ m \neq 0}}^{4} W_{m, \chi}(\theta_R, \alpha, \beta) e^{-im(\gamma + \phi)} \left\{ e^{-im\omega_R t_1} - e^{-im\omega_R t_0} \right\},$$

$$= W_{\chi}(\theta_R, \alpha, \beta)(t_1 - t_0) + \sum_{\substack{m = -4 \\ m \neq 0}}^{4} W_{m,\chi}(\theta_R, \alpha, \beta)e^{-im(\omega_R t_1 + \gamma + \phi)} - \sum_{\substack{m = -4 \\ m \neq 0}}^{4} W_{m,\chi}(\theta_R, \alpha, \beta)e^{-im(\omega_R t_0 + \gamma + \phi)}, \quad (S.271)$$

where

$$W_{\chi}(\theta_R, \alpha, \beta) = \sum_{L=0,2,4} \varpi_{L,0}(\theta_R, \alpha, \beta), \quad \text{and} \quad W_{m,\chi}(\theta_R, \omega_R, \alpha, \beta) = \sum_{L=2,4} \frac{\varpi_{L,m}(\theta_R, \alpha, \beta)}{im\omega_R}.$$
 (S.272)

Also, note that

$$W_{m,\chi}^*(\theta_R,\omega_R,\alpha,\beta) = \sum_{L=2,4} \frac{\varpi_{L,m}^*(\theta_R,\alpha,\beta)}{-im\omega_R} = \sum_{L=2,4} \frac{\varpi_{L,-m}(\theta_R,\alpha,\beta)}{i(-m)\omega_R} = W_{-m,\chi}(\theta_R,\omega_R,\alpha,\beta). \tag{S.273}$$

Following Mehring [24],  $u_{\chi}(t|\alpha,\beta,\gamma)$  can be rewritten using the property of Dirac delta functions of a periodic function

$$\int_{\text{all }\Phi} d\Phi \delta(\Phi - \theta) f(\Phi) = f(\theta), \tag{S.274}$$

to obtain

$$u_{\chi}(t_{1},t_{0}|\alpha,\beta,\gamma) = e^{-iW_{\chi}(\theta_{R},\alpha,\beta)(t_{1}-t_{0})}$$

$$\times \frac{1}{2\pi} \int_{0}^{2\pi} d\Phi_{1}\delta(\Phi_{1}-\omega_{R}t_{1}-\gamma-\phi) \exp\left\{-i\sum_{\substack{m=-4\\m\neq 0}}^{4} W_{m,\chi}(\theta_{R},\omega_{R},\alpha,\beta)e^{-im\Phi_{1}}\right\}$$

$$\times \frac{1}{2\pi} \int_{0}^{2\pi} d\Phi_{2}\delta(\Phi_{2}-\omega_{R}t_{0}-\gamma-\phi) \exp\left\{i\sum_{m=-4}^{4} W_{m,\chi}(\theta_{R},\omega_{R},\alpha,\beta)e^{-im\Phi_{2}}\right\}. \quad (S.275)$$

The Dirac delta functions can then be expanded as sums using the identity

$$\delta(\Theta - \theta) = \sum_{N = -\infty}^{\infty} e^{\pm iN(\Theta - \theta)},$$
 (S.276)

giving

$$u_{\chi}(t_{1}, t_{0} | \alpha, \beta, \gamma) = e^{-iW_{\chi}(\theta_{R}, \alpha, \beta)(t_{1} - t_{0})} \times \frac{1}{2\pi} \int_{0}^{2\pi} d\Phi_{1} \sum_{N_{1} = -\infty}^{\infty} e^{iN_{1}(\Phi_{1} - \omega_{R}t_{1} - \gamma - \phi)} \exp \left\{ -i \sum_{\substack{m = -4 \\ m \neq 0}}^{4} W_{m,\chi}(\theta_{R}, \omega_{R}, \alpha, \beta) e^{-im\Phi_{1}} \right\} \times \frac{1}{2\pi} \int_{0}^{2\pi} d\Phi_{2} \sum_{N_{2} = -\infty}^{\infty} e^{-iN_{2}(\Phi_{2} - \omega_{R}t_{0} - \gamma - \phi)} \exp \left\{ i \sum_{\substack{m = -4 \\ m \neq 0}}^{4} W_{m,\chi}(\theta_{R}, \omega_{R}, \alpha, \beta) e^{-im\Phi_{2}} \right\}. \quad (S.277)$$

After regrouping, we obtain

$$u_{\chi 0}(\alpha, \beta, \gamma) = e^{-iW_{\chi}(\theta_{R}, \alpha, \beta)(t_{1} - t_{0})}$$

$$\times \sum_{N_{1} = -\infty}^{\infty} \left[ \frac{1}{2\pi} \int_{0}^{2\pi} d\Phi_{1} \exp\left\{ iN_{1}\Phi_{1} - i\sum_{\substack{m = -4\\ m \neq 0}}^{4} W_{m,\chi}(\theta_{R}, \omega_{R}, \alpha, \beta)e^{-im\Phi_{1}} \right\} \right] e^{-iN_{1}(\gamma + \phi)}e^{-iN_{1}\omega_{R}t_{1}}$$

$$\times \sum_{N_{2} = -\infty}^{\infty} \left[ \frac{1}{2\pi} \int_{0}^{2\pi} d\Phi_{2} \exp\left\{ -iN_{2}\Phi_{2} + i\sum_{\substack{m = -4\\ m \neq 0}}^{4} W_{m,\chi}(\theta_{R}, \omega_{R}, \alpha, \beta)e^{-im\Phi_{2}} \right\} \right] e^{iN_{2}(\gamma + \phi)}e^{iN_{2}\omega_{R}t_{0}}. \quad (S.278)$$

Thus, we write

$$u_{\chi 0}(\alpha, \beta, \gamma) = e^{-iW_{\chi}(\theta_R, \alpha, \beta)(t_1 - t_0)}$$

$$\sum_{N_{1}=-\infty}^{\infty} \sum_{N_{2}=-\infty}^{\infty} A_{\chi}(N_{1}|\theta_{R},\omega_{R},\alpha,\beta) A_{\chi}^{*}(N_{2}|\theta_{R},\omega_{R},\alpha,\beta) e^{-iN_{1}(\gamma+\phi)} e^{iN_{2}(\gamma+\phi)} e^{-iN_{1}\omega_{R}t_{1}} e^{iN_{2}\omega_{R}t_{0}}, \quad (S.279)$$

defining

$$A_{\chi}(N|\theta_R, \omega_R, \alpha, \beta) = \frac{1}{2\pi} \int_0^{2\pi} a_{\chi}(\Phi|\theta_R, \omega_R, \alpha, \beta) e^{iN\Phi} d\Phi,$$
 (S.280)

where

$$a_{\chi}(\Phi|\theta_R,\omega_R,\alpha,\beta) = \exp\left\{-i\sum_{\substack{m=-4\\m\neq 0}}^4 W_{m,\chi}(\theta_R,\omega_R,\alpha,\beta)e^{-im\Phi}\right\}.$$
 (S.281)

From Eq. (S.281) we obtain

$$a^*(\Phi|\theta_R, \omega_R, \alpha, \beta) = \exp\left\{i \sum_{\substack{m=-4\\m\neq 0}}^4 W_m^*(\theta_R, \omega_R, \alpha, \beta) e^{im\Phi}\right\} = \exp\left\{i \sum_{\substack{m=-4\\m\neq 0}}^4 W_{-m}(\theta_R, \omega_R, \alpha, \beta) e^{im\Phi}\right\}$$
$$= \exp\left\{i \sum_{\substack{m=-4\\m\neq 0}}^4 W_m(\theta_R, \omega_R, \alpha, \beta) e^{-im\Phi}\right\}. \quad (S.282)$$

and obtain

$$A_{\chi}^{*}(N|\theta_{R},\omega_{R},\alpha,\beta) = \frac{1}{2\pi} \int_{0}^{2\pi} a_{\chi}^{*}(\Phi|\theta_{R},\omega_{R},\alpha,\beta)e^{-iN\Phi}d\Phi.$$
 (S.283)

Equation (S.280) also reveals the important discrete Fourier relationships [13, 22] between sideband order, N, and rotor pitch,  $\Phi$ , i.e.,

$$A(\pm N) = \frac{1}{2\pi} \int_{-\pi}^{\pi} a(\Phi) e^{\pm iN\Phi} d\Phi. \text{ and } a(\Phi) = \sum_{N=-\infty}^{\infty} A(\pm N) e^{\mp iN\Phi},$$
 (S.284)

$$A^*(\pm N) = \frac{1}{2\pi} \int_{-\pi}^{\pi} a^*(\Phi) e^{\mp iN\Phi} d\Phi. \text{ and } a^*(\Phi) = \sum_{N=-\infty}^{\infty} A^*(\pm N) e^{\pm iN\Phi}.$$
 (S.285)

The numerical calculation of the  $A(N|\theta_R, \omega_R, \alpha, \beta, 0)$  proceeds as follows. We expand the  $\pm m$  pairs in the exponential term as

$$W_{-m}(\theta_R, \omega_R, \alpha, \beta)e^{im\theta} + W_m(\theta_R, \omega_R, \alpha, \beta)e^{-im\theta}$$

$$= 2X_m(\theta_R, \omega_R, \alpha, \beta)\cos m\theta - 2Y_m(\theta_R, \omega_R, \alpha, \beta)\sin m\theta, \quad (S.286)$$

to substitute into the expression for  $a(\Phi|\theta_R,\omega_R,\alpha,\beta,0)$  in Eq. (S.281) to obtain

$$a(\Phi|\theta_R, \omega_R, \alpha, \beta) = \exp\left[i\sum_{m=1}^4 \left\{2X_m(\theta_R, \omega_R, \alpha, \beta)\cos m\Phi - 2Y_m(\theta_R, \omega_R, \alpha, \beta)\sin m\Phi\right\}\right]. \tag{S.287}$$

For a given value of  $\alpha$  and  $\beta$ , this function is numerically evaluated from  $\Phi = 0$  to  $2\pi$  with a  $\Delta\Phi$  increment. Following Eq. (S.284), we transform  $a(\Phi|\theta_R, \omega_R, \alpha, \beta)$  into  $A(N|\theta_R, \omega_R, \alpha, \beta)$ . To avoid aliasing of signals in the sideband order dimension, the  $\Delta\Phi$  increment must be smaller than  $\pi/|N_{\rm band}|$ , where  $|N_{\rm band}|$  is the highest order sideband present in the sideband pattern.

Further rearranging of Eq. (S.279) gives

$$u_{\chi}(t_1, t_0 | \alpha, \beta, \gamma) = \sum_{N,N'} A_{\chi}(N | \theta_R, \omega_R, \alpha, \beta) A_{\chi}^*(N' | \theta_R, \omega_R, \alpha, \beta)$$

$$\times e^{i(N'-N)(\gamma+\phi)} e^{i(N'-N)\omega_R t_0} e^{-i(W_{\chi}(\theta_R, \alpha, \beta) + N\omega_R)\Delta t_1}. \quad (S.288)$$

where  $\Delta t_1 = t_1 - t_0$ . In the discussions that follow, we drop the explicit orientation and rotor angle dependence, i.e., take  $A_{\chi}(N|\omega_R) \equiv A_{\chi}(N|\theta_R,\omega_R,\alpha,\beta), \ W_{\chi} \equiv W_{\chi}(\theta_R,\alpha,\beta), \ u_{\chi}(t_1,t_0|\alpha,\beta,\gamma) \equiv u_{\chi}(t_1,t_0)$  and write the "propagator"

$$u_{\chi}(t_1, t_0) = \sum_{N, N'} A_{\chi}(N|\theta_R, \omega_R) A_{\chi}^*(N'|\theta_R, \omega_R) e^{i(N'-N)(\gamma+\phi)} e^{i(N'-N)\omega_R t_0} e^{-i(W_{\chi} + N\omega_R)\Delta t_1}.$$
 (S.289)

At infinite spinning speed, i.e.,  $\omega_R \to \infty$ , we have  $W_{m,\chi}(\theta_R, \omega_R) \to 0$  giving  $A_{\chi}(0|\theta_R, \omega_R) = 1$  and  $A_{\chi}(N \neq 0|\theta_R, \omega_R) = 0$ , and Eq. (S.268) becomes

$$\lim_{\omega_{R} \to \infty} u_{\chi}(t_1, t_0) = e^{-iW_{\chi}\Delta t_1}.$$
(S.290)

Also note that when  $t_1 = t_0$ , we expect that

$$u_{\chi}(t_0, t_0) = \sum_{N,N'} A_{\chi}(N|\theta_R, \omega_R) A_{\chi}^*(N'|\theta_R, \omega_R) e^{i(N'-N)(\gamma+\phi)} e^{i(N'-N)\omega_R t_0} = 1.$$
 (S.291)

For this to be true for arbitrary  $\gamma + \phi$  and  $t_0$  requires N = N', giving

$$u_{\chi}(t_0, t_0) = \sum_{N} A_{\chi}(N|\theta_R, \omega_R) A_{\chi}^*(N|\theta_R, \omega_R) = 1.$$
 (S.292)

Similarly, at finite spinning speeds with stroboscopic sampling, i.e.,  $t_1 - t_0 = n\tau_R$ , we find that  $u_{\chi}(n\tau_R + t_0, t_0) = e^{-iW_{\chi}n\tau_R}$ .

### S8.1 Evolution through one transition - The $\hat{\chi}$ spectrum

Consider the signal from a transition  $\hat{\chi}$ 

$$s_{\chi}(t_1, t_0) = u_{\chi}(t_1, t_0)u_{\chi, 0}(\alpha, \beta, \gamma), \tag{S.293}$$

where  $u_{\chi,0}(\alpha,\beta,\gamma)$  is the initial complex amplitude of the  $\hat{\chi}$  transition signal. If we can assume that  $u_{\chi,0}(\alpha,\beta,\gamma) = u_{\chi,0}$  is independent of orientation, then we can perform the integral over  $\gamma$  analytically. In this case, the signal becomes

$$\langle s_{\chi}(t_1, t_0) \rangle_{\gamma} = u_{\chi, 0} \sum_{N} \left[ A_{\chi}(N|\omega_R) \sum_{N'} A_{\chi}^*(N'|\omega_R) e^{i(N'-N)\omega_R t_0} \int_0^{2\pi} e^{i(N'-N)(\gamma+\phi)} d\gamma \right] e^{-i(W_{\chi}+N\omega_R)\Delta t_1}.$$
 (S.294)

The integral over  $\gamma$  is non-zero only when N' = N. Thus, the signal becomes

$$\langle s_{\chi}(t_1, t_0) \rangle_{\gamma} = u_{\chi, 0} \sum_{N} I(N) e^{-i(W_{\chi} + N\omega_R)\Delta t_1}, \tag{S.295}$$

where  $I(N) = 2\pi |A_{\chi}(N|\omega_R)|^2$ . Defining  $t = \Delta t_1$ , a Fourier transform of  $\langle s_{\chi}(t) \rangle_{\gamma}$  gives the  $\hat{\chi}$  transition spectrum as

$$\langle s_{\chi}(\omega) \rangle_{\gamma} = u_{\chi,0} \sum_{N} I(N) \delta(W_{\chi} + N\omega_R - \omega),$$
 (S.296)

and only a numerical integration over the angles  $\alpha$  and  $\beta$  remains to obtain the spectrum from the polycrystalline sample. Notice that the dependence on  $t_0$  and the initial rotor phase,  $\phi$ , has been eliminated from the spectrum by the integral over  $\gamma$ .

## S8.2 Free evolution through two transitions - The $\hat{\chi}_A \rightarrow \hat{\chi}_B$ spectrum

Consider a transition pathway,  $\hat{\chi}_A \to \hat{\chi}_B$  signal written as

$$s_{AB}(t_2, t_1, t_0 | \alpha, \beta, \gamma) = u_B(t_2, t_1) \ u_{BA}(\alpha, \beta, \gamma) \ u_A(t_1, t_0) \ u_{A,0}(\alpha, \beta, \gamma), \tag{S.297}$$

where  $u_{A,0}(\alpha,\beta,\gamma)$  is the initial complex amplitude of the  $\hat{A}$  transition signal,  $u_{BA}(\alpha,\beta,\gamma)$  is the complex amplitude of the  $\hat{\chi}_A \to \hat{\chi}_B$  coherence transfer, and  $u_A(t_1,t_0)$  and  $u_B(t_2,t_1)$  are the propagators for the  $\hat{\chi}_A$  and  $\hat{\chi}_B$  transitions, respectively. Again, assuming there is no advance of the rotor phase during  $u_{BA}(\alpha,\beta,\gamma)$ , and further assume that  $u_{A,0}(\alpha,\beta,\gamma) = u_{A,0}$  and  $u_{BA}(\alpha,\beta,\gamma) = u_{BA}$  are both independent of orientation, the signal becomes

 $s_{AB}(t_2, t_1, t_0, \alpha, \beta, \gamma) = u_{BA}u_{A,0}$ 

$$\times \left[ \sum_{N_{B},N_{B}'} A_{B}(N_{B}|\theta_{R},\omega_{R}) A_{B}^{*}(N_{B}'|\theta_{R},\omega_{R}) e^{i(N_{B}'-N_{B})\omega_{R}t_{1}} e^{i(N_{B}'-N_{B})(\gamma+\phi)} e^{-i(W_{B}+N_{B}\omega_{R})\Delta t_{2}} \right]$$

$$\times \left[ \sum_{N_{A},N_{A}'} A_{A}(N_{A}|\theta_{R},\omega_{R}) A_{A}^{*}(N_{A}'|\theta_{R},\omega_{R}) e^{i(N_{A}'-N_{A})\omega_{R}t_{0}} e^{i(N_{A}'-N_{A})(\gamma+\phi)} e^{-i(W_{A}+N_{A}\omega_{R})\Delta t_{1}} \right], \quad (S.298)$$

where  $\Delta t_2 = t_2 - t_1$ . We rearrange and perform a partial integration over  $\gamma$ ,

$$\langle s_{AB}(t_{2}, t_{1}, t_{0}, \alpha, \beta) \rangle_{\gamma} = u_{BA} u_{A,0}$$

$$\times \sum_{N_{A}, N_{B}} \sum_{N'_{A}, N'_{B}} e^{-i(W_{A} + N_{A}\omega_{R})\Delta t_{1}} e^{-i(W_{B} + N_{B}\omega_{R})\Delta t_{2}} A_{A}(N_{A}|\omega_{R}) A_{A}^{*}(N'_{A}|\omega_{R}) A_{B}(N_{B}|\omega_{R}) A_{B}^{*}(N'_{B}|\omega_{R})$$

$$\times e^{i(N'_{A} - N_{A})\omega_{R}t_{0}} e^{i(N'_{B} - N_{B})\omega_{R}t_{1}} e^{i(N'_{A} - N_{A})\phi} e^{i(N'_{B} - N_{B})\phi} \int_{0}^{2\pi} e^{i(N'_{A} - N_{A})\gamma} e^{i(N'_{B} - N_{B})\gamma} d\gamma, \quad (S.299)$$

which integrates to a non-zero value only when  $(N'_A - N_A) + (N'_B - N_B) = 0$ , leaving

$$\langle s_{AB}(\Delta t_2, \Delta t_1, \alpha, \beta) \rangle_{\gamma} = u_{BA} u_{A,0} \sum_{N_A, N_B, N_B'} I(N_A, N_B, N_A', N_B')$$

$$\times e^{-i(W_A + (N_A - (N_B' - N_B))\omega_R)\Delta t_1} e^{-i(W_B + N_B\omega_R)\Delta t_2}$$
 (S.300)

where

$$I(N_A, N_B, N_A', N_B') = 2\pi A_A(N_A|\omega_R) A_A^*(N_A'|\omega_R) A_B(N_B|\omega_R) A_B^*(N_B'|\omega_R),$$

and  $N'_A = N_A - (N'_B - N_B)$ . In this example, we can simplify the expression to

$$\langle s_{AB}(\Delta t_2, \Delta t_1, \alpha, \beta) \rangle_{\gamma} = u_{BA} u_{A,0} \sum_{N_A, N_B} I(N_A', N_B) e^{-i(W_A + N_A' \omega_R) \Delta t_1} e^{-i(W_B + N_B \omega_R) \Delta t_2}, \tag{S.301}$$

where

$$I(N_A', N_B) = 2\pi A_A^*(N_A'|\omega_R) A_B(N_B|\omega_R) \sum_{N_B'} A_B^*(N_B'|\omega_R) A_A(N_B' + (N_A' - N_B)|\omega_R).$$
 (S.302)

We recognize the summation is a discrete convolution of  $A_B^*(N)$  and  $A_A(N)$ , where  $N_{AB} = N_A' - N_B$ , i.e.,

$$\{A_B^* \otimes A_A\}(N_{AB}) = \sum_{N_B' = -\infty}^{\infty} A_B^*(N_B') A_A(N_B' + N_{AB}). \tag{S.303}$$

One can show that the discrete Fourier transform of the convolution is the product of the discrete Fourier transforms of the individual functions,  $a_B^*(\Phi)a_A(\Phi)$ , i.e.,

$$\sum_{N_{AB}=-\infty}^{\infty} \{A_{B}^{*} \otimes A_{A}\}(N_{AB})e^{-iN_{AB}\Phi} = \sum_{N_{AB}=-\infty}^{\infty} \left(\sum_{N_{B}'=-\infty}^{\infty} A_{B}^{*}(N_{B}')A_{A}(N_{B}'+N_{AB})\right)e^{-iN_{AB}\Phi}$$

$$= \sum_{N_{B}'=-\infty}^{\infty} A_{B}^{*}(N_{B}')\left(\sum_{N_{AB}=-\infty}^{\infty} A_{A}(N_{AB}+N_{B}')e^{-iN_{AB}\Phi}\right) = \sum_{N_{B}'=-\infty}^{\infty} A_{B}^{*}(N_{B}')\left(a_{A}(\Phi)e^{iN_{B}'\Phi}\right)$$

$$= a_{A}(\Phi)\sum_{N_{B}'=-\infty}^{\infty} A_{B}^{*}(N_{B}')e^{iN_{B}'\Phi} = a_{B}^{*}(\Phi)a_{A}(\Phi). \quad (S.304)$$

Therefore, Eq. (S.302) becomes

$$I(N_A', N_B) = 2\pi A_A^*(N_A'|\omega_R) A_B(N_B|\omega_R) A_{AB}(N_A' - N_B|\omega_R), \tag{S.305}$$

where

$$A_{AB}(N_{AB}|\omega_R) = \{A_B^* \otimes A_A\}(N_{AB}) = \frac{1}{2\pi} \int_0^{2\pi} a_B^*(\Phi) a_A(\Phi) e^{-iN_{AB}\Phi} d\Phi.$$
 (S.306)

A Fourier transform with respect to  $t_A = \Delta t_1$  and  $t_B = \Delta t_2$  gives the  $\hat{\chi}_A \to \hat{\chi}_B$  transition pathway spectrum for a given crystallite orientation,  $(\alpha, \beta, \gamma)$ , as

$$\langle s_{AB}(\omega_A, \omega_B, \alpha, \beta) \rangle_{\gamma} = u_{BA}u_{A,0} \sum_{N_A', N_B} I(N_A', N_B) \quad \delta(W_A + N_A'\omega_R - \omega_A) \, \delta(W_B + N_B\omega_R - \omega_B) \,, \quad (S.307)$$

and only a numerical integration over the angles  $\alpha$  and  $\beta$  remains to obtain the spectrum from the polycrystalline sample.

#### S8.2.1 <sup>2</sup>H 2D PASS

In a PASS sequence, [11, 12, 3, 2, 39], illustrated in Fig. S8A, an effective time coordinate,  $\epsilon$ , is created during a constant time period, T, during which only pure chemical shift anisotropy influences the signal phase. This is achieved with an initial excitation pulse applied at t=-T followed by a series of  $\pi$  pulses applied at specific times during the constant time period. The direct acquisition of the signal begins at the end of the constant time period, i.e., at t=0. Recall that the effect of a  $\pi$ -pulse on transition symmetries is  $\mathbb{p}_I \xrightarrow{\pi} -\mathbb{p}_I$  and  $\mathbb{d}_I \xrightarrow{\pi} \mathbb{d}_I$ . Since frequency contributions with  $d_I$  symmetry remain invariant through a  $\pi$  pulse, we can focus our attention on the effect of the  $\pi$  pulses on the signal phase due to frequency contributions with  $p_I$  symmetry, treating the  $d_I$  contributions as a constant signal phase contribution at the end of T.

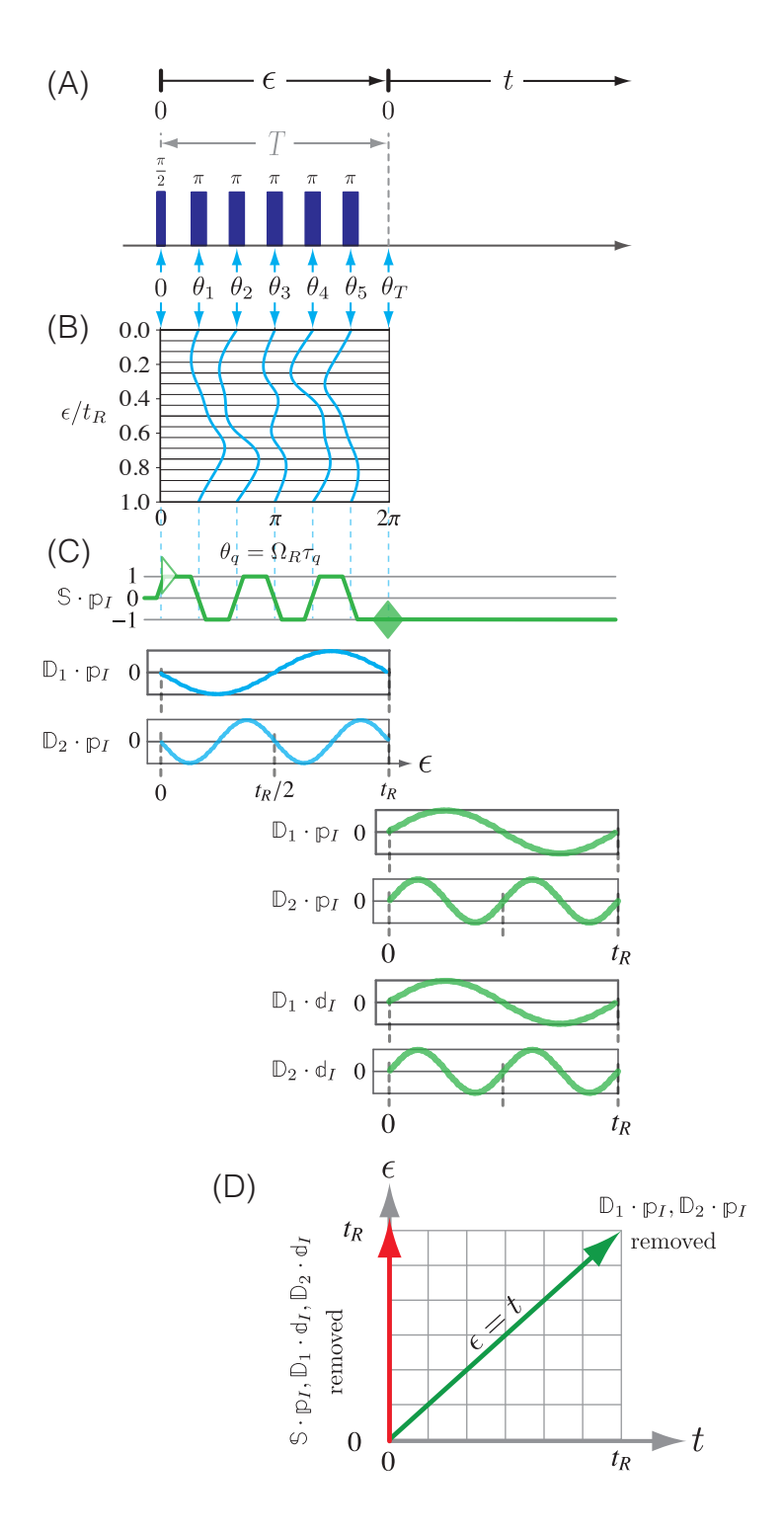


Figure S8: Pulse sequence and spatial-transition symmetry pathways for 2D Phase Adjusted Spinning Sideband (2D-PASS) sequence applied to a  ${}^2\mathrm{H}$  (I=1) nucleus. In this sequence, the  $\pi$  pulse spacings are varied during a constant time period, T, to produce a desired effective signal evolution of duration  $\epsilon$  between 0 to  $t_R$ —depending the  $\pi$ -pulse spacings—from only the  $D_1 \cdot \mathrm{p}$  and  $D_2 \cdot \mathrm{p}$  frequency contributions. During the second time period, t, the transition evolves under all frequency contributions, i.e.,  $\mathbb{S} \cdot \mathbb{p}_I$ ,  $\mathbb{D}_1 \cdot \mathbb{p}_I$ ,  $\mathbb{D}_1 \cdot \mathbb{d}_I$  and  $D_2 \cdot \mathbb{d}_I$ . During this time period, the  $\mathbb{D}_1 \cdot \mathbb{p}_I$ ,  $\mathbb{D}_2 \cdot \mathbb{p}_I$  contributions are refocussed into an echo along  $\epsilon = t$ , as shown by the green arrow in (B). As shown by Aleksis et al.[1] the resulting spectrum can be sheared to produce a correlation of spinning sidebands produced by pure shift anisotropy to isotropic chemical shift and first-order quadrupolar frequency anisotropy.

Between the initial excitation pulse and signal acquisition are Q  $\pi$ -pulses, applied at times  $-T + \tau_1, -T + \tau_2, \ldots, -T + \tau_Q$ . The signal phase contribution at the end of T is given by

$$\Phi_Q = (-1)^Q \sum_{q=0}^{Q} (-1)^q \int_{-T+\tau_a}^{-T+\tau_{q+1}} \Omega(s) ds,$$
 (S.308)

where  $\tau_0 = 0$ ,  $\tau_{Q+1} = T$  and  $\Omega(s)$  is the time dependent transition frequency of the observed  $\mathbb{p}_I = -1$  transition. Given

$$\int_{-T+\tau_{q}}^{-T+\tau_{q+1}} \Omega(s)ds = W_{0}(\tau_{q+1} - \tau_{q}) + \sum_{m \neq 0} W_{m}e^{-im(\gamma+\phi)}e^{im\omega_{R}T} \left\{ e^{-im\omega_{R}\tau_{q+1}} - e^{-im\omega_{R}\tau_{q}} \right\}, \tag{S.309}$$

the signal phase at the end of the constant time period is given by

$$\Phi_{Q} = W_{0} \left[ (-1)^{Q} \sum_{q=0}^{Q} (-1)^{q} (\tau_{q+1} - \tau_{q}) \right] + \sum_{m \neq 0} W_{m} e^{-im(\gamma + \phi)} e^{im\omega_{R}T} \left[ (-1)^{Q} \sum_{q=0}^{Q} (-1)^{q} \left\{ e^{-im\omega_{R}\tau_{q+1}} - e^{-im\omega_{R}\tau_{q}} \right\} \right]. \quad (S.310)$$

This can be further simplified to

$$\Phi_{Q} = W_{0} \left[ T - 2(-1)^{Q} \sum_{q=1}^{Q} (-1)^{q} \tau_{q} \right] - \sum_{m \neq 0} W_{m} e^{-im(\gamma + \phi)} \left[ 2(-1)^{Q} \sum_{q=1}^{Q} (-1)^{q} e^{-im\theta_{q}} e^{im\theta_{T}} + (-1)^{Q} e^{im\theta_{T}} - 1 \right],$$
(S.311)

where  $\theta_T = \omega_R T$ , and  $\theta_q = \omega_R \tau_q$ .

In PASS, the timings of the  $\hat{Q}$   $\pi$  pulses are manipulated so the signal phase at the end of the constant time period, i.e., at t = 0, matches the phase of a  $p_I = +1$  transition evolving under only the anisotropic frequency contribution with  $p_I$  symmetry for a duration  $\epsilon$ , given by

$$\Phi_{\text{PASS}}(\epsilon) = -\int_0^{\epsilon} \Omega(s)ds = -\sum_{m \neq 0} W_m e^{-im(\gamma + \phi)} \left[ e^{-im\omega_R \epsilon} - 1 \right]. \tag{S.312}$$

Evolving forward from t=0, the 2D PASS signal phase then becomes

$$\Phi(\epsilon, t) = \Phi_{\text{PASS}}(\epsilon) + \Phi(t) = W_0 t + \sum_{m \neq 0} W_m e^{-im(\gamma + \phi)} \left[ e^{-im\omega_R t} - e^{-im\omega_R \epsilon} \right]. \tag{S.313}$$

The timings for the  $\pi$  pulses that give the signal phase of Eq. (S.312) comes from equating Eqs. (S.311) and (S.312) to obtain the PASS equations:

$$\theta_T - 2(-1)^Q \sum_{q=1}^Q (-1)^q \theta_q = 0,$$
 (S.314)

and

$$2(-1)^{Q} \sum_{q=1}^{Q} (-1)^{q} e^{im\theta_{q}} e^{-im\theta_{T}} + (-1)^{Q} e^{-im\theta_{T}} = e^{-im\Theta},$$
(S.315)

where  $\Theta = \omega_R \epsilon$ . Levitt and coworkers[3] suggested a five  $\pi$  pulse (Q = 5) 2D PASS sequence, of constant duration T, with  $\theta_T = 2\pi$ , yielding the equations

$$2\sum_{q=1}^{5}(-1)^{q}\theta_{q} + 2\pi = 0, \quad \text{and} \quad -2\sum_{q=1}^{5}(-1)^{q}e^{im\theta_{q}} - 1 = e^{-im\Theta}, \quad \text{for} \quad m = 1, 2.$$
 (S.316)

These non-linear equations can be solved numerically for the  $\pi$  pulse timings, which are plotted as a function of  $\epsilon$  in Fig. S8B. Tabulated values can be found elsewhere[3].

The 2D PASS experiment in terms of spatial-transition symmetry product pathways is illustrated in Fig. S8C. In this perspective, the  $\mathbb{S} \cdot \mathbb{p}_I$  spatial-transition symmetry product pathway leads to an echo at the end of the constant time period, i.e., its contribution averages to zero at the end of T. In contrast, the averaged  $\mathbb{D}_1 \cdot \mathbb{p}_I$  and  $\mathbb{D}_2 \cdot \mathbb{p}_I$  spatial-transition symmetry product pathways at the end of T mimic the  $\mathbb{D}_1 \cdot \mathbb{p}_I$  and  $\mathbb{D}_2 \cdot \mathbb{p}_I$  pathways experienced by the free evolution of a transition with  $\mathbb{p}_I = +1$  under MAS with the effective evolution time  $\epsilon$ . With all frequency contributions present during the forward evolution of the  $\mathbb{p}_I = -1$  transition in t, there is a refocusing of the  $\mathbb{D}_1 \cdot \mathbb{p}_I$  and  $\mathbb{D}_2 \cdot \mathbb{p}_I$  contributions into an echo along the  $\epsilon + t = 0$  line, along which only the isotropic chemical shift and the first-order quadrupolar anisotropy modulate the signal phase. Since the isotropic chemical shift and the first-order quadrupolar frequency anisotropy contributions are removed during  $\epsilon$  evolution, the resulting spectrum can be sheared to produce a correlation of spinning sidebands produced by pure shift anisotropy along  $\epsilon$  to isotropic chemical shift and first-order quadrupolar frequency anisotropy along the along the  $\epsilon + t = 0$  line, as shown by Aleksis et al.[1].

In Fig. S9 is full density matrix simulation of the 2D PASS sequence, shown in Fig. S8, for a <sup>2</sup>H nucleus, reproducing Fig. 2 from Aleksis et al.[1].<sup>3</sup> The 2D spectra were obtained by applying a shear of  $\kappa^{(\omega_1)} = -1$  parallel to the  $\omega_1$  dimension (Fourier conjugate of  $\epsilon$ ), i.e., the  $D_1 \cdot \mathbf{p}_I$ ,  $D_2 \cdot \mathbf{p}_I$  dimension. This is followed by a frequency domain reversal of the  $D_1 \cdot \mathbf{p}_I$ ,  $D_2 \cdot \mathbf{p}_I$  dimension to make the 2D spectrum correspond to the  $p_I = -1 \rightarrow -1$  and  $d_I = \pm 1 \rightarrow \pm 1$  transition symmetry pathways.

An equivalent 2D spectrum can be simulated significantly more efficiently in the frequency domain using Eq. (S.307). In this case, the 2D PASS spectrum is obtained from two transition pathway signals, i.e.,

$$|-1\rangle\langle 0| \rightarrow |-1\rangle\langle 0|$$
 and  $|0\rangle\langle +1| \rightarrow |0\rangle\langle +1|$ ,

which map to the  $p_I = -1 \rightarrow -1$  and  $d_I = \pm 1 \rightarrow \pm 1$  transition symmetry pathways. In  $\omega_1$  the spectrum contains the  $\mathbb{D}_1 \cdot \mathbb{p}_I$  and  $\mathbb{D}_2 \cdot \mathbb{p}_I$  frequency contributions, while in  $\omega_2$  the spectrum contains all frequency contributions, i.e.,  $\mathbb{S} \cdot \mathbb{p}_I$ ,  $\mathbb{D}_1 \cdot \mathbb{p}_I$ ,  $\mathbb{D}_2 \cdot \mathbb{p}_I$ ,  $\mathbb{D}_1 \cdot \mathbb{d}_I$  and  $\mathbb{D}_2 \cdot \mathbb{d}_I$ . In this case, the 2D PASS spectrum were obtained from the simulated spectrum by applying a shear of  $\kappa^{(\omega_1)} = 1$  parallel to the  $\omega_1$  dimension. The resulting 2D spectra, shown in Fig. S10, are identical to those in Fig. S9 obtained with the full 2D PASS sequence in a full density matrix simulation. The simulations were performed on a laptop computer (Apple MacBook Air, 3.49 GHz M2 processor with 8 cores and 24 GB RAM) and completed in approximately 50 ms.

<sup>&</sup>lt;sup>3</sup>While the 2D spinning sideband patterns are in agreement, there appears to be a discrepancy with Aleksis et al.[1] with regard to the frequency domain reversal of the  $D_1 \cdot \mathbf{p}_I$ ,  $D_2 \cdot \mathbf{p}_I$  dimension. Without access to their time-domain simulations or experimental datasets, it was not possible to track down the origin of this discrepancy.

## Density Matrix Simulation - 2D PASS

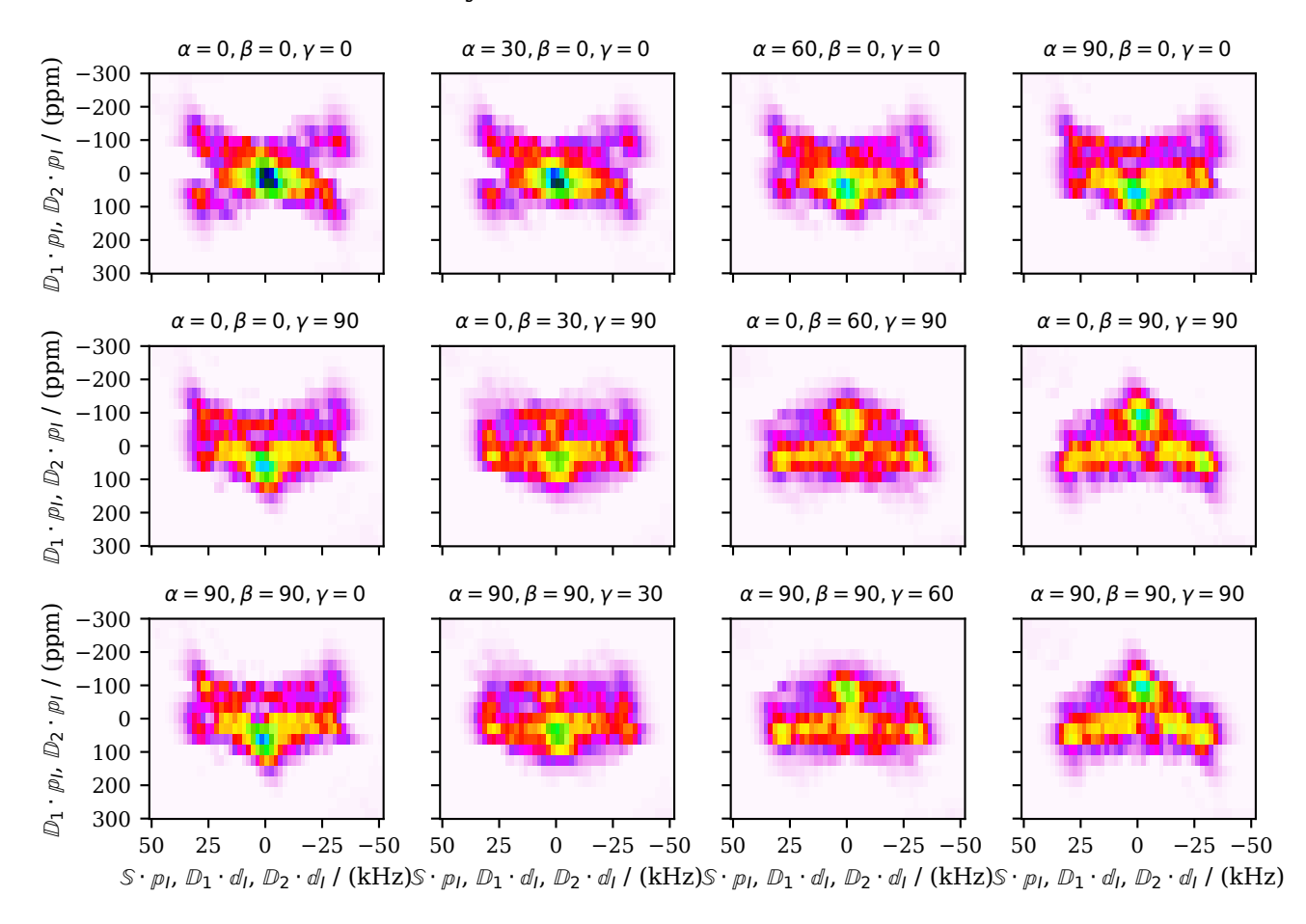


Figure S9: Density Matrix Simulation of the 2D PASS spectra, using the pulse sequence shown in Fig. S8, for a  $^2$ H nucleus with  $C_q = 50 \,\mathrm{kHz}$ ,  $\eta_q = 0.9$  and  $\zeta_\sigma = 150 \,\mathrm{ppm}$  and  $\eta_\sigma = 0.7$  for various relative orientations of the shielding to EFG tensor while spinning at  $\omega_R/(2\pi) = 2 \,\mathrm{kHz}$ . The 2D spectrum was obtained by applying a shear of  $\kappa^{(\omega_1)} = -1$  parallel to the  $\omega_1$  dimension (Fourier conjugate of  $\epsilon$ ), i.e., the  $D_1 \cdot \mathrm{p}_I$ ,  $D_2 \cdot \mathrm{p}_I$  dimension. This is followed by a frequency domain reversal of the  $D_1 \cdot \mathrm{p}_I$ ,  $D_2 \cdot \mathrm{p}_I$  dimension to make the 2D spectrum correspond to the  $p_I = -1 \to -1$  and  $d_I = \pm 1 \to \pm 1$  transition symmetry pathways. These simulations were performed to reproduce Fig. 2 from Aleksis et al.[1]. Simulations were performed using density matrix code of Trease et al.[36]. To ensure convergence of the spectral amplitudes, simulations were averaged over 131,072 orientations on the hemisphere using three-angle integration sets described by Haber[18]. Each simulation was completed in approximately 200 s on a laptop computer (Apple MacBook Air, 3.49 GHz M2 processor with 8 cores and 24 GB RAM).

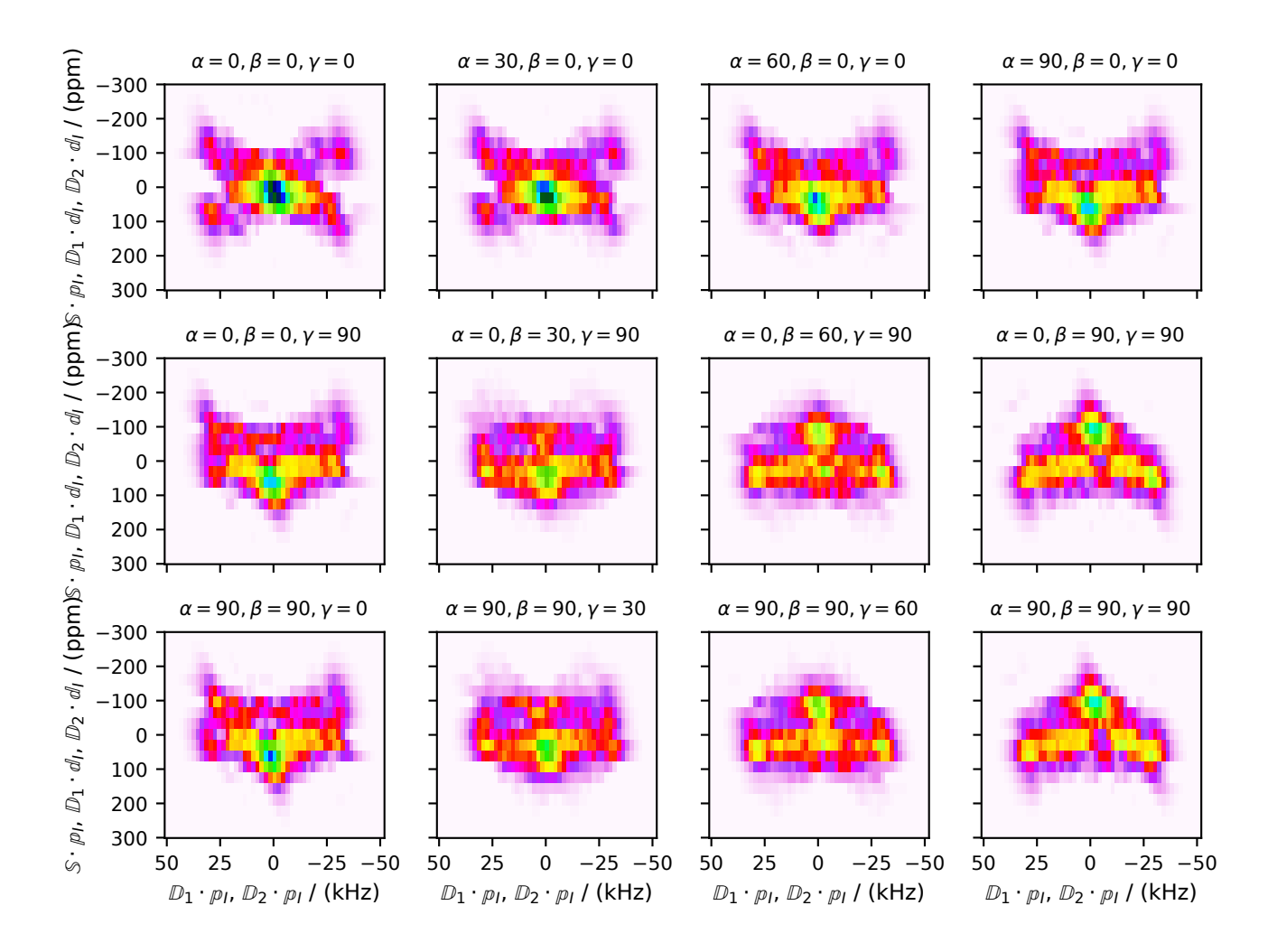


Figure S10: Frequency domain simulation of the 2D PASS spectra using Eq. (S.307) for a <sup>2</sup>H nucleus with  $C_q = 50$  kHz,  $\eta_q = 0.9$  and  $\zeta_\sigma = 150$  ppm and  $\eta_\sigma = 0.7$  for various relative orientations of the shielding to EFG tensor while spinning at  $\omega_R/(2\pi) = 2$  kHz, in agreement with the full density matrix simulations in Fig. S9. These simulations employ the two transition pathways  $|-1\rangle\langle 0| \to |-1\rangle\langle 0|$  and  $|0\rangle\langle +1| \to |0\rangle\langle +1|$ , which map to the transition symmetry pathways  $p_I = -1 \to -1$  and  $d_I = \pm 1 \to \pm 1$ . Each simulation was completed in approximately 50 ms on a laptop computer (Apple MacBook Air, 3.49 GHz M2 processor with 8 cores and 24 GB RAM).

#### S8.2.2 Stroboscopic sampling during one time domain

If the spinning speed is infinite, i.e.,  $\omega_R \to \infty$ , or stroboscopically sampled during one of the evolution periods, e.g.,  $\Delta t_1 = n\tau_R$ , then  $A_A(0|\omega_R) = 1$  and  $A_A(N|\omega_R) = 0$  for  $N \neq 0$ . In this case, a partial integration of Eq. (S.298) over  $\gamma$  becomes

$$\langle s_{AB}(t_{2}, t_{1}, t_{0}, \alpha, \beta) \rangle_{\gamma} = u_{BA} u_{A,0}$$

$$\times \sum_{N_{B}} \sum_{N'_{B}} e^{-iW_{A}\Delta t_{1}} e^{-i(W_{B} + N_{B}\omega_{R})\Delta t_{2}} A_{B}(N_{B}|\omega_{R}) A_{B}^{*}(N'_{B}|\omega_{R})$$

$$\times e^{i(N'_{B} - N_{B})\omega_{R}t_{1}} e^{i(N'_{B} - N_{B})\phi} \int_{0}^{2\pi} e^{i(N'_{B} - N_{B})\gamma} d\gamma, \quad (S.317)$$

which integrates to a non-zero value only when  $N'_B = N_B$ , leaving

$$\langle s_{AB}(t_2, t_1, t_0, \alpha, \beta) \rangle_{\gamma} = u_{BA} u_{A,0} e^{-iW_A \Delta t_1} \sum_{N_B} I(N_B) e^{-i(W_B + N_B \omega_R) \Delta t_2},$$
 (S.318)

where

$$I(N_B) = 2\pi |A_B(N_B|\omega_R)|^2.$$
 (S.319)

#### S8.2.3 Skew projection

When the two free evolution periods combine to form a single evolution period, i.e.,  $\Delta t = x_A \Delta t_1 + x_B \Delta t_1$ , the time-domain signal becomes

$$\langle s_{AB}(\Delta t, \alpha, \beta) \rangle_{\gamma} = u_{BA} u_{A,0} \sum_{N_A', N_B} I(N_A', N_B) e^{-i \left[ x_A (W_A + N_A' \omega_R) + x_B (W_B + N_B \omega_R) \right] \Delta t}. \tag{S.320}$$

In the special case of  $x_A = x_B = 1/2$ , this can be expanded and rewritten as

$$\langle s_{AB}(\Delta t, \alpha, \beta) \rangle_{\gamma} = u_{BA} u_{A,0} e^{-i(W_A + W_B)\Delta t/2} \sum_{N_A', N_B} I(N_A', N_B) e^{-i(N_A' + N_B)\omega_R \Delta t/2},$$
 (S.321)

where  $W_{AB} = (W_A + W_B)/2$ . Defining  $N = N'_A + N_B$ , we obtain

$$\langle s_{AB}(\Delta t, \alpha, \beta) \rangle_{\gamma} = u_{BA} u_{A,0} e^{-iW_{AB}\Delta t} \sum_{N} I(N) e^{-iN\omega_{R}\Delta t/2}, \tag{S.322}$$

where, since  $N'_A = N - N_B$ , we have

$$I(N) = 2\pi \sum_{N_B} A_A^* (N - N_B | \omega_R) A_B(N_B | \omega_R) A_{AB}(N - 2N_B | \omega_R).$$
 (S.323)

#### **S8.2.4** Rotor phase advance during $u_{BA}(\alpha, \beta, \gamma)$

Consider the case where the rotor phase advances during the coherence transfer, i.e.,  $u_{BA}(\alpha, \beta, \gamma)$ , but we have no transition frequency evolution. In this case, we write the signal in Eq. (S.298) as

$$s_{AB}(t_3, t_2, t_1, t_0, \alpha, \beta, \gamma) = u_{BA}u_{A,0}$$

$$\times \left[ \sum_{N_{B},N_{B}'} A_{B}(N_{B}|\theta_{R},\omega_{R}) A_{B}^{*}(N_{B}'|\theta_{R},\omega_{R}) e^{i(N_{B}'-N_{B})\omega_{R}t_{2}} e^{i(N_{B}'-N_{B})(\gamma+\phi)} e^{-i(W_{B}+N_{B}\omega_{R})\Delta t_{3}} \right]$$

$$\times \left[ \sum_{N_{A},N_{A}'} A_{A}(N_{A}|\theta_{R},\omega_{R}) A_{A}^{*}(N_{A}'|\theta_{R},\omega_{R}) e^{i(N_{A}'-N_{A})\omega_{R}t_{0}} e^{i(N_{A}'-N_{A})(\gamma+\phi)} e^{-i(W_{A}+N_{A}\omega_{R})\Delta t_{1}} \right], \quad (S.324)$$

where  $\Delta t_3 = t_3 - t_2$ . We rearrange and perform a partial integration over  $\gamma$ ,

$$\langle s_{AB}(t_{3}, t_{2}, t_{1}, t_{0}, \alpha, \beta) \rangle_{\gamma} = u_{BA}u_{A,0}$$

$$\times \sum_{N_{A}, N_{B}} \sum_{N'_{A}, N'_{B}} e^{-i(W_{A} + N_{A}\omega_{R})\Delta t_{2}} e^{-i(W_{B} + N_{B}\omega_{R})\Delta t_{3}} A_{A}(N_{A}|\omega_{R}) A^{*}_{A}(N'_{A}|\omega_{R}) A_{B}(N_{B}|\omega_{R}) A^{*}_{B}(N'_{B}|\omega_{R})$$

$$\times e^{i(N'_{A} - N_{A})\omega_{R}t_{0}} e^{i(N'_{B} - N_{B})\omega_{R}t_{2}} e^{i(N'_{A} - N_{A})\phi} e^{i(N'_{B} - N_{B})\phi} \int_{0}^{2\pi} e^{i(N'_{A} - N_{A})\gamma} e^{i(N'_{B} - N_{B})\gamma} d\gamma, \quad (S.325)$$

which integrates to a non-zero value only when  $(N'_A - N_A) + (N'_B - N_B) = 0$ , leaving

$$\langle s_{AB}(t_3, t_2, t_1, t_0, \alpha, \beta) \rangle_{\gamma} = u_{BA} u_{A,0} \times \sum_{N_A, N_B} \sum_{N_A', N_B'} e^{-i(W_A + N_A \omega_R) \Delta t_2 s} e^{-i(W_B + N_B \omega_R) \Delta t_3} I(N_A, N_B, N_A', N_B') e^{i(N_B' - N_B) \omega_R(t_2 - t_0)}.$$
 (S.326)

Rewriting  $\omega_R(t_2-t_0) = \omega_R(t_2-t_1-t_0+t_1) = \omega_R\Delta t_2 + \omega_R\Delta t_1$ , we obtain

$$\langle s_{AB}(t_3, t_2, t_1, t_0, \alpha, \beta) \rangle_{\gamma} = u_{BA} u_{A,0} \sum_{N_A', N_B} I(N_A', N_B) e^{-i(W_A + N_A' \omega_R) \Delta t_2} e^{-i(W_B + N_B \omega_R) \Delta t_3}, \tag{S.327}$$

where

$$I(N'_A, N_B) = 2\pi A_A^*(N'_A|\omega_R) A_B(N_B|\omega_R) \sum_{N'_B} A_B^*(N'_B|\omega_R) A_A(N'_B + (N'_A - N_B)|\omega_R) e^{i(N'_B - N_B)\omega_R \Delta t_1}.$$
 (S.328)

Thus, we see that a rotor advance during the coherence transfer,  $u_{BA}(\alpha, \beta, \gamma)$ , with no transition frequency evolution, results in a phase modulation of the sideband amplitudes.

### S8.3 Free evolution through n transitions

Finally, we consider a transition pathway through n transitions, whose signal can be written as

$$s(t_1, ..., t_n, \alpha, \beta, \gamma) = \prod_{\varepsilon=1}^n u_{\varepsilon}(t_{\varepsilon}, \alpha, \beta, \gamma) u_{\varepsilon, \varepsilon - 1}(\alpha, \beta, \gamma), \tag{S.329}$$

where  $u_{\varepsilon,\varepsilon-1}(\alpha,\beta,\gamma)$  is the complex amplitude of the  $\hat{\chi}_{\varepsilon-1} \to \hat{\chi}_{\varepsilon}$  coherence transfer, and  $u_{\varepsilon}(t_{\varepsilon},\alpha,\beta,\gamma)$  is the propagator for the  $\hat{\chi}_{\varepsilon}$  transition. Inferring from the previous sections, we can write the sideband amplitudes after free evolution through n transitions as

$$s(\mathbf{t}) = s(\mathbf{0}) \left[ \sum_{N_1} \sum_{N_1'} A_1(N_1 | \theta_R, \omega_R) A_1^*(N_1' | \theta_R, \omega_R) e^{i(N_1' - N_1)\omega_R t_0} e^{i(N_1' - N_1)(\gamma + \phi)} e^{-i(W_1 + N_1 \omega_R)\Delta t_1} \right] \dots \times \left[ \sum_{N_n} \sum_{N_n'} A_n(N_n | \theta_R, \omega_R) A_n^*(N_n' | \theta_R, \omega_R) e^{i(N_n' - N_n)\omega_R t_{n-1}} e^{i(N_n' - N_n)(\gamma + \phi)} e^{-i(W_n + N_n \omega_R)\Delta t_n} \right], \quad (S.330)$$

where

$$s(\mathbf{0}) = \prod_{j=1}^{n} u_{j,j-1},\tag{S.331}$$

and  $\Delta t_{\varepsilon} = t_{\varepsilon} - t_{\varepsilon-1}$ . Regrouping gives

$$s(\mathbf{t}) = s(\mathbf{0}) \sum_{N_1} \cdots \sum_{N_n} \sum_{N_1'} \cdots \sum_{N_n'} \left[ \prod_{\varepsilon=1}^n A_{\varepsilon}(N_{\varepsilon} | \theta_R, \omega_R) A_{\varepsilon}^*(N_{\varepsilon}' | \theta_R, \omega_R) \right] \times \left[ \prod_{\varepsilon=1}^n e^{i(N_{\varepsilon}' - N_{\varepsilon})\omega_R t_{\varepsilon-1}} e^{i(N_{\varepsilon}' - N_{\varepsilon})(\gamma + \phi)} e^{-i(W_{\varepsilon} + N_{\varepsilon}\omega_R)\Delta t_{\varepsilon}} \right], \quad (S.332)$$

and

$$s(\mathbf{t}) = s(\mathbf{0}) \sum_{N_1} \cdots \sum_{N_n} \sum_{N'_1} \cdots \sum_{N'_n} I(\mathbf{N}, \mathbf{N}') e^{i\sum_{\varepsilon} (N'_{\varepsilon} - N_{\varepsilon})\omega_R t_{\varepsilon - 1}} e^{i\sum_{\varepsilon} (N'_{\varepsilon} - N_{\varepsilon})(\gamma + \phi)} e^{-i\sum_{\varepsilon} (W_{\varepsilon} + N_{\varepsilon}\omega_R)\Delta t_{\varepsilon}}, \quad (S.333)$$

where

$$I(\mathbf{N}, \mathbf{N}') = 2\pi \prod_{\varepsilon=1}^{n} A_{\varepsilon}(N_{\varepsilon}|\theta_{R}, \omega_{R}) A_{\varepsilon}^{*}(N_{\varepsilon}'|\theta_{R}, \omega_{R}),$$
(S.334)

and  $\mathbf{N} = (N_1, N_2, ..., N_n)$  and  $\mathbf{N}' = (N_1', N_2', ..., N_n')$ Integrating  $s(\mathbf{t})$  over  $\gamma$ ,

$$s(\mathbf{t}) = s(\mathbf{0}) \sum_{N_1} \cdots \sum_{N_n} \sum_{N_1'} \cdots \sum_{N_n'} \frac{I(\mathbf{N}, \mathbf{N}')}{2\pi} \left[ e^{i \sum_{\varepsilon} (N_{\varepsilon}' - N_{\varepsilon}) \omega_R t_{\varepsilon - 1}} e^{-i \sum_{\varepsilon} (W_{\varepsilon} + N_{\varepsilon} \omega_R) \Delta t_{\varepsilon}} \int_0^{2\pi} e^{i \sum_{\varepsilon} (N_{\varepsilon}' - N_{\varepsilon}) (\gamma + \phi)} d\gamma \right],$$
(S.335)

leads to a non-zero value only when  $\sum_{\varepsilon=1}^{n} (N'_{\varepsilon} - N_{\varepsilon}) = 0$  or  $N'_{1} = N_{1} - \sum_{\varepsilon=2}^{n} (N'_{\varepsilon} - N_{\varepsilon})$ , leaving

$$s(\mathbf{t}) = s(\mathbf{0}) \sum_{N_1} \cdots \sum_{N_n} \sum_{N_2'} \cdots \sum_{N_n'} I(\mathbf{N}, \mathbf{N}') e^{i \sum_{\varepsilon} (N_{\varepsilon}' - N_{\varepsilon}) \omega_R t_{\varepsilon - 1}} e^{-i \sum_{\varepsilon} (W_{\varepsilon} + N_{\varepsilon} \omega_R) \Delta t_{\varepsilon}}.$$
 (S.336)

#### S8.3.1 Simplifying the frequency expression

$$\sum_{\varepsilon=1}^{n} (N_{\varepsilon}' - N_{\varepsilon}) \omega_{R} t_{\varepsilon-1} - \sum_{\varepsilon=1}^{n} N_{\varepsilon} \omega_{R} \Delta t_{\varepsilon}$$

Examine the case of n = 2, n = 3, and n = 4 transitions.

n=2 case: With the constraint  $(N'_2-N_2)=-(N'_1-N_1)$ , we expand the summation:

$$(N'_{1} - N_{1})\omega_{R}t_{0} + (N'_{2} - N_{2})\omega_{R}t_{1} - N_{1}\omega_{R}\Delta t_{1} - N_{2}\omega_{R}\Delta t_{2}$$

$$(N'_{1} - N_{1})\omega_{R}t_{0} - (N'_{1} - N_{1})\omega_{R}t_{1} - N_{1}\omega_{R}\Delta t_{1} - N_{2}\omega_{R}\Delta t_{2}$$

$$-(N'_{1} - N_{1})\omega_{R}\Delta t_{1} - N_{1}\omega_{R}\Delta t_{1} - N_{2}\omega_{R}\Delta t_{2}$$

$$-N'_{1}\omega_{R}\Delta t_{1} - N_{2}\omega_{R}\Delta t_{2}$$

n=3 case: With the constraint  $(N_2'-N_2)=-(N_1'-N_1)-(N_3'-N_3)$ , we expand the summation:

$$(N'_1 - N_1)\omega_R t_0 + (N'_2 - N_2)\omega_R t_1 + (N'_3 - N_3)\omega_R t_2 - N_1\omega_R \Delta t_1 - N_2\omega_R \Delta t_2 - N_3\omega_R \Delta t_3$$

$$(N'_1 - N_1)\omega_R t_0 + (-(N'_1 - N_1) - (N'_3 - N_3))\omega_R t_1 + (N'_3 - N_3)\omega_R t_2 - N_1\omega_R \Delta t_1 - N_2\omega_R \Delta t_2 - N_3\omega_R \Delta t_3$$

$$(N'_1 - N_1)\omega_R t_0 - (N'_1 - N_1)\omega_R t_1 - (N'_3 - N_3)\omega_R t_1 + (N'_3 - N_3)\omega_R t_2 - N_1\omega_R \Delta t_1 - N_2\omega_R \Delta t_2 - N_3\omega_R \Delta t_3$$

$$-(N'_1 - N_1)\omega_R \Delta t_1 + (N'_3 - N_3)\omega_R \Delta t_2 - N_1\omega_R \Delta t_1 - N_2\omega_R \Delta t_2 - N_3\omega_R \Delta t_3$$

$$-(N'_1 - N_1)\omega_R \Delta t_1 + (N'_3 - N_3)\omega_R \Delta t_2 - N_1\omega_R \Delta t_1 - N_2\omega_R \Delta t_2 - N_3\omega_R \Delta t_3$$

$$-(N'_1 \omega_R \Delta t_1 - (N_2 - (N'_3 - N_3))\omega_R \Delta t_2 - N_3\omega_R \Delta t_3$$

n = 4 case: With the constraint  $(N'_2 - N_2) = -(N'_1 - N_1) - (N'_3 - N_3) - (N'_4 - N_4)$ , we expand the summation:

$$(N'_{1} - N_{1})\omega_{R}t_{0} + (N'_{2} - N_{2})\omega_{R}t_{1} + (N'_{3} - N_{3})\omega_{R}t_{2} + (N'_{4} - N_{4})\omega_{R}t_{3} - N_{1}\omega_{R}\Delta t_{1} - N_{2}\omega_{R}\Delta t_{2} - N_{3}\omega_{R}\Delta t_{3} - N_{4}\omega_{R}\Delta t_{4}$$
$$-N'_{1}\omega_{R}\Delta t_{1} + (N'_{3} - N_{3} - N_{2})\omega_{R}\Delta t_{2} - (N'_{4} - N_{4})\omega_{R}t_{1} + (N'_{4} - N_{4})\omega_{R}t_{3} - N_{3}\omega_{R}\Delta t_{3} - N_{4}\omega_{R}\Delta t_{4}$$
$$-N'_{1}\omega_{R}\Delta t_{1} - (N_{2} - (N'_{3} - N_{3}) - (N'_{4} - N_{4}))\omega_{R}\Delta t_{2} - (N_{3} - (N'_{4} - N_{4}))\omega_{R}\Delta t_{3} - N_{4}\omega_{R}\Delta t_{4}$$

The pattern that emerges is given by

$$\sum_{\varepsilon=1}^{n} (N'_{\varepsilon} - N_{\varepsilon}) \omega_{R} t_{\varepsilon-1} - \sum_{\varepsilon=1}^{n} N_{\varepsilon} \omega_{R} \Delta t_{\varepsilon} = -N'_{1} \omega_{R} \Delta t_{1} - \sum_{\varepsilon=2}^{n} \left( N_{\varepsilon} - \sum_{\varepsilon'=\varepsilon+1}^{n} (N'_{\varepsilon'} - N_{\varepsilon'}) \right) \omega_{R} \Delta t_{\varepsilon}.$$

Since  $N_1' = N_1 - \sum_{\varepsilon=2}^n (N_\varepsilon' - N_\varepsilon)$ , we can further simplify to

$$\sum_{\varepsilon=1}^{n} (N'_{\varepsilon} - N_{\varepsilon}) \omega_{R} t_{\varepsilon-1} - \sum_{\varepsilon=1}^{n} N_{\varepsilon} \omega_{R} \Delta t_{\varepsilon} = -\sum_{\varepsilon=1}^{n} \left( N_{\varepsilon} - \sum_{\varepsilon'=\varepsilon+1}^{n} (N'_{\varepsilon'} - N_{\varepsilon'}) \right) \omega_{R} \Delta t_{\varepsilon}.$$

Thus, an n-dimensional signal from free evolution through n transitions is given by

$$\langle s(\mathbf{t}) \rangle_{\gamma} = s(\mathbf{0}) \sum_{N_1} \cdots \sum_{N_n} \sum_{N'_2} \cdots \sum_{N'_n} I(\mathbf{N}, \mathbf{N}') \exp \left\{ -i \sum_{\varepsilon=1}^n \left[ W_{\varepsilon} + \left( N_{\varepsilon} - \sum_{\varepsilon'=\varepsilon+1}^n (N'_{\varepsilon'} - N_{\varepsilon'}) \right) \omega_R \right] \Delta t_{\varepsilon} \right\}, \quad (S.337)$$

where  $N_1' = N_1 - \sum_{\varepsilon=2}^n (N_\varepsilon' - N_\varepsilon)$ .

A method will have  $n_{\text{dim}}$  spectral dimensions,  $v = 1 \dots n_{\text{dim}}$ . Inside the  $v^{\text{th}}$  spectral dimension are  $v^{\text{th}}$  spectral events.  $n_{\rm v} = n_{\rm v}^{\rm mx} + n_{\rm v}^{\rm de} + n_{\rm v}^{\rm se}$  events (or propagators), where  $n_{\rm v}^{\rm mx}$  are mixing,  $n_{\rm v}^{\rm de}$  are delay, and  $n_{\rm v}^{\rm se}$  are spectral events. The total number of free evolution events (i.e., delay and spectral events) is given by  $n = \sum_{v=1}^{n_{\text{dim}}} (n_v^{\text{de}} + n_v^{\text{se}})$ . The free evolution events, ordered by time and indexed by  $\varepsilon = 1 \dots n$ , are partitioned into disjoint subsets of delay events,  $\mathfrak{D}_1, \mathfrak{D}_2, \dots, \mathfrak{D}_{n_{\dim}}$  and spectral events,  $\mathfrak{S}_1, \mathfrak{S}_2, \dots, \mathfrak{S}_{n_{\dim}}$ .

Similarly, the mixing events, ordered by time and indexed by  $\mu = 1 \dots m$ . We assume that mixing events occur instantaneously, with no rotor phase advance and no free evolution of transitions. Furthermore, we assume that mixing events are independent of  $\alpha$ ,  $\beta$ , and  $\gamma$ . Thus, we redefine Eq. (S.331) as

$$s(\mathbf{0}) = \prod_{\mu=1}^{m} u_{\mu},\tag{S.338}$$

and write the  $n_{\rm dim}$ -dimensional time domain signal as

$$\langle s(\mathbf{t}, \boldsymbol{\tau}, \alpha, \beta) \rangle_{\gamma} = s(\mathbf{0}) \sum_{N_{1}} \cdots \sum_{N_{n}} \sum_{N'_{2}} \cdots \sum_{N'_{n}} I(\mathbf{N}, \mathbf{N}') \exp \left\{ -i \sum_{v=1}^{n_{\text{dim}}} \sum_{\varepsilon \in \mathfrak{D}_{v}} \left( W_{\varepsilon} - \left( N_{\varepsilon} - \sum_{\varepsilon' = \varepsilon + 1}^{n} (N'_{\varepsilon'} - N_{\varepsilon'}) \right) \omega_{R} \right) \tau_{\varepsilon} \right\}$$

$$\times \exp \left\{ -i \sum_{v=1}^{n_{\text{dim}}} \sum_{\varepsilon \in \mathfrak{S}_{v}} \left( W_{\varepsilon} - \left( N_{\varepsilon} - \sum_{\varepsilon' = \varepsilon + 1}^{n} (N'_{\varepsilon'} - N_{\varepsilon'}) \right) \omega_{R} \right) x_{\varepsilon} t_{v} \right\}. \quad (S.339)$$

Here,  $x_{\varepsilon}$  is assigned to the corresponding fraction  $x_{v,k}$  for the  $k^{th}$  propagator in the  $v^{th}$  spectral dimension. The  $n_{\rm dim}$ -dimensional Fourier transform of this signal is

$$\langle s(\boldsymbol{\omega}, \boldsymbol{\tau}, \alpha, \beta) \rangle_{\gamma} = s(\mathbf{0}) \sum_{N_{1}} \cdots \sum_{N_{n}} \sum_{N_{2}'} \cdots \sum_{N_{n}'} I(\mathbf{N}, \mathbf{N}') \exp \left\{ -i \sum_{v=1}^{n_{\text{dim}}} \sum_{\varepsilon \in \mathfrak{D}_{v}} \left( W_{\varepsilon} - \left( N_{\varepsilon} - \sum_{\varepsilon' = \varepsilon + 1}^{n} (N_{\varepsilon'}' - N_{\varepsilon'}) \right) \omega_{R} \right) \tau_{\varepsilon} \right\}$$

$$\times \prod_{v=1}^{n_{\text{dim}}} \delta \left( \sum_{\varepsilon \in \mathfrak{S}_{v}} \left( x_{\varepsilon} W_{\varepsilon} - \left( N_{\varepsilon} - \sum_{\varepsilon' = \varepsilon + 1}^{n} (N_{\varepsilon'}' - N_{\varepsilon'}) \right) x_{\varepsilon} \omega_{R} \right) - \omega_{v} \right). \quad (S.340)$$

This expression for the transition pathway spectrum is the solution of the quantum master equation using our theoretical assumptions. Only a numerical integration over the angles  $\alpha$  and  $\beta$  remains to obtain the spectrum from the polycrystalline sample.

# S9 Czjzek Distribution

The Czjzek distribution[10, 9, 40]—originally developed to model random distributions of electric field gradient (EFG) tensors in glasses—is a model for anisotropic line shapes arising from structures producing random deviations from a mean anisotropy of zero, and is given by

$$f(\zeta, \eta | \sigma_{\zeta}) = \frac{\zeta^4 \eta}{\sqrt{2\pi} \sigma_{\zeta}^5} \left( 1 - \frac{\eta^2}{9} \right) \exp \left\{ -\frac{\zeta^2 \left( 1 + \frac{\eta^2}{3} \right)}{2\sigma_{\zeta}^2} \right\}, \tag{S.341}$$

where  $\zeta$  and  $\eta$  are the two independent parameters of the second-rank traceless symmetric tensor, and  $\sigma_{\zeta}$  is the width parameter. The Czjzek distribution assumes uncorrelated Gaussian distributions of second-rank spherical tensor components with a single width parameter, that is,

$$\mathbf{S} = \begin{bmatrix} \sqrt{3}U_5 - U_1 & \sqrt{3}U_4 & \sqrt{3}U_2 \\ \sqrt{3}U_4 & -\sqrt{3}U_5 - U_1 & \sqrt{3}U_3 \\ \sqrt{3}U_2 & \sqrt{3}U_3 & 2U_1 \end{bmatrix},$$
 (S.342)

where the components,  $U_1$ ,  $U_2$ ,  $U_3$ ,  $U_4$ , and  $U_5$ , are the five components of the second-rank traceless symmetric tensor, randomly drawn from a five-dimensional multivariate normal distribution with the mean of  $\langle U_i \rangle = 0$  and the variance of  $\langle U_i^2 \rangle = \sigma_c^2$ . It is a general model for identifying anisotropic line shapes arising from a random distribution of second-rank NMR tensors.

For a derivation of the Czjzek distribution, see Werner-Zwanziger et al. [40]. As noted in ref. [40], any scaling of the Czjzek distribution can be absorbed into a renormalized standard deviation parameter. Therefore, the distribution parameterized in terms of  $\zeta_{\sigma}$  or  $\zeta_{q}$  is given by Eq. (S.341). The distribution parameterized in terms of  $C_{q}$  is given by

$$f(C_q, \eta | \sigma_{C_q}) = \frac{C_q^4 \eta}{\sqrt{2\pi} \sigma_{C_q}^5} \left( 1 - \frac{\eta^2}{9} \right) \exp \left\{ -\frac{C_q^2 \left( 1 + \frac{\eta^2}{3} \right)}{2\sigma_{C_q}^2} \right\}, \tag{S.343}$$

where  $\sigma_{C_q}$  is the standard deviation of the distribution.

### References

- [1] Rihards Aleksis and Andrew J. Pell. Separation of quadrupolar and paramagnetic shift interactions in high-resolution nuclear magnetic resonance of spinning powders. J. Chem. Phys., 155, 2021.
- [2] O. N. Antzutkin. Sideband manipulation in magic-angle-spinning nuclear magnetic resonance. Prog. NMR Spect., 35:203–266, OCT 1999.
- [3] O. N. Antzutkin, S. C. Shekar, and M. H. Levitt. Two-dimensional sideband separation in magic-angle spinning NMR. J. Magn. Reson. A, 115:7–19, 1995.
- [4] A. D. Bain. A simple proof that third-order quadrupole perturbations of the NMR central transition of half-integral nuclei are zero. J. Magn. Reson., 179:308–310, 2006.
- [5] G. J. Bowden and W. D. Hutchison. Tensor operator formalism for multiple-quantum NMR. 1. spin-1 nuclei. J. Magn. Reson, 67:403-414, 1986.
- [6] G.J. Bowden, J.P.D. Martin, and M.J. Prandolini. Non-square tensor algebra and applications in the NMR of multiply connected spin systems: I. *Molec. Phys.*, 74:985 – 998, 1991.
- [7] H. A. Buckmaster, R. Chatterjee, and Y. H. Shing. The application of tensor operators in the analysis of EPR and ENDOR spectra. Phys. Stat. Sol. A, 13:9–50, 1972.
- [8] R. L. Cook and F. C. DeLucia. Application of the theory of irreducible tensor operators to molecular hyperfine structure. Am. J. Phys., 39:1433–1454, 1971.
- [9] G. Czjzek. Distribution of nuclear quadrupole splittings in amorphous materials and the topology of the  $(V_{zz}, \eta)$ -parameter space. Hyperfine Interactions, 14:189 194, 1983.

- [10] G. Czjzek, J. Fink, F. Götz, H. Schmidt, J. M. D. Coey, J.-P. Rebouillat, and A. Liénard. Atomic coordination and the distribution of electric field gradients in amorphous solids. *Phys. Rev. B*, 23:2513–2530, Mar 1981.
- [11] W. T. Dixon. Spinning-sideband-free NMR-spectra. J. Magn. Reson., 44:220–223, 1981.
- [12] W. T. Dixon. Spinning-sideband-free and spinning-sideband-only NMR spectra in spinning samples. *J. Chem. Phys.*, 77:1800, 1982.
- [13] M. Eden and M. H. Levitt. Computation of orientational averages in solid-state NMR by gaussian spherical quadrature. *J. Magn. Reson.*, 132:220–239, 1998.
- [14] A. R. Edmonds. Angular Momentum in Quantum Mechanics. Princeton University Press, 1960.
- [15] Z. H. Gan, P. Srinivasan, J. R. Quine, S. Steuernagel, and B. Knott. Third-order effect in solid-state NMR of quadrupolar nuclei. *Chem. Phys. Lett.*, 367(1-2):163–169, 2003.
- [16] M. Goldman, P. J. Grandinetti, A. Llor, Z. Olejniczak, J. R. Sachleben, and J. W. Zwanziger. Theoretical aspects of higher-order truncations in solid-state NMR. J. Chem. Phys., 97:8947–8960, 1992.
- [17] P. J. Grandinetti, J. T. Ash, and N. M. Trease. Symmetry pathways in solid-state NMR. *Prog. Nucl. Mag. Res. Sp.*, 59:121–196, 2011.
- [18] Seymour Haber. Parameters for integrating periodic functions of several variables. *Mathematics of Computation*, 41:115, 1983.
- [19] R. K. Harris, E. D. Becker, S. M. Cabral De Menezes, Pierre Grangerd, R. E. Hoffman, and K. W. Zilm. Further conventions for NMR shielding and chemical shifts, IUPAC recommendations 2008. Solid State Nucl. Mag., 33:41–56, 2008.
- [20] J. G. Hexem, M. H. Frey, and S. J. Opella. Influence <sup>14</sup>N on <sup>13</sup>C NMR spectra of solids. J. Am. Chem. Soc., 103:224–226, 1981.
- [21] J. G. Hexem, M. H. Frey, and S. J. Opella. Molecular and structural information from <sup>14</sup>N-<sup>13</sup>C dipolar couplings manifested in high resolution <sup>13</sup>C NMR spectra of solids. *J. Chem. Phys.*, 77:3847, 1982.
- [22] Malcolm H. Levitt and MATTIAS EDÉN. Numerical simulation of periodic nuclear magnetic resonance problems: fast calculation of carousel averages. *Molecular Physics*, 95:879 890, Mar-12-1998 1998.
- [23] P A Lindgard and O Danielsen. Bose-operator expansions of tensor operators in the theory of magnetism. *J. Phys. C: Solid State Physics*, 7:1523 1535, 1974.
- [24] M. Mehring. Principles of High Resolution NMR in Solids, volume 11. Springer-Verlag, Berlin, 1983.
- [25] A. Messiah. Quantum Mechanics, volume 2. Wiley, Amsterdam, 1965.
- [26] A. Naito, S. Ganapathy, and C. A. McDowell. High resolution solid state <sup>13</sup> C NMR spectra of carbons bonded to nitrogen in a sample spinning at the magic angle. *J. Chem. Phys.*, 74:5393–5397, 1981.
- [27] A. Naito, S. Ganapathy, and C. A. McDowell. <sup>14</sup>N quadrupole effects in CP-MAS <sup>13</sup>C NMR spectra of organic compounds in the solid state. *J. Magn. Reson.*, 48:367–381, 1982.
- [28] A. C. Olivieri. Quadrupolar effects in the CPMAS NMR spectra of spin-1/2 nuclei. *J. Magn. Reson.*, 81:201, 1989.
- [29] A. C. Olivieri, L. Frydman, and L. E. Diaz. A simple approach for relating molecular and structural information to the dipolar coupling <sup>13</sup>C-<sup>14</sup>N in <sup>13</sup>C CPMAS NMR. *J. Magn. Reson.*, 75:50–62, 1987.
- [30] S. J. Opella, M. H. Frey, and T. A. Cross. Detection of individual carbon resonances in solid proteins. J. Am. Chem. Soc., 101:5856–5857, 1979.
- [31] Giulio Racah. Theory of complex spectra. ii. Phys. Rev., 62:438–462, Nov 1942.
- [32] M. E. Rose. Elementary Theory of Angular Momentum. John Wiley and Sons, 1955.
- [33] B. L. Silver. Irreducible Tensor Methods. Academic Press Inc., San Diego, 1976.

- [34] Deepansh J. Srivastava and Philip J. Grandinetti. Statistical learning of NMR tensors from 2D isotropic/anisotropic correlation nuclear magnetic resonance spectra. *J. Chem. Phys.*, 153:134201, Jul-10-2020 2020.
- [35] M. E. Stoll, R. W. Vaughan, R. B. Saillant, and T. Cole.  $^{13}$ C chemical shift tensor in  $K_2Pt(CN)_4Br_{0.3} \cdot 3 H_2O$ . J. Chem. Phys., 61:2896, 1974.
- [36] N. M. Trease and P. J. Grandinetti. Solid-state nuclear magnetic resonance in the rotating tilted frame. *J. Chem. Phys.*, 128(5):052318, 2008.
- [37] D. L. VanderHart, H. S. Gutowsky, and T. C. Farrar. Dipole-dipole interactions of a spin-1/2 nucleus with a quadrupole-coupled nucleus. J. Am. Chem. Soc., 89:5056, 1967.
- [38] D. A. Varshalovich, A. N. Moskalev, and V. K. Khersonskii. *Quantum Theory of Angular Momentum*. World Scientific, Teaneck, NJ, 1988.
- [39] B. J. Walder, K. K. Dey, D. C. Kaseman, J. H. Baltisberger, and P. J. Grandinetti. Sideband separation experiments in NMR with phase incremented echo train acquisition. *J. Chem. Phys.*, 138, 2013.
- [40] U. Werner-Zwanziger, A.L. Paterson, and J.W. Zwanziger. The Czjzek distribution in solid-state NMR: Scaling properties of central and satellite transitions. *J. Non-Cryst. Solids*, 550:120383, 2020.
- [41] N. Zumbulyadis, P. M. Henrichs, and R. H. Young. Quadrupolar effects in the magic-angle-spinning spectra of spin-1/2 nuclei. *J. Chem. Phys.*, 75:1603–1611, 1981.